POLITECNICO
MILANO 1863

SCUOLA DI INGEGNERIA INDUSTRIALE
E DELL'INFORMAZIONE

Executive Summary of the Thesis

A method to study the water activation with FLUKA and LSC for a hadron therapy facility

Laurea Magistrale in Nuclear Engineering - Ingegneria Nucleare

Author: Benedetta Brusasco

Advisor: Prof. Marco Caresana

Co-advisor: Ing. Michele Ferrarini

Academic year: 2020-2021

1. Introduction

The goal of this project is to present a method to analyze the water activation in an hadrontheraphy centre. The importance of the water activation analysis is generated by the fact that the accelerated high energies particles can activate structural elements, air and water, and produce radiation, that lasts in time.
The investigation is developed at the CNAO foundation with the radioprotection office, where an important expansion is projected: it will be the first centre in the world to have a synchrotron dedicated to the acceleration of ions, a synchrotron for protons, thanks to the collaboration with Hitachi, and a BNCT facility in partnership with TAE. For these reasons, the water activation studio is based on the analysis of the production of different radionuclides according to the involved field and facility. Two kind of water systems are studied: the cooling circuit of the accelerators, characterized by demineralized water, and the cooling circuit of the utilities, composed of softened water. The work is developed with FLUKA for the computational side and LSC for the experimental one. In this paper, the main questions and results are presented following this path: starting with the characteristics of the employed water to provide a better understanding of the radionuclide production, subsequently the simulations of the accelerations are presented with a particular accidental scenario, to end with the experimental evaluation.

2. Water characteristics

For studying a conservative scenario, water with more impurities is investigated and simulated. In this way, the obtained results are the worst conditions that can be supposed for the facility. Therefore, the demineralized water is simulated with the composition of the analysis of DAFNE accelerator from INFN, National Laboratory of Frascati, and the softened water is simulated with the potable water from the water supply of Pavia. In the water analysis of DAFNE from INFN, some micrograms of Cu, Fe and Cr are present, while in the potable water of Pavia some milligrams of Na, Cl and Ca are present and lead to the production of traces of important radionuclides as ^{41}Ca, ^{36}Cl and ^{24}Na.

3. Synchrotron simulation

The simulations of the two water cooling circuits are performed not only for carbon ions and protons, that is to say the actual therapies, but also for the future accelerated particles: ^{4}He, ^{7}Li, ^{16}O and ^{56}Fe.

Table 1: Data for the employment of the simulated particles

Particles	Energy [MeV/u]	[particles/seconds]
p	250	2.0E+10
^{12}C	400	3.0E+08
^{4}He	320	5.0E+08
^{7}Li	306	4.5E+08
^{16}O	400	7.3E+07
^{56}Fe	306	3.6E+07

The beam is characterized by different losses, some of them are due to the working principles, such as to stop the beam a damp is necessary, or if a structural material is hit or by chance. They are all considered in a routine written in Fortran and compiled in FLUKA.

3.1. Geometry

The idea of the simulated structure comes from the original planimetry adapted to FLUKA, in order to make it the most similar to reality. The synchrotron cooling circuit is composed of the internal ring pipeline 1, the pipes along the HEBT line and the dipole 3. On the other hand, the utilities cooling circuit is the perimetrical pipeline and it appears with the number 4. The dimensions of the pipes are the following:

- Volume 1= 2612.5 l
- Volume 2=549.2 l
- Volume 3= 29.2 l
- Volume 4= 4235.9 l

The water volume of the designed dipole is bigger than the real one, because it was chosen to represent the water of all the dipoles, that are present in the ring, in one. This dipole is selected because of its strategic position, as it appears in the 1 figure, with the number 3, where the beam losses have bigger rate.

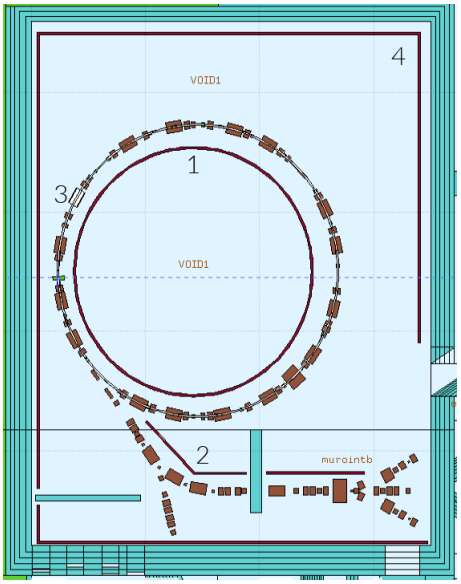

Figure 1: Simulated pipeline in the Synchrotron room, top view at beam height

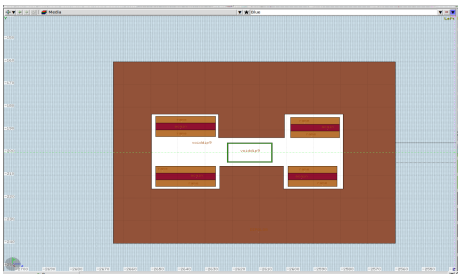

Figure 2: Dipole n° 3 in detail. Inside: in red water, surrounded by two layers of copper, in an iron structure

Studying and employing the routine that describes the beam losses and the track of the primary particles, a problem came out: the primary beam was hitting directly the water area. This situation is not describing the reality, because structural parts and other elements, such as controlling and measuring monitors, are present and stopping a great part of the losses. The proposed solution is to increase of some centimeters the dimensions of the magnets. This choice is employed because the elements that interfere consist of iron, the same material as the magnets. Nevertheless, for the protons the proposed solution is not enough and statistical problems are found. This is due to the fact that the generated activity is very low, so the program finds difficulties to detect some radionuclides. Hence, to implement the statistic a bigger volume is placed to detect the utilities cooling system and then is

re scaled through the specific activity.

3.2. Results

Among, all the obtained results, it is pointed out that the carbon ions are able to produce more activities than all the other ions. Hence, as an example, the result from the acceleration of the carbon ions are reported. The two water cooling circuits are studied after 1 s and 900 s, to remove the short half-life radionuclides. All the simulations are performed for a year.

Table 2: Ring pipeline results after 900 s

A	Z	A [Bq]	A_s [Bq/g]	Statistical error
15	8	3.46E+02	1.33E-04	6
14	6	3.95E+00	1.51E-06	14
14	8	7.27E-02	2.78E-08	29
13	7	1.06E+03	4.05E-04	21
11	6	1.53E+04	5.86E-03	25
10	4	4.82E-03	1.84E-09	23
7	4	7.93E+03	3.04E-03	12
3	1	2.76E+03	1.06E-03	6

Table 3: Perimetrical pipeline results after 900 s

A	Z	A [Bq]	A_s [Bq/g]	Statistical error
41	20	5.98E-03	1.41E-09	19
36	17	1.27E-02	3.00E-09	10
24	11	4.24E+02	1.00E-04	33
19	8	1.02E-08	2.41E-15	26
15	8	2.30E+02	5.44E-05	5
14	6	2.68E+00	6.33E-07	5
14	8	3.57E-02	8.43E-09	46
13	7	8.64E+02	2.04E-04	15
11	6	1.05E+04	2.49E-03	6
10	4	2.17E-03	5.11E-10	13
7	4	6.63E+03	1.56E-03	10
3	1	1.45E+03	3.42E-04	6

Reading the tables of the results coming from the perimetrical pipeline, it is remarkable the presence of ^{41}Ca, ^{36}Cl and ^{24}Na produced by neutron capture from the parent nuclide of impurities from the analysis of potable water of Pavia. Even though ^{41}Ca, ^{36}Cl, ^{14}C and ^{10}Be are produced in traces or in less quantity, it is important to keep them monitored, because they have a long half life. The production of ^{7}Be [fig:4] and ^{3}H [fig:3] is salient against all the other particles: in the zone at the centre, that is the closest one to the beam, the production of some kBq is seen. For these reasons, here the visual plot of their total activation is listed. The main produced radionuclides are ^{3}H, ^{7}Be, ^{11}C and ^{13}N. The results here listed are a summary of all the accelerated particles in the different regions.

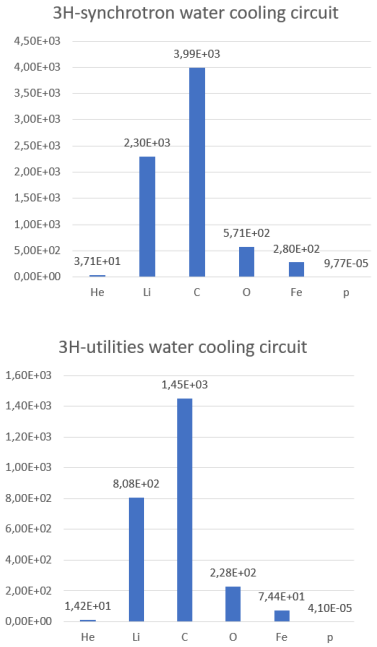

Figure 3: ^{3}H activity [Bq] per year

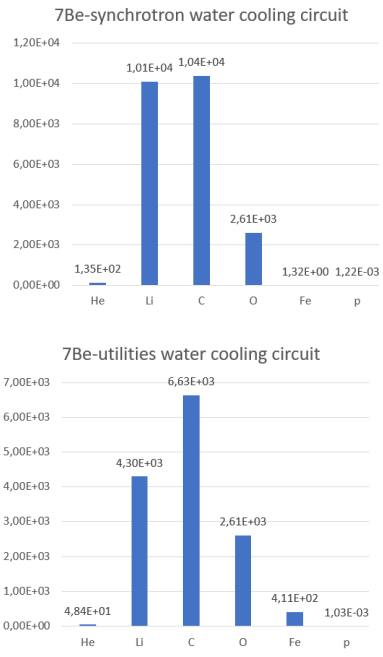

Figure 4: ^{7}Be activity [Bq] per year

4. Protontherapy

In the Hitachi protonteraphy facility, the water coolong circuit of the utilities is studued and simulated for 20 $years$. This evaluation is performed for a future decommissioning.
Moreover, this structure is characterized by a synchrotron with 4 dipoles and a gantry at the end of the line to deliver the therapy. In particular the gantry is an element that plays a fundamental role: with its 360° of rotation the beam losses hit all the surroundings. They are simulated like a cross and performed through a routine Source.f, written in Fortran and compiled by FLUKA.

4.1. Geometry

The geometry is composed of a perimetrical pipeline that is located in the room of the synchrotron and the gantry for a total volume equal to 611.7 l.

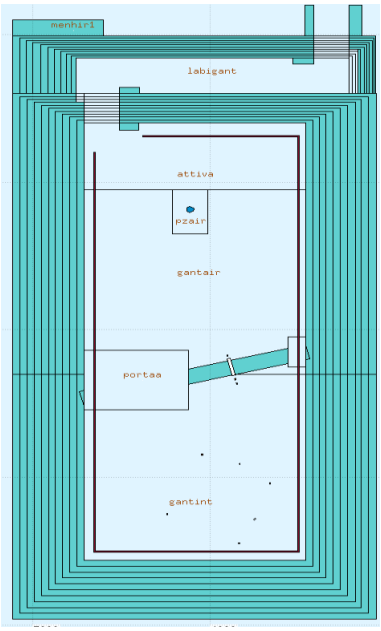

Figure 5: Hitachi simulated structure, top view at beam height

4.2. Results

In this section the tables of water activation results are placed. The investigated area is detected after 1 s and after 900 s. Moreover, the results show the same produced radionuclides as for the acceleration of protons in the actual synchrotron, but in more quantities. This effect is due to the gantry with its 360° degrees rotation added to the synchrotron and its losses.

Table 4: Wall pipeline results after 1 s

A	Z	A [Bq]	A_s [Bq/g]	Statistical error
41	20	5.87E-02	9.59E-08	26
36	17	9.93E-02	1.62E-07	25
24	11	1.68E+02	2.75E-04	28
16	7	3.05E+04	4.98E-02	10
15	6	3.48E+02	5.69E-04	91
15	8	8.60E+04	1.41E-01	7
14	6	8.99E+01	1.47E-04	13
14	8	8.32E+02	1.36E-03	20
13	7	2.94E+03	4.80E-03	35
11	6	4.83E+04	7.89E-02	12
10	4	1.43E-01	2.33E-07	26
10	6	2.84E+03	4.64E-03	21
7	4	1.26E+04	2.06E-02	15
3	1	4.48E+04	7.32E-02	11

Table 5: Wall pipeline results after 900 s

A	Z	A [Bq]	A_s [Bq/g]	Statistical error
41	20	5.87E-02	9.59E-08	26
36	17	9.93E-02	1.62E-07	25
24	11	1.66E+02	2.72E-04	28
15	8	5.26E+02	8.59E-04	7
14	6	8.99E+01	1.47E-04	13
14	8	1.22E-01	2.00E-07	20
13	7	1.04E+03	1.69E-03	35
11	6	2.90E+04	4.74E-02	12
10	4	1.43E-01	2.33E-07	26
7	4	1.26E+04	2.06E-02	15
3	1	4.48E+04	7.32E-02	11

Analyzing the results, the most relevant particles are ^{41}Ca, ^{36}Cl, ^{7}Be, ^{3}H and ^{14}C, due to their major production and their long half life. ^{41}Ca, ^{36}Cl and ^{24}Na are present for the employment of the analysis of potable water of Pavia, showing that milligrams of the added impurities can conduce to the production of other radiactive elements. Furthermore, traces of ^{10}Be are formed, an other long life particle that can not be neglected. ^{15}C has an higher error, because for the program it is more difficult to provide a valid estimation when the half life is really short or for the occurrence of exotic reactions.

5. BNCT

As regards the water activation, this facility has two circuits: the cooling system of the target area and the cooling circuit of the utilities, which

is located in the HEBL room.

5.1. HEBL room

The water activation studio is performed for 20 years to evaluate the produced radionuclides for the decommissioning. The water of the utilities cooling circuit is composed of the Pavia potable water, as in the previous simulations.

5.1.1 Geometry

In the next picture, it is noticeable the position of the HEBL room respect to the structure and the simulated pipes have a volume equals to 111 l.

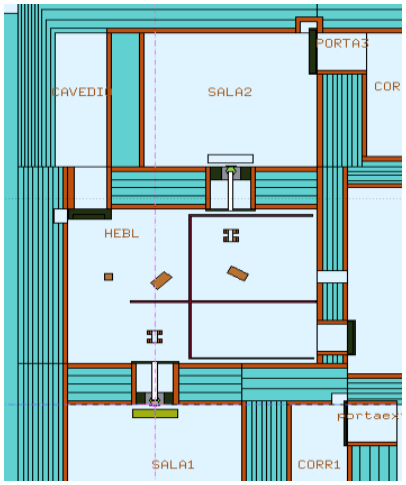

Figure 6: BNCT facility: layout from a top view

5.1.2 Results and comparison

In BNCT facility, it is present a total different field respect to the synchrotron: just ^{14}C and ^{36}Cl have a production that is detectable for FLUKA. These two particles are relevant for their long half life.

Table 6: Pipeline results from HEBL room

A	Z	A [Bq]	A_s [Bq/g]	Statistical error
36	17	1.58E+00	1.42E-05	14
14	6	2.30E+02	2.07E-03	28

Hence, to validate the obtained results, offline calculus are developed and the produced activity is estimated through:

$$A = N \cdot \lambda \tag{1}$$

where the population of the produced radionuclide N is obtained through the reaction rate and λ is the decay constant. The missing element to evaluate the RR is the thermal neutron fluence rate ϕ_{th} can be calculated through the use of the formula of Patterson and Wallace (1958), as it is suggested in the NCRP 144 [3]:

$$\phi_{th} = \frac{c * Q_F}{S} \tag{2}$$

where Q_F is the yield of fast neutrons, S is the internal area of the considered room and c is a constant that depends on the thermalization process of the fast neutrons, they slow down with their interaction with the walls. The c constant is equal to 5 [1] and a corrective factor is added $1/\eta$ to keep in count of the boron loaded concrete walls.

Reaction	Reaction Rate [particles/s]	λ [1/s]	Activity per second [Bq/s]	Activity per year [Bq/y]	Acitivity per 20 years [Bq]
H2(n,γ)H3	5,58E-01	1,78E-09	9,96E-10	7,17E-03	1,43E-01
O17(n,α)C14	3,54E+02	3,84E-12	1,36E-09	9,77E-03	1,95E-01
Ca40(n,γ)Ca41	3,68E-02	3,08E-13	1,13E-14	8,15E-08	1,63E-06
Ca40(n,α)Ar37	1,84E-04	2,29E-07	4,22E-11	3,04E-04	6,07E-03
Ca44(n,γ)Ca45	1,58E-03	4,92E-08	7,79E-11	5,61E-04	1,12E-02
Ca46(n,γ)Ca47	2,66E-06	1,77E-06	4,69E-12	3,38E-05	6,76E-04
Na23(n,γ)Na24	2,59E-02	1,29E-05	3,34E-07	2,40E+00	4,80E+01
Cl35(n,γ)Cl36	2,90E-01	7,30E-14	2,11E-14	1,52E-07	3,04E-06
Cl35(n,p)S35	2,90E-03	9,17E-08	2,66E-10	1,91E-03	3,82E-02
Cl35(n,α)P32	4,05E-07	5,61E-07	2,27E-13	1,64E-06	3,28E-05
Na23(n,γ)Na24	2,59E-02	1,29E-05	3,34E-07	2,40E+00	4,80E+01
Cd108(n,γ)Cd109	3,23E-09	1,77E-08	5,72E-17	4,12E-10	8,24E-09
Cd114(n,γ)Cd115	2,32E-08	1,82E-07	4,22E-15	3,04E-08	6,08E-07
Cd116(n,γ)Cd117	2,11E-09	5,82E-05	1,23E-13	8,86E-07	1,77E-05
Cr50(n,γ)Cr51	5,26E-07	2,90E-07	1,52E-13	1,10E-06	2,19E-05
Cr54(n,γ)Cr55	2,46E-09	3,30E-03	8,14E-12	5,86E-05	1,17E-03
Fe54(n,γ)Fe55	6,91E-07	8,14E-09	5,63E-15	4,05E-08	8,10E-07
Fe58(n,γ)Fe59	5,83E-08	4,87E-10	2,84E-17	2,05E-10	4,09E-09
Ni58(n,γ)Ni59	4,71E-07	2,93E-13	1,38E-19	9,95E-13	1,99E-11
Ni62(n,γ)Ni63	1,12E-07	2,20E-10	2,46E-17	1,77E-10	3,54E-09
Ni64(n,γ)Ni65	2,14E-09	7,64E-05	1,63E-13	1,18E-06	2,35E-05
Pb204(n,γ)Pb205	2,14E-10	1,47E-15	3,13E-25	2,25E-18	4,51E-17
Pb208(n,γ)Pb209	8,00E-12	5,92E-05	4,74E-16	3,41E-09	6,82E-08

Figure 7: Offline calculus in the HEBL room-results

The offline calculus shows that no relevant productions of other radionuclides are present. On the other hand, some differences are observed: some radionuclides, as ^{3}H and ^{24}Na, show an increase of activity, at the same time ^{36}Cl and ^{14}C has a decrease. This phenomenon is due to the employed approximation in this calculus, while a Monte Carlo method can consider all the phenomena and the statistic events at the same time. Nevertheless, this evaluation was needed to assure that no other radionuclides are produced with an important quantity.

5.2. Target region

The target simulation is a crucial point: it is where the production of neutrons takes place, through the reaction of accelerated protons on a

target of ^7Li, that produces ^7Be and neutrons and the highest energies of the facility are focused. The study is performed to estimate which particles and their quantity are produced in a year, to assure the safety to all the workers and to execute the ordinary maintenance.

5.2.1 Geometry

The target zone is composed of an Al void chamber with a cylindrical shape, in which protons are accelerated, followed by a thin layer of Li supported on a thicker part made of Cu. The total volume of the simulated pipeline is equal to $0.15\,l$. The simulated structure is an exact reproduction of the original structure and it is not publicly available. For this reason, no figure of the target are placed.

5.2.2 Results and comparison

The beam data are simulated for $655\,d$, that is the supposed lifetime of the target with 1E+13 particles per second. The areas immediately after the target and the three pipes are investigated after 1 s and after 900 s, but due to the fact that only long half life radionuclides are present, only a time interval is represented. Therefore, the water circulation forms a total activity of ^{14}C equal to $5.61E+02\,Bq$ and a specific activity of $3.74\,\frac{Bq}{g}$. These values are relevant due to the quantity of the produced radionuclide and the long half life. It was surprising the absence of tritium, so this is investigated with an offline calculus.
The production of ^3H and ^{14}C is due to the following reactions: $^2H(n,\gamma)^3H$ and $^{17}O(n,\alpha)^{14}C$. Their quantities are estimated through the reaction rate and the activity through the formula employed in the 5.1.2 section.
Once again, the missing element is the flux that is recovered through to the fluence. The FLUKA card USERTRACK allows to estimate the fluence of the neutrons passing through the region of ^7Li target in $[particles * cm^{-2} * GeV * primaries^{-1}]$. The investigated energy range is from $100\,\mu eV$ to $100\,keV$, after this energy value the fluence is equal to zero. Therefore, the total fluence can be obtained:

$$Total fluence = \Sigma_i \sigma_i E_i * primaries \quad (3)$$

where E_i stands for the average energy of the energy interval for that corresponding σ cross section of ^2H and ^{17}O, provided by Janis Web [2].

Element	RR	$\lambda\ [s^{-1}]$	Activity [Bq]
^3H	2.84E+04	1,796E-09	4.42E-05
^{14}C	5.56E+06	3.836E-12	2.12E-05

Table 7: Results from the offline analysis

As it appears in the 7 table, the calculus of the activity shows a low value of activity for both particles. This can explain the absence of ^3H from the results obtained by FLUKA. At the same time, the ^{14}C does not fit the expectation. This phenomenon is explained by statistical evaluations: even though the simulation was performed with $4E+09$ particles, it could be difficult for the simulator to provide an accurate results in presence of low activity in a little volume. Moreover, the simulation could overestimate some resonance peaks in the epithermal energies.

6. The Pavia Sewer case: dose estimation to workers

The CNAO water cooling system is composed of a closed loop in ordinary condition, thanks to the employment of ion exchange resin for the purification. On the other hand, in case of a failure or an accident in the circuit, an emergency pool is placed under the synchrotron room to collect its cooling water. Particularly, two possible risky situations are faced:

- a worker of the Pavia drainage system is near a pipeline and the radionuclides are passing at $1\,m$ of distance with the corrivation speed of $3\,ms^{-1}$;
- a person that is on the walkway over the depuration tanks or that is near the sludge for $200\,h$ per year.

6.1. Dose estimation to workers during corrivation

The dose estimation to workers during corrivation at a distance of $1\,m$ can be outlined in the following way:

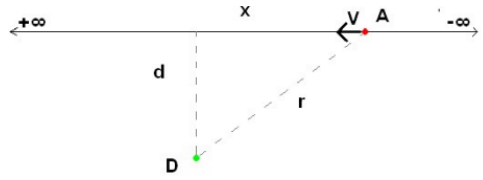

Figure 8: Sewer schematic model for dose estimation

The estimation of the ambient dose equivalent H*(10) in the point D at $1\,m$ of distance is performed along the path thanks to the integral:

$$H = \int_{-\infty}^{+\infty} \dot{H}(t)\,dt \tag{4}$$

with $\dot{H}(t) = \frac{\dot{H}_0}{r^2}$ and $\dot{H}_0$ can be evaluated in $\frac{\mu Sv}{h}$, thanks to the employment of the specific Gamma-ray costant Γ.
At this point, knowing $\dot{H}_0$, $D = 1\,m$ and $v = 0.3\,ms^{-1}$, H*(10) is equal to $H = 202\,nSv$ in the case of ^{18}F and for all the rest of radionuclides $H = 9\,nSv$. This evaluation is strongly conservative for the facts that usually the pipeline are placed underground and the radioactive decay is not considered during the corrivation. Therefore, no actual risk is present for the workers or any person that is close to the drain pipeline between CNAO and the dupuration facility.

6.2. Dose estimation to people from deputation tank and sludge line

To provide a proper estimation, the employment of FLUKA was required. Thanks to the simulation code, a dose map of the H*(10) is provide in $\frac{nSv}{primaries}$ and can be adapted to different activity.

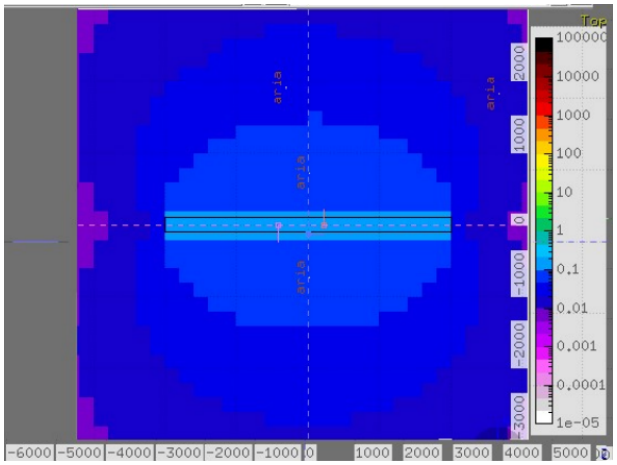

Figure 9: Equivalent dose map - $\beta+$ emitters

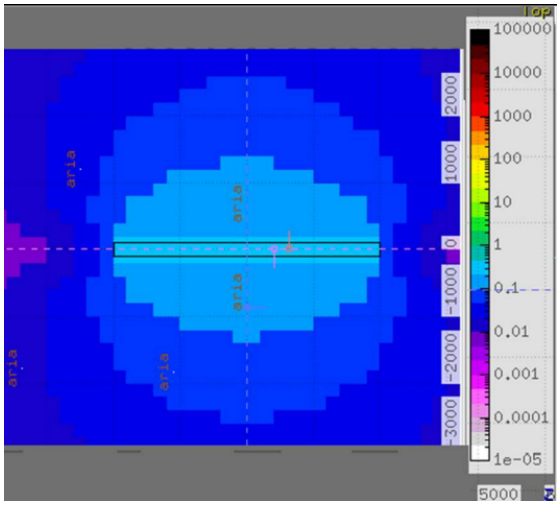

Figure 10: Equivalent dose map - $2\,MeV$

6.2.1 Dose evaluation from depuration tank

The H*(10) dose rate at $1\,m$ from the water depuration tank are $0.2\,\frac{nSv}{h}$ for $1\,MBq$ by a $2\,MeV$ photons emitters and inferior to $0.1\,\frac{nSv}{h}$ for $\beta+$ emitters.

6.2.2 Dose evaluation from sludge tank

This section is dedicated to the evaluation of the case in which the radionuclides are absorbed in the sludge line after the wastewater treatment. The short lived radionuclides are decayed, because all the collection and extraction of the drain lasts one day.
Using the same dose map of H*(10) [fig:10, 9], at a distance $1\,m$ from the sludge line a H*(10) dose is equal to $10\,nSv/h$ almost entirely due to ^{24}Na. However, after a pair of days, the dose rate will be $2\,nSv/h$, provided by ^{48}V, ^{7}Be, ^{22}Na and ^{54}Mn.
Considering the shield of the tank wall and the fact that the radionuclides would decay, the total dose to the personnel will be less then $1\,\mu Sv$, that is under the radioprotection dose limit of $1\,mSv$ per year for the population.

7. Experimental measurements

An experimental method is propose to perform an implementation to the water analysis: the HPGe can be applied as a first check and it is followed by a liquid scintillator counter. The available instrument at CNAO is the Triathler.

7.1. HPGe measurement

The analysis with the HPGe is the first step of the experimental part. The need to employ an accurate gamma spectroscopy is due to the possible presence of other radionuclides that can interfere with the liquid scintillation measurement. The presence of gamma emitters can derive from the oxidation of the material that composed the pipes due to the water action. The water spills from the LINAC circuit and synchrotron are measured for $1\,h$. The resulting spectra do not show any presence of radionuclides.

7.2. LSC measurement

In this work, it is developed the triathler calibration respect to the ^3H. The first trial was to perform the quench curve with the addition of a known quantity of ^3H. Different tests are performed: 8 vials composed of $10\,ml$ distilled water + $10\,ml$ cocktail with $314\,Bq$ of activity each; followed by 4 vials $10\,ml$ distilled water + $10\,ml$ cocktail with $3113\,Bq$ and the last attempt was performed with 3 vials $8\,ml$ distilled water + $12\,ml$ cocktail with $3113\,Bq$. Nevertheless, it is not possible to print the quench curves due to the machine characteristics (1 PMT). Hence, the photoluminiscence peak is overlapped to the ^3H spectrum, particularly increasing the quenching level, the plot is shifted and reduced towards left so the centre of gravity was in the photoluminescence peak. At this point, the instrument was not able to differentiate the increasing levels of quenching.

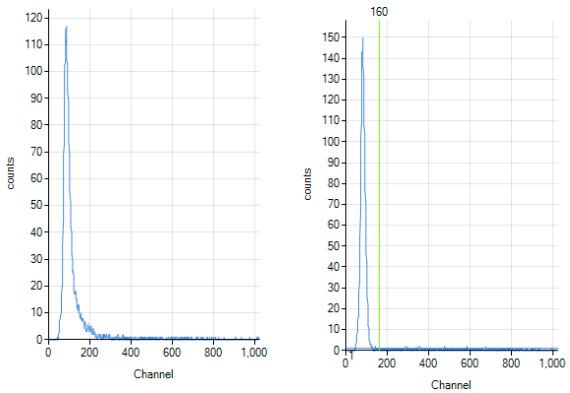

Figure 11: $10\,ml$ distilled water+$10\,ml$ cocktail+$314\,Bq$ ^3H spectrum vs $20\,ml$ cocktail spectrum

Then, the optimal solution is the internal standard method [4], that allows a quench correction thanks to an estimation of the efficiency. The evaluation is performed with two measurements: the first counts CPM_x are the measurement of the vial $15\,ml$ of cocktail+$5\,ml$ demineralized water, then after the an addition of a known activity $DPM_{standard}$ of the studied radionuclide the second measurement is registered with its countrate CPM_{x+std}. The employed $DPM_{standard}$ is a ^3H capsule source with an activity equals to $3101\,Bq$.

$$efficiency = \frac{CPM_{x+std} - CPM_x}{DPM_{standard}} \qquad (5)$$

The triathler characteristics outlines the best working condition analyzing $5\,ml$ or less of water. Hence, trials with the addition of $1\,ml$, $2\,ml$ and $5\,ml$ of demineralized water with the corresponding part of cocktail are performed in plastic vials of $20\,ml$.

vial	CPM_x	CPM_{x+std}	efficiency
$19\,ml$+$1\,ml$	120	19100	10.2 %
$18\,ml$+$2\,ml$	124	15580	8.3 %
$15\,ml$+$5\,ml$	133	10564	5.6 %

Table 8: Internal standard method result

Due to the results obtained, $15\,ml$+$5\,ml$ is chosen as the optimal solution, because it allows to analyze more volume of water and is a good compromise between efficiency and detection limit. In fact, considering the vial with $5\,ml$ of water, it is possible to reach almost $0.3\,Bq/g$ in $2\,h$. Hence, the internal standard was the correct solution to perform a calibration. It is followed by the evaluation of the correct concentration according to the measured efficiency, analyzed volume and corresponding MDA. Subsequently, the obtained efficiency are corroborated with the preparation of other samples, by validating the procedure.
Therefore, it follows an evaluation of consistency and reproducibility of the sample to validate the value of efficiency. Others samples with the same characteristics are measured and their statistic is following the Poisson distribution.

8. Conclusions

This executive summary represents the main themes developed in the water activation stu-

dio. The levels of activity produced in the water are useful to provide the future decommissioning and a safe environment to workers and patients. Therefore, proposing a method of evaluating an hadrontheraphy facility through FLUKA can guarantee the proper estimation of activity. At the same time, it can be implemented by offline calculus. Moreover, the last evaluation is an experimental part composed of two measurements with an HPGe and a LSC.

References

[1] Cheol Woo Lee, Young-Ouk Lee, Young-Sik Cho, and Sohyun Ahn. Analysis of the neutron thermalization in an accelerator room. *Journal of Nuclear Science and Technology*, 45(sup5):39–41, 2008.

[2] NEA. Janis web.

[3] National Council on Radiation Protection and Measurements. *NCRP Report No. 144. Radiation protection for Particle Accelerator Facilities*. 2003.

[4] CT Peng. Quenching correction in liquid scintillation counting. *Advances in tracer methodology*, pages 81–94, 1966.

POLITECNICO
MILANO 1863

SCUOLA DI INGEGNERIA INDUSTRIALE
E DELL'INFORMAZIONE

A method to study the water activation with FLUKA and LSC for a hadron therapy facility

Tesi di Laurea Magistrale in
Nuclear Engineering - Ingegneria nucleare

Author: **Benedetta Brusasco**

Student ID: 919964
Advisor: Prof. Marco Caresana
Co-advisors: Ing. Michele Ferrarini
Academic Year: 2020-21

Abstract

Nowadays, the number of facilities that accelerates ions and protons for treating tumors is increasing. The radioprotection is a fundamental framework to guarantee the safety for the workers, the patients, the neighbours and the environment. The goal of this project is to present a method to analyze the water activation in an hadrontherapy centre.

The investigation is developed at the CNAO foundation: an Italian excellence, that will be the first centre in the world to have a synchrotron dedicated to the acceleration of ions, a synchrotron for protons, thanks to the collaboration with Hitachi, and a BNCT facility in partnership with TAE. In radioprotection the importance of the water activation analysis is generated by the fact that the accelerated high energies particles can activate the structural elements, the air and the water, and produce radiation, that lasts in time.

The dissertation is composed of two main sections: the computational codes, preceded by an analysis of the expected particles, and the experimental measurements. The computational evaluation is performed through FLUKA, a Monte Carlo method software which provides different evaluations, including the activation in particular regions. The FLUKA codes are tailored according to the examined facility: important studios are dedicated to the different geometries, fields and water compositions.

As regards the actual synchrotron, the simulations deal with the water cooling circuit of the synchrotron and its utilities. Moreover, they are performed not only for carbon ions and protons, that is to say the actual therapies, but also for the future accelerated particles: ^{4}He, ^{7}Li, ^{16}O and ^{56}Fe.

In the Hitachi protontherapy, the simulation addresses to the water cooling utilities, that is placed in a particular location that includes not only the synchrotron, but also the gantry to deliver the therapy.

On the other hand, the BNCT facility is characterized by an electrostatic tandem accelerator to accelerate protons and subsequently to produce neutrons. In this setting, the water activation is studied for the target and the utilities in the HEBL room. Nevertheless, the FLUKA results reveal low activity levels, so they are complemented with offline

calculus, that are consistent with the computational work.

Furthermore, the water cooling system is a closed loop, but it is studied an accidental scenario, in which the cooling water is collected in the emergency pool and then it fails. Hence, the radionuclides are ended in the sewer and the dose to workers is estimated in the corrivation phase, depuration tank and sludge phase.

The experimental evaluation achieves the goal to perform an analysis on site of the water cooling system of the synchrotron. It is articulated in two phases: first the HPGe detector allows a general screening, followed by the Liquid Scintillation Counter. The instrument available at CNAO is the Triathler. In this work, it is developed its calibration respect to the ^3H. The calibration consists on a quench correction through the quench curve with the addition of a known ^3H quantity as a first trial and then, the internal standard method. Hence, the internal standard was the correct solution to perform a calibration. It is followed by the evaluation of the correct concentration according to the measured efficiency, analyzed volume and corresponding MDA. Subsequently, the obtained efficiency are corroborated with the preparation of other samples, by validating the procedure.

Keywords: water activation, FLUKA, LSC

Abstract in lingua italiana

Oggigiorno, il numero di strutture che utilizzano acceleratori per la cura di determinati tumori sta crescendo sempre più. In questo contesto, la radioprotezione è una disciplina fondamentale per garantire la sicurezza ai lavoratori, ai pazienti, alla popolazione circostante e all'ambiente. L'obbiettivo di questa tesi è presentare un metodo per analizzare l'attivazione dell'acqua in un centro di adroterapia.

Lo studio è svolto presso la fondazione CNAO: un'eccellenza italiana, che vanterà di essere il primo centro al mondo ad avere un sincrotrone dedicato all'accelerazione di ioni, un sincrotrone per la protonterapia grazie alla collaborazione con Hitachi e una struttura per la BNCT in collaborazione con TAE. In radioprotezione l'importanza dell'analisi di attivazione dell'acqua risiede nel fatto che le particelle accelerando possono attivare radiazioni elementi strutturali, aria e acqua, e generare radiazioni, che durano nel tempo.

Questo lavoro è composto da due parti principali: i codici computazionali, preceduti da un'analisi delle particelle che si sarebbero aspettate, e le misure sperimentali. La valutazione di carattere computazionale è sviluppata grazie a FLUKA, un software basato sul metodo Monte Carlo che fornisce l'attivazione nelle aree richieste. I codici FLUKA sono stati personalizzati secondo le caratteristiche di ogni struttura: importanti focus sono dedicati alle differenti geometrie e campi.

Per quanto riguarda il sincrotrone attuale, le simulazioni affrontano il circuito di raffreddamento del sincrotrone e delle utenze. Esse sono state effettuate non solo per gli ioni carbonio e per i protoni, ovvero le terapie attuali, ma anche per le particelle che verranno accelerate in futuro: ^{4}He, ^{7}Li, ^{16}O and ^{56}Fe.

Nella struttura di protonterapia, la simulazione è rivolta solo al circuito di raffreddamento delle utenze, che è posto in un luogo particolare che include il sincrotrone, ma anche il gantry per effettuare la terapia.

Dall'altro lato, la struttura dedicata alla BNCT è caratterizzata da un acceleratore elettrostatico tandem per accelerare protoni e successivamente produrre neutroni. In questo contesto, sono state sviluppate simulazioni per quanto rigurda il target e le utenze nella

sala HEBL. Siccome i risultati provenienti da FLUKA rilevano poca attività, sono stati affiancati da conti offline che sono in linea con il lavoro simulato.

Inoltre, il sistema di raffreddamento è un circuito chiuso, ma è stato studiato un scenario incidentale, in cui l'acqua di raffreddamento è raccolta nella piscina di emergenza e il sistema di contenimento fallisce. Quindi, i radionuclidi sono portati nella fogna e sono state valutate le dosi durante la fase di corrivazione, dalla vasca di depurazione e dallo smistamento dei fanghi.

La valutazione sperimentale raggiunge l'obbiettivo di realizzare un analisi sul posto del circuito di raffreddamento dell'acqua del sincrotrone. Essa si articola in due fasi: dapprima il detector HPGe permette uno screening generale, seguito dalla misura con la scintillazione liquida. Lo strumento disponibile allo CNAO è il Triatler. In questo lavoro, è stato calibrato rispetto all' ^3H. La calibrazione consiste nella correzione del quenching attraverso in un primo momento le curve di calibrazione con l'aggiunta di una quantità nota di ^3H e successivamente con il metodo dello standard interno. Conseguentemente, lo standard interno era la soluzione corretta per realizzare la calibrazione. L'analisi segue con la valutazione della corretta concentrazione sulla base dell'efficienza misurata, volume analizzato e la corrispondente minima attività rilevabile. Successivamente i risultati di efficienza ottenuti sono corroborati attraverso la preparazione di altri campioni, validando così la procedura.

Parole chiave: attivazione dell'acqua, FLUKA, LSC

Contents

1 | Introduction

This introductory chapter aims to describe the involved physical quantities, to provide a global understanding in the activation process, and to the method to recreate a realistic situation through a simulator.

Parallel to the physical description, a simulation code was needed to perform the water activation for the radioprotection analysis: not only to realize the complex geometry, in order to make it as realistic as possible, but also to take in consideration all the physic events that are happening at the same time. For this reason, it was necessary to use a powerful software as FLUKA, FLUktuierende KAskade, that is based on the Monte Carlo simulation.

In the first and second sections, the needed quantities for having a complete description are analyzed, followed by the description of Monte Carlo simulation and FLUKA code in the third one.

1.1. Field quantities

For being able to provide a detailed analysis, here, an overview of physical quantities is placed: starting with field quantities, used to describe radiations, that allows to understand the following radio-protection and dosimetric properties, used in this project.

1.1.1. Particle fluence

In a point P of the irradiated body, as it appears in the figure 1.1, particle fluence Φ is evalueted by:

$$\Phi = \frac{dN}{da} \tag{1.1}$$

where da is the maximum surface hit by the flux, considering a sphere with an infinitesimal radius and the unit of measurement is $[m^{-2}]$.

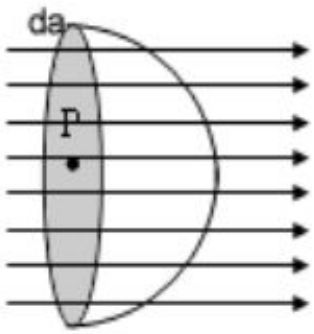

Figure 1.1: Generic P point in a sphere of infinitesimal radius *da* [7]

1.1.2. Flux

Flux, ϕ, is a quantity that allows to quantify the number of particles, dN, in time dt, that collide with a sphere of maximum section *da*, as described in the picture 1.1

$$\phi = \frac{dN}{da \cdot dt} = \frac{\Phi}{dt} \tag{1.2}$$

ϕ is measured in $[m^{-2} \cdot s^{-1}]$.

To provide a correct estimation of released energy is necessary to define the following quantities.

1.2. Dosimetric quantities

This part has the goal to highlight the main quantities involved in this project, providing a complete description of quantities used for radioprotection and dosimetric purpose.

1.2.1. Imparted energy

In a volume, the imparted energy $\bar{\epsilon}$ from the radiation is expressed by the next energy balance:

$$\bar{\epsilon} = R_{in} - R_{out} + \Sigma Q(J) \tag{1.3}$$

R_{in}= imparted energy of all the particles entering the considered volume.

R_{out}= imparted energy of all the particles exiting the same volume.

ΣQ= the sum of all the released energies, once subtracted the energetic consumption from

the nuclear reaction and transformation.

$\bar{\epsilon}$ can vary considerably if a little volume or a low flux is considered, so important oscillations are registered.

1.2.2. Absorbed dose

In an infinitesimal volume of mass dm, the absorbed dose D is:

$$D = \frac{d\bar{\epsilon}}{dm} \tag{1.4}$$

where $\bar{\epsilon}$ is the average imparted energy (1.2.1).

A special focused on dm, which is not the derivative of the function mass, but is expressed by the mass limit to zero:

$$D = \lim_{m \to 0} \frac{\bar{\epsilon}}{m} = \lim_{V \to 0} \frac{1}{\rho} \frac{\bar{\epsilon}}{V} \tag{1.5}$$

The measurement unit is Gray: $1\,Gy = 1\,J/Kg$; while the RAD is still used: $1\,RAD = 100\,\frac{erg}{g} = 10^{-2}\,\frac{J}{Kg} = 10^{-2}\,Gy$.

Nevertheless, the absorbed dose is not able to express the real damage, because it does not keep in consideration biological effect and characteristics of the radiation or particles. For this reasons, other quantities are described.

1.2.3. Organ absorbed dose

For analyzing the absorbed dose in a mass, it is effective to estimate D_T, the organ absorbed dose, defined by ICPR 2007 [27]:

$$D_T = \frac{1}{m_T} \int_{m_T} D\, dm_T = \frac{\bar{e}_T}{m_T} \tag{1.6}$$

where m_T is the mass of the organ T and D the absorbed dose of dm. In addition, the last result shows that D_T can be estimate by the the ratio of the imparted energy $\bar{e}_T$ in the organ T with the organ mass dm.

1.2.4. Equivalent dose

The equivalent dose, defined by [14] and [10], is evaluated through :

$$H_{T,R} = w_R \, D_{T,R} \tag{1.7}$$

where w_R is a constant depending on the type of radiation R, called radiation weighting factor, and D_T the organ absorbed dose (1.2.3). In this way, $H_{T,R}$ is a value able to correlate the effect of that kind of radiation to the considered organ.

Table 1.1: w_R values

Type of Radiation	w_R
Photons	1
Muons and electron	1
α particles, heavy ions, fission fragments	20
neutrons	continuous function depending on energy

Here, it is placed the plot 1.2 that shows the function of the weighting factor w_R depending on the neutron energies [33]:

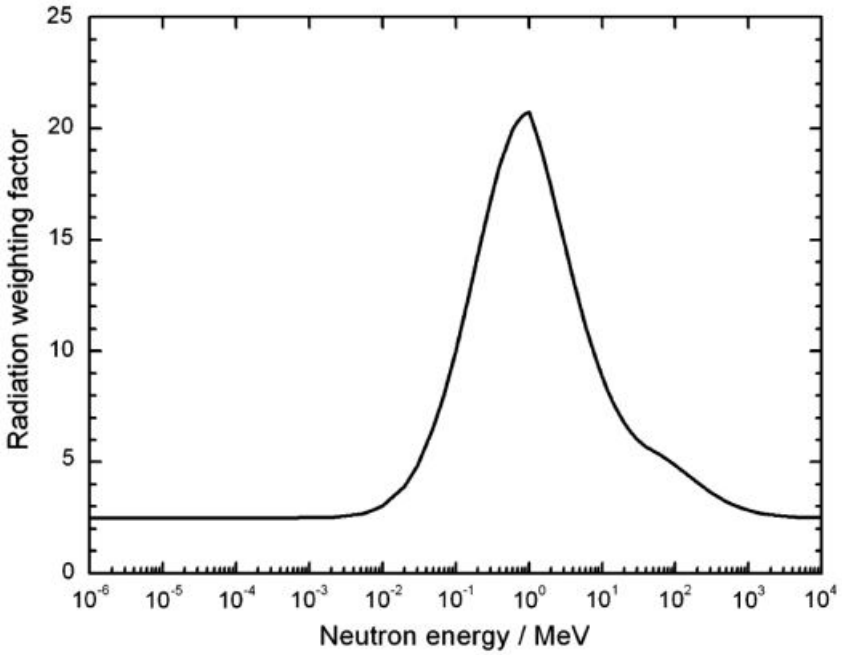

Figure 1.2: Radiation weighting factor w_R for neutrons [33]

Moreover, a global quantity, concerning all the present radiations, is the total equivalent

dose H_T:

$$H_T = \Sigma_R \, w_R \, D_{T,R} \tag{1.8}$$

1.2.5. Effective dose

The effective dose is described by [14] and [10], and can be estimated by:

$$E = \Sigma_T \, w_T \, \Sigma_R \, w_R \, D_{T,R} \tag{1.9}$$

with E measured in *sievert*, $[Sv]$. A new quantity is introduced, w_T, a weighting factor that is able to keep in consideration the different effects that a radiation can affect that organ instead of an another one.

Table 1.2: Effective Dose

Organ	number of tissue	w_T	total weight
Lungs, colon, stomach, bone-marrow, remaining tissue	6	0.12	0.72
Gonad	1	0.08	0.08
Thyroid, esophagus, liver, bladder	6	0.12	0.72
Bones, brain, skin, salivary gland	4	0.01	0.04

1.2.6. Ambient dose equivalent

The ambient dose equivalent H*(10) is defined by ICRP Publication 103:

The dose equivalent at a point in a radiation field that would be produced by the corresponding expanded and aligned field in the ICRU sphere at a depth of 10 mm on the radius vector opposing the direction of the aligned field. [27]

Its unit of measurement is the Sievert (Sv) and $10\,mm$ stands for a standard depth for indicating a deep radiation dose.

The ICRU sphere is a $30\,cm$ diameter, made of tissue equivalent material with $1\,\frac{g}{cm^3}$ of density and the following mass composition:

Table 1.3: Composition of ICRU sphere

Element	%
O	76.2
C	11.1
H	10.1
N	2.6

1.2.7. Activity

Activity is the number of measured decays in the unit of time [7]:

$$A = \frac{dN}{dt} = -\lambda N \tag{1.10}$$

with dN the spontaneous revealed disintegration, that happens in dt and in the considered quantity of the radionuclide. In addition, activity is proportional to the atoms N of that involved element. The presence of the sign minus is due to the decrease of the considered population during the time and λ, decay constant, represents the probability that the considered radionuclide decays.

The unit of measurement is $[s^{-1}] = 1\,Bq$, *Becquerel*, while the historic unit is the *Curie*: $1\,Ci = 3,7 \cdot 10^{10}\,Bq$.

Solving the differential equation (2.10), the evolution of the population of the radionuclide in time:

$$N(t) = N_0 \cdot e^{-\lambda t} \tag{1.11}$$

For the same development of the equation (2.10), it is possible to write the equation of the activity:

$$A(t) = A_0 \cdot e^{-\lambda t} \tag{1.12}$$

1.2.8. Specific Activity

Specific activity provides a real information about the quantity of radioactive material. It is defined by the ratio of the activity and the considered mass and is measured in $[Bq/g]$:

$$A_s = \frac{A}{m} = \frac{\lambda \cdot N}{m} = \frac{\lambda \cdot N_{av} \cdot M}{m} = \frac{\lambda \cdot N_{av} \cdot m}{m \cdot PA} A_s = \lambda \cdot \frac{N_{av}}{PA} \tag{1.13}$$

The previous equation shows how to obtain a practical formula, where M is the mumber

of moles, N_{av} is Avogadro number and PA is the molecular weight.

1.2.9. LET

Linear Energy Transfer is a value able to estimate the spatial distribution of the released energy, coming from the path of charged particles.

This estimation allows to have a realistic measure of the transferred energy, because it keeps in consideration the secondary electrons. Secondaries possess a not negligible energy value, because they can create secondary ionization according to their energy. So, secondary particles have to be kept in consideration for biological effects.

LET can be defined taking in account all the process that are under a particular value indicated with $\Delta\,[eV]$:

$$L_\Delta = (\frac{dE}{dl})_\Delta \tag{1.14}$$

with dE energy loss of primary particle during in the path dl. The unit of measure is $[J/m]$, but the most used is $[KeV/\mu m]$.

1.2.10. RBE

RBE, Relative Biological Effectiveness, provides a description of biological effects depending on the present ionizing radiation relative to an other one. It allows to estimate damages of different radiation with low or high LET.

$$RBE = \frac{D_X}{D_R} \tag{1.15}$$

D_X is the reference absorbed dose of X-rays, accelerated at $150\,kV$, that is able to create a determinate damage, so D_R is the absorbed dose that is able to replicate the same damage. Instead of D_X, it can be use the radiation coming from gammas and the correspond absorbed dose D_γ, as reference.

1.3. Monte Carlo and FLUKA

1.3.1. Simulation codes

The parameters just mention can be simulated in a complex structure through the use of Monte Carlo method. In fact in this project, a computational part is developed by FLUKA, a powerful tool that is based on Monte Carlo.

1.3.2. Monte Carlo

Monte Carlo methods are computational algorithms based on random samples of an unknown value through the use of distribution probability.

Particularly, a Monte Carlo simulation allows us to estimate a value using the principles of inferential statistics. Inferential statistics is based on a population, made of a set of samples, that are composed of subsets of the population. The key is the fact that the simulation chooses a random sample: the randomness tends to expresses the same characteristic as the entire population. Thanks to this, the simulation allows to describe the probability of occurrence of a particular physical quantity, starting from running some variables through a model. The model is customized describing the occurring physical events, taking in consideration all the phenomena that can affect the model with probability of them. After having analyzed the probability distribution of the starting domain, the simulation goes on generating inputs randomly and subsequently performing a deterministic computation on the input. At this point, the results are aggregated from the different inputs with a statistical error.

For the first time in history, the Monte Carlo method was used by Enrico Fermi for studying the neutron diffusion. Unfortunately, he did not published it but, his student, Emilio Segrè, witnessed it.

Some years later, during World War II, in the project Manhattan, Stanislaw Ulam proposed a modern version of it studying the development of weapons. John von Neumann was fascinating by the Ulam's method, so created the first computer able to develop the algorithm. Due to the fact that the project was secret, they gave to this method the code name: Monte Carlo, in honor of the famous Monte Carlo Casino in Monaco. From this starting point, in the decades, the Monte Carlo method was expanded and improved for being used in different fields of engineering, physics, finance, biology and transport.

In this project, for analyzing the water activation, FLUktuierende Kaskade (FLUKA) code is used as a way to investigate through Monte Carlo method.

1.3.3. FLUKA

FLUKA is a general purpose instrument for the realization of Monte Carlo simulation [2], able to describe the transport of particles and interaction with matter. It covers a wide range of particles, almost sixty, including: photons and electrons from 1 keV until thousands of TeV; hadrons until $20\,TeV$; heavy ions; neutrons until thermal energies; neutrino; muons and all their antiparticles.

Thanks to the software and the user-friendly interface FLAIR, it allows to replicate difficult structures and geometries, like an accelerator, and to investigate system for radiotherapy, activation, dose delivery, calorimetry etc.

In the 1960s the first version of FLUKA was computed by Johannes Ranf at CERN, for designing the shield. The CERN project consisted of high energy proton accelerators ($300\,GeV$) and to estimate the performance of a NaI crystal for hadron calorimeters.

Thereafter, the Ranf's first code was improved with new models including modern physics. In 1988 CERN projected new proton colliders with energies closed to TeV, so the need of FLUKA became of real interest for evaluating the radiation damage and activation of machines. A team made of physicists from the Italian INFN, National Institute of Nuclear Physics, and CERN transformed FLUKA in a more powerful instrument capable of deal with different particles having a wide range of energies and above all able to interact with matter considering all the possible phenomena. For this reason, the software is distributed by INFN and CERN and they keep the copyright.

Particularly, after all the progress in the code, a Combinatory Geometry (CG) is available and not only is customized to represent difficult geometries, but also to follow correctly the path of charged particles also in presence of magnetic or electric fields. It works through bodies and regions: basic 3D structure and more complex geometric shapes are available to create the desire system. The CG package provides infinite surfaces or macro-bodies like cylinders (RCC), parallelepipeds (RPP) and other element. By combining them with the employ of Boolean operations (union, subtraction and intersection) a region is formed. Only a single material can be assigned to a region and the connection among them can consist of more contiguous part. This fact is due to the meaning of region as a fraction of space of homogeneous statistics or same settings. In addition, for taking in consideration the fact that particles cannot be traced across the external boundary and for absorbing

all the escaping particles, a black-hole region is needed and should be quite big to not interfere.

1.3.4. Software settings

To run a FLUKA simulation, an input is uploaded in FLAIR: it is a view editor, that helps the use of the software through CARDS. Every CARD allows an important setting.

Here, some of the most important and use CARDs, to simulate the water activation, are described [11]. Starting with the Default card, the simulator offers a group of physical settings, that can be selected according to the event to describe. After having outlined the regions, material and compound have to be assigned to each region to accredit the chemical composition and density of the material.

Beam definition on FLUKA

For defining the transport of the primary particles, the crucial card is the BEAM: it allows to set the type of particles, their energy, their position in the space and other features like isotropic, rectangular and so on. Instead of using this card, it is possible to design the beam modifying one characteristic of the interface routines with SOURCE.f, a subroutine written in Fortran77, that superimposes its data to the BEAM card. This can be implemented with the use of the card SOURCE, that permits to open the SOURCE.f. To perform the water activation analysis various SOURCE.f files were employed according to the features of each structure.

Activation and scoring cards

Particularly, to achieve the activation analysis, specific cards are utilized. First of all, RADDECAY demands simulation of radioactive decays and establishes the corresponding transport conditions. To perform an irradiation profile varying in time, IRRPROFIL permits to indicate the quantity of particles per seconds and for how much time they are irradiating. Coupling with DCYTIMES, the times are set to score the selected quantities in relation to the end of irradiation. Then, RESNUCLEi scores the radioactive nuclei that stops on a region basis and is associated to DCYSCORE, that actives the time selected to estimate the results. In order to obtain trustable results, the card PHYSICS is activated for taking into account physical phenomena, that are not considered in the defaults. In this case, coalescence and evaporation are activated. Moreover, to estimate the scoring other two cards are selected: USERBIN to value various relevant quantities, such as dose and particle fluence, giving as a result a map of the investigating measure, that is

geometrical independent and superimposed to the simulated geometry; USERTRACK to estimate the fluence for a track-length detector.

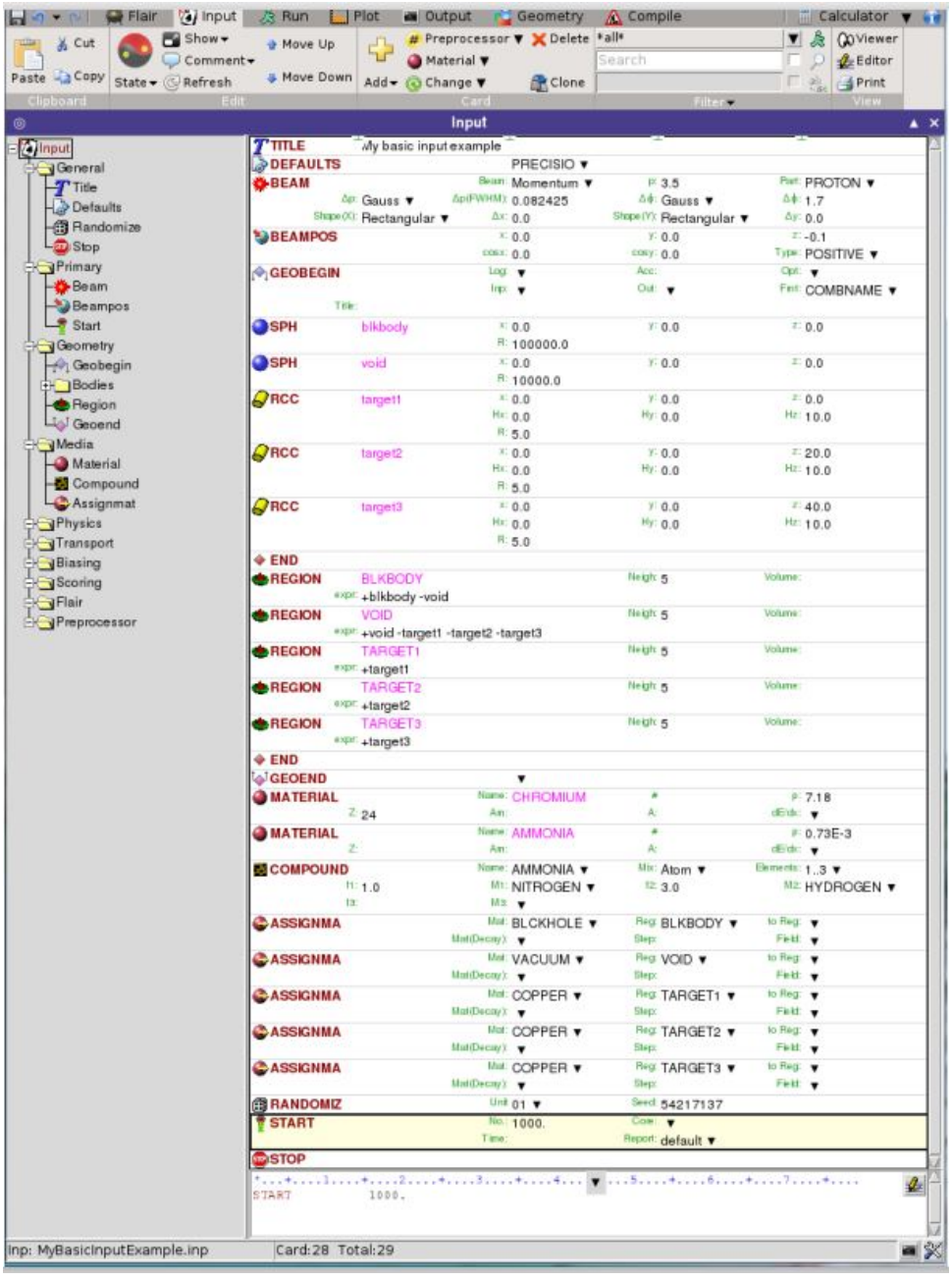

Figure 1.3: Flair - FLUKA interface

2 | CNAO Foundation

This chapter describes the CNAO foundation and the project concerning a future expansion. Moreover, every research activity is developed with the purpose to improve the structure and to provide a better treatment quality for the patients.

CNAO, National Center for Oncological Hadrontherapy, is the first center in Italy that employs hadrons as a therapy, substituting the conventional radiotherapy, with the carbon ions and proton to treat tumors [8]. Around the world, there are only six structures to perform this therapy. Furthermore, the center has gained prestige also for clinical and radiobiology research to discover effective instruments to fight against cancer.

The center is based in Pavia and its inauguration occurred in 2010; since 2014 hadrontherapy is included in the treatments paid by the National Health Service. Nowadays the structure is following 700 patients for year.

The advantages of using heavier particles than X-rays are: to be able to damage radio resistant or inoperable tumors, including those located in difficult zone; to be much more precise and to avoid delivering high doses to healthy tissues. In addition, it has been observed that in young patients, the risk of metastasis is reduced.

Actually, CNAO Synchrotron is providing the extraction of the particles at high energy: $250\,MeV$ for protons and $400\,MeV/u$ for carbon ions as maximum values.

2.1. Synchrotron

The CNAO's Synchrotron is designed specifically for treating oncological patients: it is similar to the one in the CERN in Geneva, but it has some features for tailoring the beam for the purpose of therapies, such as splitting and sending the beam towards the treatment rooms.

It is a circular accelerator with a diameter of $25\,m$ and a circumference of $80\,m$. A specific bunker of $1600\,m^2$ was built to keep a safe surrounding environment for the neighbourhood and workers. So for radioprotection reasons, reinforced concrete walls of a range from 2

to $6\,m$ were designed.

Figure 2.1: Synchrotron at CNAO [8]

2.1.1. Synchrotron structure

The structure of the synchrotron is composed of: two sources for the production of carbon ions and protons; a LINAC for a pre-acceleration phase; followed by an injection line to transfer the particles to the synchrotron ring where they will be additionally accelerated and extracted at energies until $250\,MeV$ for protons and $400\,MeV/u$ for carbon ions.

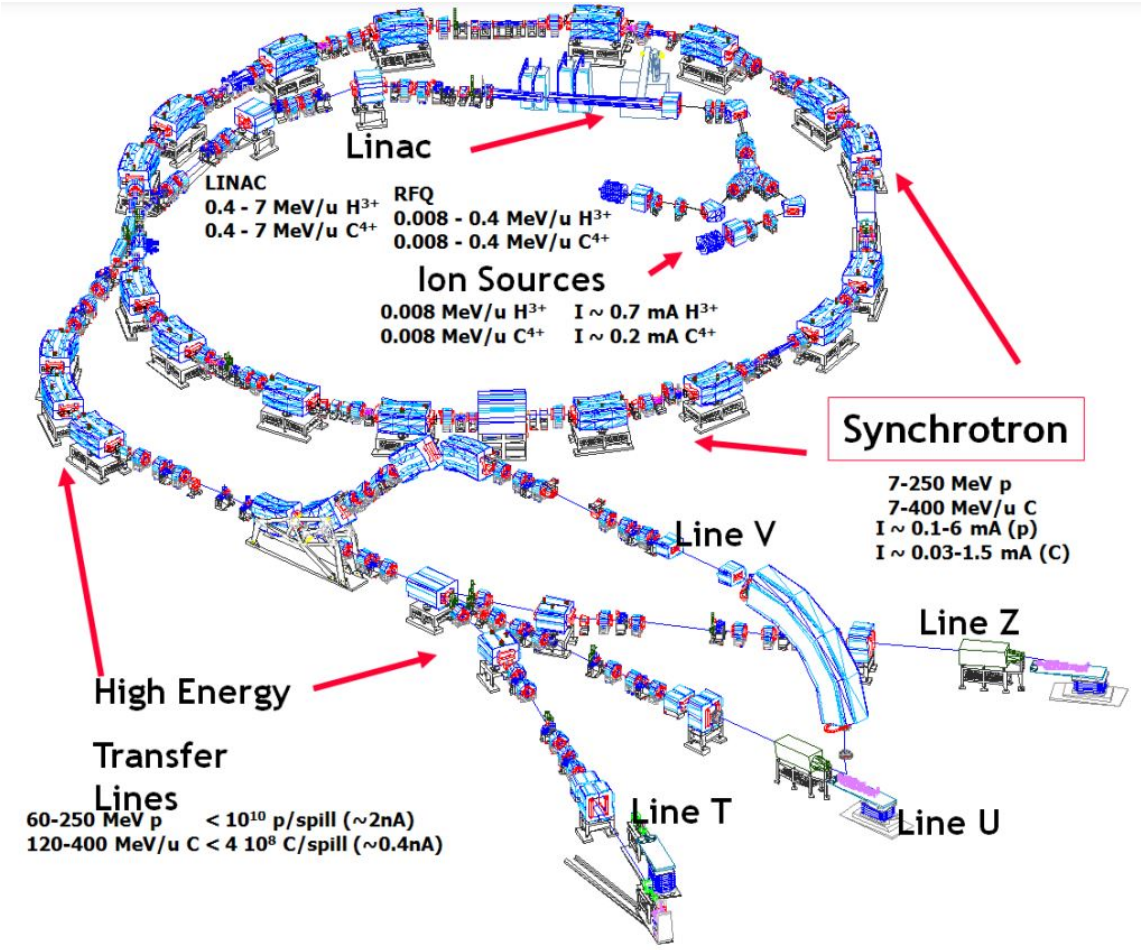

Figure 2.2: CNAO Synchrotron scheme [29]

The two sources, called Electron Cyclotron Resonance (ECR), are identical and, exploiting radiofrequences and magnetic fields, create an ionization. In normal working condition, they produce a type of particle each, by having H and CO_2 gases, to create the plasma. Now, particles are extracted through a positive voltage difference of $20\,kV$ and are ready to be accelerated according to the requested treatment. The acceleration process takes place through different stages of the synchrotron. First of all, the Low Energy Beam Transfer Lines (LEBT) is placed.

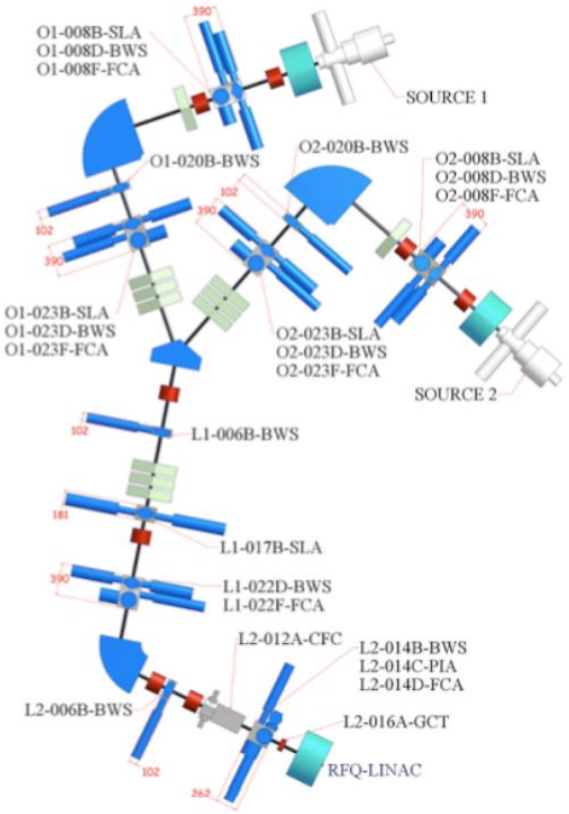

Figure 2.3: LEBT - detailed description [28]

In the Low Energy Beam Transfer Lines, the injection energy is $8\,keV/u$ and correspond to the kinetic energy of the particles. So the LEBT is starting from each source with a double line, O1 and O2, followed by a first line L1, including quadrupoles and spettrometers, and a second L2, that has a solenoid and a RFQ.

The Radio Frequency Quadrupole RFQ customizes the beam for entering the LINAC, impressing a longitudinal acceleration until $400\,keV/u$ and focusing it on the transversal direction.

The Linear Particle Accelerator is $3,8\,m$ long and gives a further acceleration from $400\,keV/u$ until $7\,MeV/u$, through a resonance frequency of $216.8\,MHz$ and a pulse repetition frequency of $10\,Hz$.

The following goal is to have a clean beam and is realized by the actions of some quadrupoles, that direct the beam on a stripping foil and assemble the particles in bunch of protons and carbon ions. At the same time the stripping foil removes the unwanted particles such as remaining electrons.

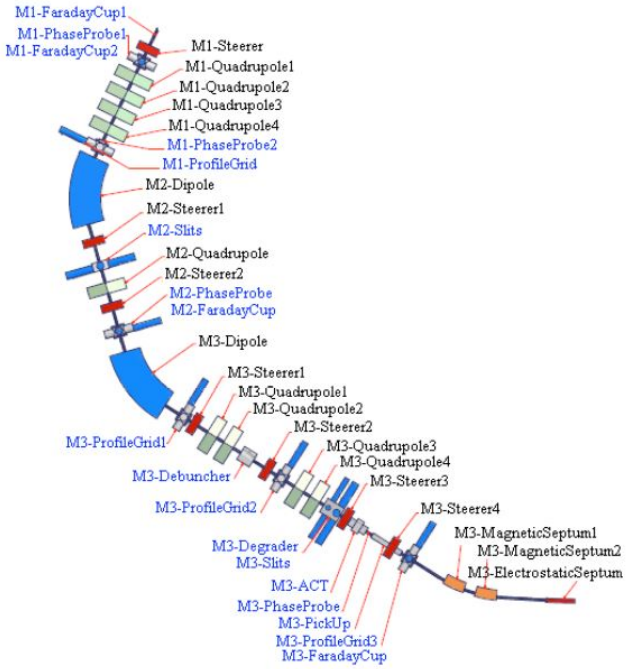

Figure 2.4: MEBT - description of each element [8]

It follows the MEBT line, Medium Energy Beam Transfer, that transmits the particles from the stripping foil to the point of injection. Along this line, divided in three segments M1, M2 and M3, lots of process take place in order to reduce leakages and to tailor even more the beam. For this purpose, Faraday cups FFC and wire scanners are placed, where the former measure the current and the latter check beam profile and evaluate the divergence.

Reaching MEBT part, the synchrotron ring is the protagonist: it is composed of 16 dipoles and 24 quadrupoles to focus and direct the beam, 5 sestupoles to correct the chromaticity and 20 correctors. Starting with an energy of 7 MeV/u, through the use of a RF cavity, the beam is accelerated until energies among 60 and 400 MeV/u. First of all, the RF cavity chases adiabatically the beam to accelerate it, but, at the same time, it synchronizes the frequency with the same value of the revolution frequency of the synchrotron beam.

At the end of the process, the RF cavity is still used for the extraction: this is the most crucial part because an uniform transversal distributed spill should come out for being used. Then, the last part of the extraction phase is constituted of a betratron-core, a particular induction accelerator, that exploits a particular resonance to break the stability of the beam.

To reach the treatment rooms, a High Energy Beam Transfer (HEBT) line is employed.

It is composed of 5 lines, one of these is the HEBT XPR, the experimental line at high energy, employed for research purpose. At centre of HEBT line, the HEBT chopper is placed: its role is to stop or to direct the beam to irradiate the patience. For doing this task, four fast dipoles are activate to guide the beam to the treatment rooms or turned off to stop it on the dump, which is an absorbing obstacle.

The dose delivery system is designed to irradiate the cancer in slabs: it means uniform parts, that are irradiated ideally with same energy distribution through a pencil beam. In this way, it is possible to give a different dose in the tumor and to reach compromising areas of the body without hitting healthy tissue.

One cycle, to develop a proper beam, takes 4 or 5 seconds: the extraction phase lats 1.5 seconds and the remaining time is used to adjust the characteristics such as energy and intensity. For each spill, the average number of protons for second is in range among 10^8 and 10^{10} and for carbon ions is $4 \cdot 10^6$ and $4 \cdot 10^8$.

In the following section, a brief sum up for describing how hadrontherapy works.

2.1.2. Hadrontherapy

Hadrontherapy is a variety of radiotherapy that employs neutrons, protons and positive ions. The name derives from the kind of particles involved: hadrons, particles composed of quarks, held together by strong interaction.

After the invention of the cyclotron by Lawrence and Livingston, neutrons were used as the first hadrons in radiotherapy. Unfortunately, due to the fact that dose distribution of neutrons is not so better than using photons, this kind of hadrontherapy was abandoned. On the other hand, charged hadrons are able to deliver a dose more precisely for a treatment purpose. The main advantage is described by the collision stopping power, dE/dx:

$$-\frac{dE}{dx} \propto \frac{\rho \cdot Z \cdot z^2}{A \cdot \beta^2} \tag{2.1}$$

with A and Z respectively mass and atomic number of the target, $\beta = v/c$ ion speed and z charge of the particle.

As it appears in the plot 2.5, the dE/dx is increasing with depth. This is a fundamental point, because it allows the beam to reach deep position with an high energy, releasing a very low superficial dose, but hitting powerfully the lesion with its maximum, called Bragg peak. Also for this reason, hadrontherapy is optimal for deep tumor, while the use

of X-rays would develop a consistent damage to healthy tissue.

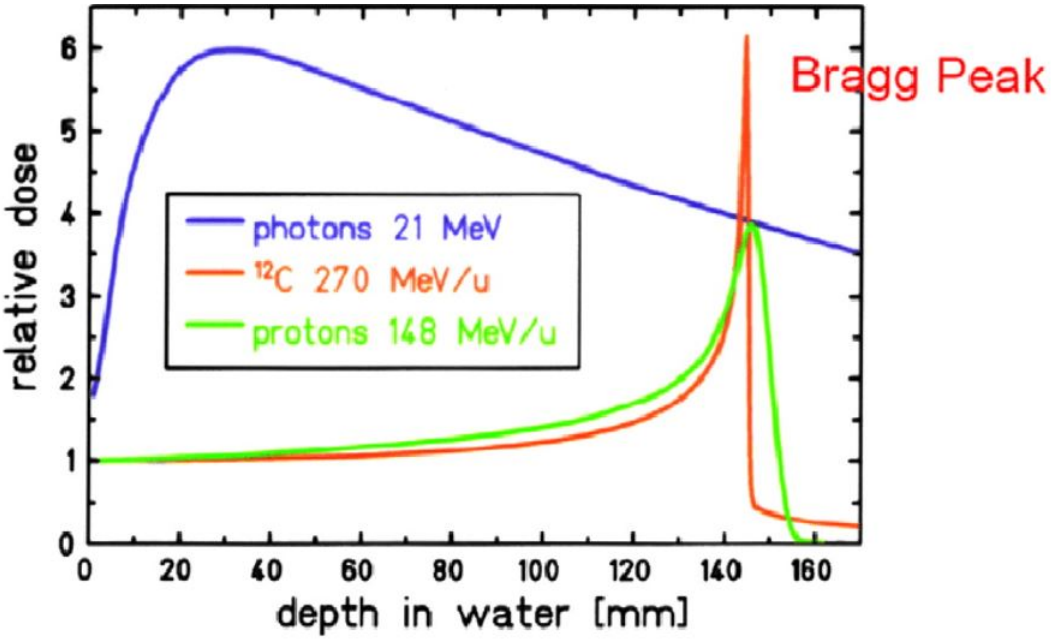

Figure 2.5: Bragg Peak [13]

Moreover, the Bragg peak can be moved in depth varying the energy of the beam. The maximum reachable point is described by the following formula:

$$R = \int_{E_0}^{0} \left(\frac{dE}{dx} \right)^{-1} dE \propto \beta^2 \tag{2.2}$$

where R is the range, that means the path that that type of particle can cover. As it can be seen, the range decreases with the increase of the collision stopping power per energy. The range highlights the fact that the majority part of dose of proton and carbon ions doses is released at almost $20\,cm$, evaluated from the point that the beam enters in the body.

An other advantage of hadrontherapy is the fact that conventional radiotherapy works better in an environment, such as a tissue that contains oxygen, for the creation of radicals, while, in the poorly oxygenated ones, the effectiveness decreases. On the other hand, hadrontherapy with carbon ions does not resent of the oxygen concentration, so it is optimal for hypoxic tumors. Considering the radiobiology, carbon ions are able to deliver an energy 24 times higher than protons, even though they have the same range.

The Radio Biological Effectiveness, RBE, is generally 3 times higher, because of the ability to create a more dense ionizing path in proximity to the Bragg peak. The sum of Bragg

peaks is applied to bigger lesions or radioresistant one, creating the SOBP, Spread-out Bragg Peak, as appears in the picture. Unfortunately, the released dose increases to the proximal part of heathy tissues but it remains the only option to treat this kind of tumors or not operable one.

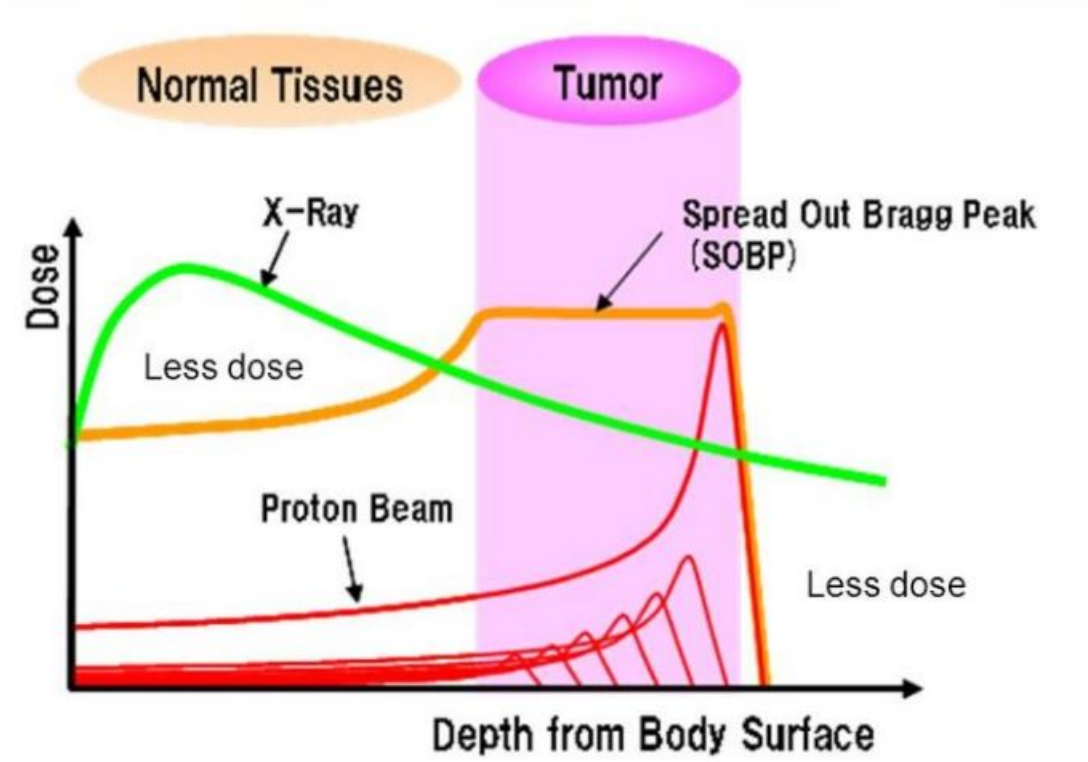

Figure 2.6: Spread Out Bragg Peak [5]

2.2. Future Expansion at CNAO

CNAO Foundation has planned an expansion concerning: an enlargement for hadron-therapy, exploiting new ions; a new building for protontherapy and a facility for the construction of BNCT, Boron Neutron Capture Therapy.

Referring to the hadrontherapy, with the purpose of both treating patients and scientific research, the new ions are:

Table 2.1: Data for the employment of new ions

Particles	Energy [MeV/u]	[particles/seconds]
^{4}He	320	5 E+08
^{7}Li	306	4.5 E+08
^{16}O	400	7.3 E+07
^{56}Fe	306	3.6 E+07

Moreover, these values are the maximum allowed energies according to the structure of the synchrotron and the facility. For a conservative problem, the maximum numbers, here represented, are also the ones used in the simulation.

In the following two sections, BNCT and protontherapy are discussed.

2.3. BNCT

Boron Neutron Capture Therapy is a hadrontherapy treatment, which involves the absorption of ^{10}B in tumoral cells: a selective process developed through the use of tailored molecules and followed by the irradiation with a neutron flux, that reaches the lesion at thermal energies. The involved reaction $^{10}B(n,\alpha)^{7}Li$ allows a consistent delivered dose through the high LET reaction products [1].

^{10}B is an isotope of boron present in nature with a concentration of 20%.

Analyzing in detail the reaction data, it is important to highlight the cross section equals to 3800 b, where 1 barn is $10^{-24}\,cm^2$, measured at reference thermal energy ($0.025\,eV$) with Q-value is $2.9\,MeV$.

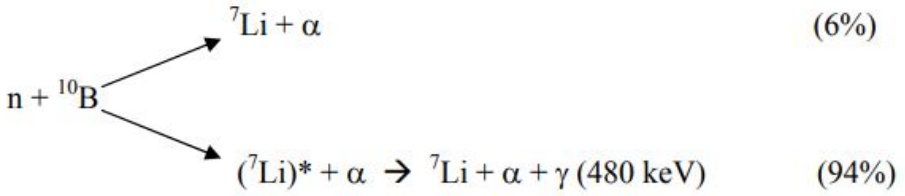

Figure 2.7: Reaction Scheme [3]

As described in the scheme, the branching ratio of the reaction is divided into: 6% production of ^{7}Li at ground state; 94% $(^{7}Li)^{*}$ that deexcites through the emission of a

gamma ray of $480\,keV$, with initial kinetic energy and range in tissue of $0.84\,MeV$ and $4\,\mu m$ for ^7Li and $1.47\,MeV$ and $8\,\mu m$ for α respectively.

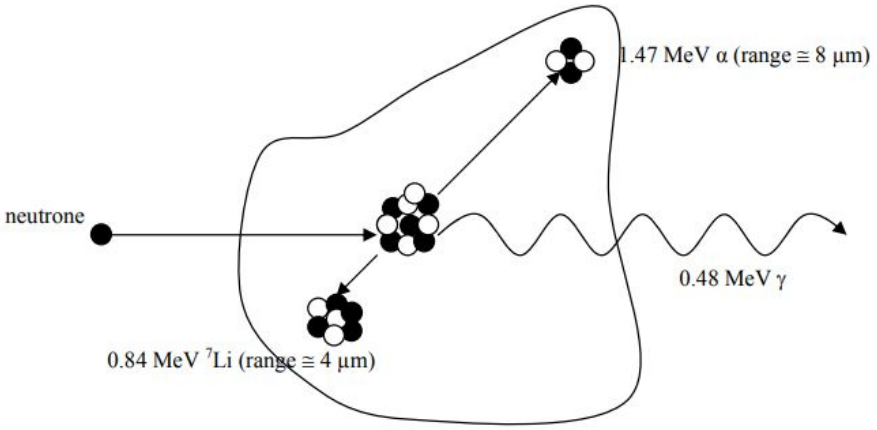

Figure 2.8: Charateristc values in Boron Neutron Capture Reaction [3]

Considering the dimension of a human cell of 10 µm, the kinetic energy, produced in the reaction, is deposited inside the cell, that is loaded with boron. For this reason, BNCT has incredibly convenience for the selectivity: through the boron carrier the reaction will occur in proximity to the cancer, saving the healthy tissue.The dose delivery is describe by the LET, Linear Energy Transfer, and RBE, Relative Biological Effectiveness. These two quantities are analyzed in the following chapter. For the Boron Neutron Capture Theraphy, the dose is released in $12\,\mu m$, due to high RBE and LET.

Therefore, the reaction products are able to reach the goal of creating an irreparable DNA damage. In this way the tumoral cellular replication is blocked.

The first project of Boron Neutron Capture Theraphy dates back to 1936, when G. Locher proposed BNCT, after the discovery of the neutron by Chadwick in 1932 and the studies of the reaction $^{10}B(n,\alpha)^7Li$ by Taylor and Goldhaber in 1935. Subsequentially, in 1951, at Brookhaven (USA) the first experiments of this reaction were applied on patients suffering of brain tumors, specifically glioblastoma multiforme. Unfortunately, they found out that the boron concentration was higher in the blood than in the tumor and the employment of thermal neutron field showed a low penetrability, so the therapy was not effective. For this reason, after ten years it was abandoned.

During the 1970s, the development of new pharmaceuticals, able to overcome the Blood

Brain Barrier, and the employment of epithermal neutron flux, made reconsider the BNCT in Japan. Particularly, epithermal neutrons, $0.5\,eV - 10\,keV$, are advantageous, because they can deliver a high dose reaching the lesion at thermal energies, thanks to scattering reactions that occurs at more superficial depth. The research of boron carries represents a major issue: the difficulty is to keep a low concentration in the healthy tissues, but at the same time an important one in the lesion. The common boron concentration ratio in BNCT is 4:1 and in the tumor ^{10}B concentration is higher than $20\,\mu$g of boron over a gram of tumor.

The last matter, that has to be considered, is the fast expulsion of the pharmaceutical from blood in the meanwhile of the treatment. Up to now, no compounds are produced that satisfied all these requirements.

During the first trials with Boron Neutron Capture Therapy, the employed boron carrier was the boric acid. This molecule showed a low selectivity and a low concentration ratio between cellular cancer and blood. Then, in the sixties two pharmaceutical were employed: the BSH, sodium mercaptoundecahydro-closo-dodecaborate, and BPA, (L)-4-dihydroxy-borylphenylalanine. These compounds revealed the advantage to keep a higher concentration ratio, not only in comparison between tumor and blood, but also between tumor and brain, for not aggravating the situation with additional toxicity. For injecting BSH and BPA in veins, they are associate to fructose to facilitate the transmission, but they show some disadvantage like not being optimal compounds for intravenous delivery.

Nowadays, investigations in pharmaco-kinetics are still being conducted: to improve the performance, to optimize the ratio of concentration in tumor respect to blood and to reach the lesion overcoming all the anatomical characteristics.

Talking about the irradiation field, BNCT works with epithermal flux, with value $\phi_{epi} = 1 \cdot 10^9 cm^{-2}\,s^{-1}$, for reaching the tumor site at thermal energies. This number is coming from the recommend values from IAEA TECDOC-1223 [31] for neutron field characteristic. Therefore, in tissue epithermal neutrons have an important penetration capability. To obtain the described flux, different solutions are in operation: moderating the fission flux by cutting down the fast neutrons and the gamma component in the spectrum or employing an accelerator to have directly the proper flux. Analyzing the moderation, even though light water has an higher deceleration capability, heavy water is employed, due to the fact that light water produces prompt gamma rays in neutron capture reactions. Otherwise, the characteristics of moderation and reflector are obtained by high purity graphite, with a density of $1.7 - 1.8\,g/cm^3$, like in a lot of nuclear reactors. In BNCT,

graphite is set in the irradiation columns.

Moreover, for customizing the spectrum, other elements are involved: aluminum, that, among the interval $5\,keV - 1\,MeV$, reveals resonances from scattering, but thanks to the complementarity of the resonances of oxygen or fluorine, they are managed. Therefore, a compound made of them is the best option to shift the spectrum. Usually, BNCT facilities employ a structure of moderation composed of alumina (Al_2O_3), aluminum trifluoride (AlF_3) and some aluminum slabs submerged in heavy water. An other part of the beam, that is tailored, is the thermal part through the use of cadmium, ^6Li or ^{10}B: materials that shows the ability to absorb neutrons at this energy, for not releasing a dose at shallower depth than the tumor. It is important to analyze the possibility to have the (n, γ) reactions, such as in the presence of cadmium, for remembering to insert bismuth or lead to stop the gamma rays.

The accelerator based BNCT will be the CNAO's solution and is discussed in the next section.

2.3.1. BNCT at CNAO

Particle accelerators assume a relevant importance for medical centers, that have not an easy access to neutron research reactor. Accelerators such as LINAC, cyclotrons and electrostatic accelerators can supply the neutron spectrum, that is needed for the therapy. Thanks to new developments, accelerator have compact dimension and can be placed inside the facility. An accelerator based BNCT structure consists of an accelerator, a target and a moderator. In the previous paragraph, it has been already discussed about the moderator. On the other hand, considering the flux and how is obtainable, proton accelerators are preferred than electron accelerators, because the latter releases a component of X rays with high energy, that add a dose. This represents a problem not only for the patience and the effectiveness of the treatment, but also for radio-protection reasons. The goal is to produce neutrons from proton capture reactions on charged particles:

$$^9Be + p \rightarrow {}^9B + n - 1.85\,MeV \quad (1)$$
$$^7Li + p \rightarrow {}^7Be + n - 1.65\,MeV \quad (2)$$
$$^9Be + d \rightarrow {}^{10}B + n + 4.36\,MeV \quad (3)$$

The last one (3) exploits the capture of deuterium on beryllium and it is favored by the exothermic properties, so it shows an absence of threshold and better thermomechanical characteristics than lithium: higher melting point $1287\,K$and higher thermal conductivity $190\,W\,m^{-1}\,K^{-1}$, compered to lithium $180.5\,K$ melting point and $85\,W\,m^{-1}\,K^{-1}$ conduc-

tivity. The disadvantage is that due to the high Q-value the produced neutrons possesses an elevated energy that should be moderated by a more complex solution. So, for this reason, they generate more activation in the surrounded materials. Contrarily, considering the first two reactions, they are characterized by a negative Q-value an important threshold energy of about $2\,MeV$. Particularly, the lithium proton capture reaction (2) generates neutrons that have energies almost in the epithermal region. For this characteristic, it is easier to place this kind of target in a medical center. An other point in favor is the high cross section, on the other hand the activation of ^{7}Be, as a reaction product, has to keep in consideration for decommission and contamination. The capture reaction on beryllium (1) shows similar properties to the lithium one, but reveals a lower neutron yield. After having described the possible solution, CNAO and TAE Life System (TLS) researched and studied the possibility to install an accelerator based BNCT. TAE Life Science (TLS) is an American company specialized in BNCT, including not only the accelerator based system but also the researching development on boron pharmaceutical.

Figure 2.9: Electrostatic tandem accelerator [30]

The proposed accelerator for CNAO is a compact electrostatic tandem accelerator: the negative ions are generated from protons with a stripping foil and then accelerated at $2.5\,MeV$ by a current of $10\,mA$. For this structure, the optimal solution of target is the ^{7}Li with its proton capture reaction. Here, it follows its cross section, where b stands for $barn$, the most used unit of measurement of cross section $1b = 10^{-24}\,cm^2$.

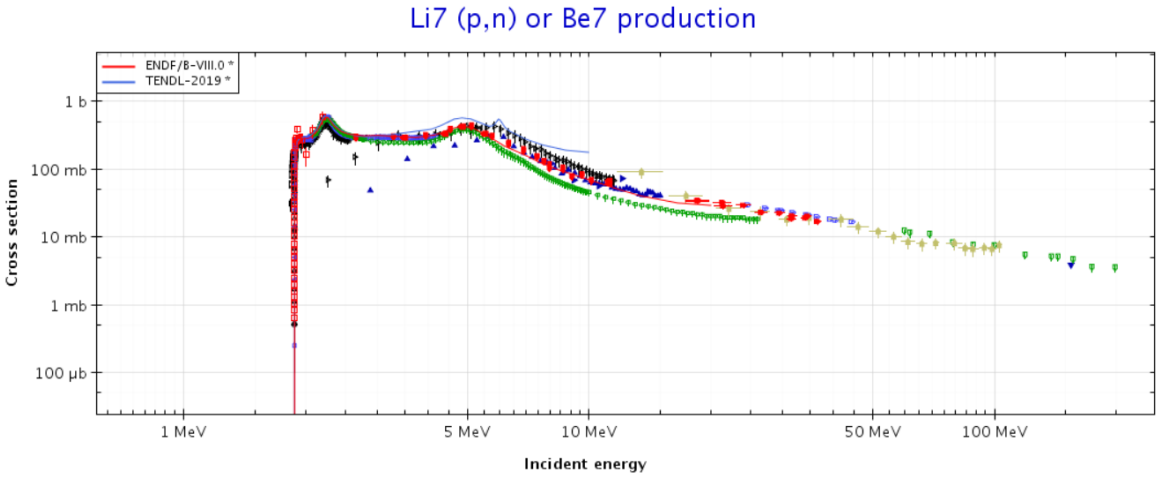

Figure 2.10: Cross section of $^{7}Li(p,n)^{7}Be$ [23]

Furthermore, the company provides an help in the construction, radioprotection analysis and a state-of-art for the research in the boron carrier providing a complete therapy. The only missing element was the moderator, that could be eligible for a correct neutron spectrum. So, TLS made a collaboration with Neuboron Therapy System (NTS) for analyzing the slowing down materials. Neuboron Therapy System is a Chinese company that investigates and produces in accelerator based BNCT. NTS proposed the Beam Shaping Assemblies (BSA) to obtain the desired epithermal flux, also with the possibility to change intensity, energy and irradiation relative to the tumor shape and characteristic. A typical BSA is composed of 2 cones made of magnesium fluoride and other elements, but no other features are public available. The radioprotection office in CNAO analyzed the shield and the activation in all the structure to provide all the technical features to build a safe environment for patience, workers and inhabitants.

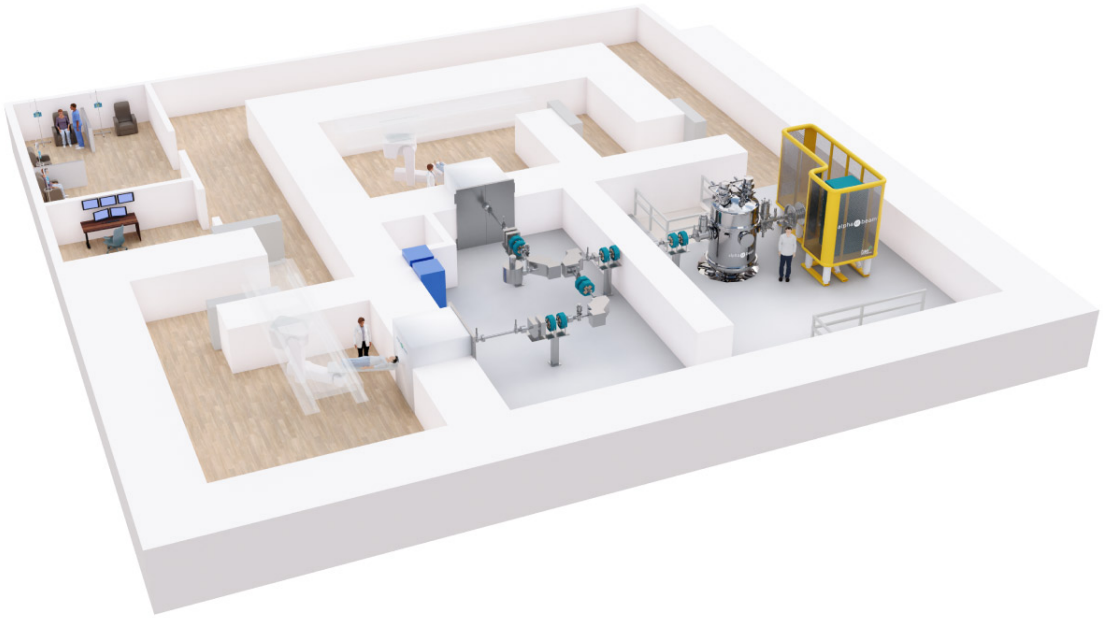

Figure 2.11: Facility proposed for BNCT at CNAO [30]

2.4. Protontherapy

CNAO and Hitachi signed a collaboration for building a new structure, dedicated only to protontherapy. In this way, CNAO will be the only center that possesses a synchrotron, reserved to accelerate ions, and another synchrotron similar to the existent one, but only for proton. This expansion is convenient not only to be able to treat more patients, but also in case of problems or damages to assure a continuity for therapies or research. Hitachi provides a state-of-art machine, able to deliver the Proton Beam Therapy modulating the intensity of the particles with a technique called IMPT, Intensity Modulated Proton Therapy. In this way, the facility provide a treatment with the last technology that releases the minimum dose as possible to the healthy tissues.

Furthermore, this facility is composed of a synchrotron with a gantry: this element introduces upgrades for having more degrees of freedom, because with this modality the patient is fixed and the beam can rotate around him.

The new building will include dedicated areas for patients and workers for a total of $6000\,m^2$. The machine will be composed of: a LINAC; an electrostatic septum ESD between two of the four magnets, that compose the accelerator ring; a magnetic septum

to guide the beam to the HEBT; a delivery line to the gantry (GABT) and an IC isocenter.

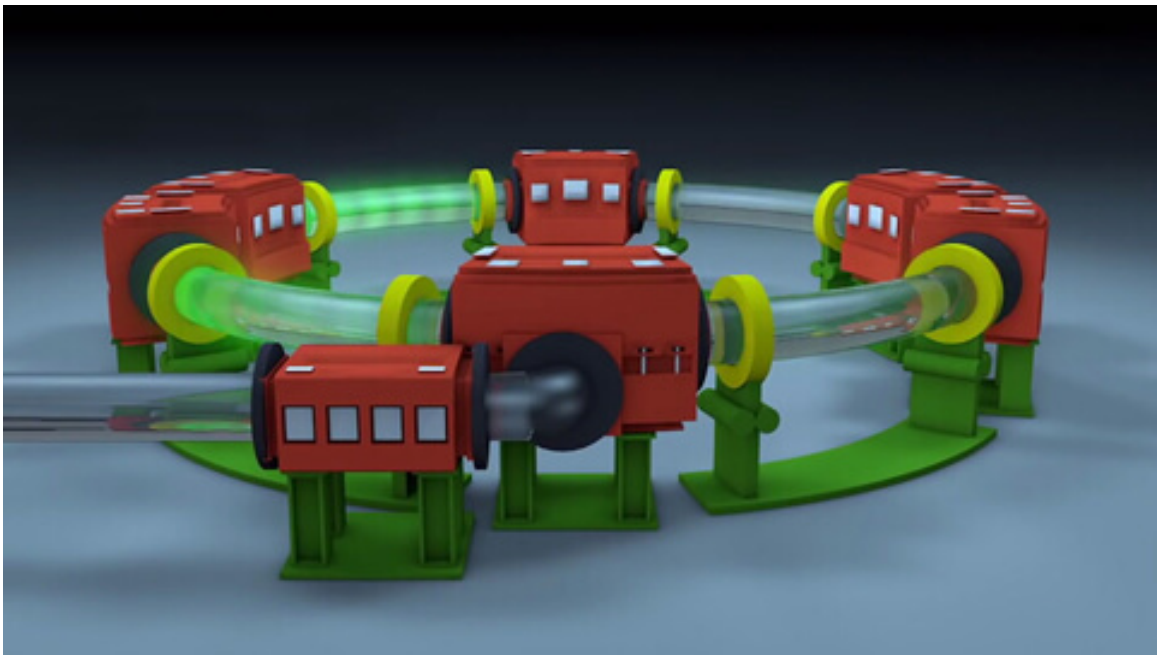

Figure 2.12: Protontherapy: Synchrotron [32]

3 | Water Activation

3.1. Activation Processes

First of all, the production of the investigated radionuclides is coming from particles interactions and they can be divided in two categories:

- scattering processes, where the hitting particle will be the reaction product. This category can be split into two subgroups: the elastic scattering characterized by the fact that particles change only energy and momentum and the inelastic scattering, where a transition to an excited state is possible for both the target and the bullet, and furthermore the production of other particles is foreseen.
- nuclear reactions: processes for which the reaction products do not keep the feature of the parents' nuclides and thanks to reassessment, different particles are generated.

For reaching the goal of this project, the main interest is on nuclear reactions: they happen when important laws of conservation of mass, energy, angular momentum, baryon number and electric charge are respected.

The interaction that are happening at high energies, around $100\,MeV/u$, can be seen as in one step, thanks to their forward angular distribution. During this event, an important quantity of energy can be transferred inside the nucleus and can lead to the intranuclear cascade: a phenomenon characterized by the movement and the interaction of nucleons that can be released by the nucleus in a short time interval, close to $10^{-22}\,s$, or can follow other processes in longer time interval of $10^{-16}\,s$. Delayed emissions can happen in the form of spallation, where new nuclei are formed, or in the form of fragmentation with the break of the parent nucleus in lighter parts and ions.

Instead, at lower energies as $1\,MeV/u$ the interaction time is slower, this leads to a greater number of collisions with the thermalization of the system, that is composed of the bullet and the target particle with an equal energy and momentum distribution among them, and so to the formation of a compound nucleus. The compound nucleus has a life time long enough to forget its previous identity, the only factor to be preserved is the

total excitation energy and decay in a different final state with the isotropic emission of nucleons and photons. The emission probability is higher for neutrons than protons for the Coulomb barrier and the final disexcitation among energetic levels is characterized by the γ emission.

For energies among 1 and 100 MeV/u pre-equilibrium or multi step reactions take place: the energy has reached this range of values through scattering and nuclei interactions and the nucleons are emitted with a similar energy to the bullet particle.

Moreover, if the produced particles has a quite high energy, they can lead to an hadronic cascade with the productions and interactions of other particles. This phenomenon arrests when the energy is not enough to allow nucleon interactions, but only with nuclear electrons or diffusion processes. The end of an hadronic cascade of neutrons is the neutron capture (n,γ). A similar phenomenon is the electromagnetic cascade: an high energetic electron or a photon creates a productive process of electrons and γ quanta thanks to bremsstralhung and pair creation. The hadronic and electromagnetic cascade coexist generally, but the first one is typical of a proton accelerator and the second one of an electrons accelerator.

Considering in detail neutrons, at lower energies can interact through elastic scattering and radioactive capture, where the creation of a compound nucleus is followed by its disexcitation with the γ emission. It is remarkable the characteristic trend at lower energies 3.1, then in the plot at intermediate energies some resonances are presents, meaning that the probability to be absorbed is higher; while increasing the energies other reactions have higher probabilities to happen such as (n, n') inelastic scattering, (n, p),$(n, 2n)$ and (n, α), followed by multi step reactions and hadronic cascade as explained before.

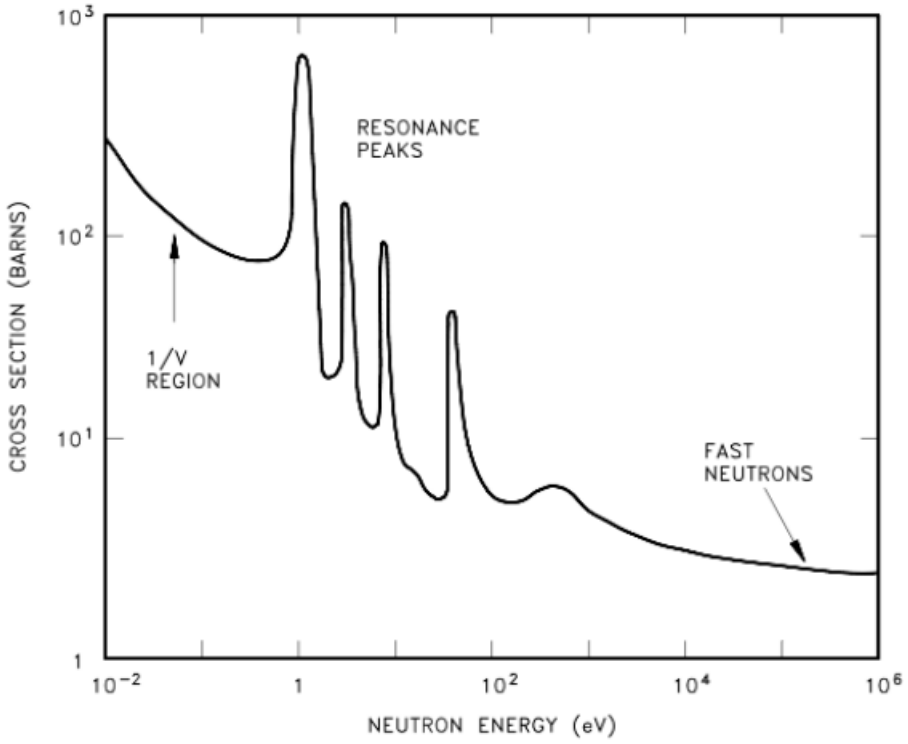

Figure 3.1: Cross section of neutrons radioactive capture varying according to the considered energy [15]

Furthermore, to reach the production of that investigated particle, other elements need to be analyzed: the presence of the parent nuclide that can generate the reaction products with its isotopic abundance and the reaction cross section. These elements are enclosed in the reaction rate formula, to evaluate how many particles are particles:

$$R.R. = \phi_{th}\sigma_i \frac{N_a}{A_i} m_i \quad [particles/s] \tag{3.1}$$

with

- ϕ_{th} thermal neutron fluence rate
- σ_i cross section of the considered i parent nuclide
- N_a Avogadro number
- A_i atomic weight of the i parent nuclide
- m_i mass of the i parent nuclide

3.2. Prompt and delayed fields at CNAO

The radiation fields present at CNAO are mainly two types:

- the prompt radiation, that is formed when an accelerator is on;
- the delayed or activation radiation, that lasts in time, even though the accelerator is off, according to the activated particles.

The prompt radiation is a mixed field composed of mainly secondary neutrons and photons with a little percentage of charged particles. This field is generated by the impinging of the primary beam on components of the machine in the so called loss-points.

On the other hand, the delayed field is generated by nuclear reactions on the structural elements of the machine, such as magnets, void chamber and water pipes, and of the room, like air and concrete shielding.

In this project, water activation is discussed and analyzed for the present synchrotron at CNAO, for the future protontheraphy and BNCT facilities.

As regards the sinchrotron's activation, the beam is accelerated in the void chamber, so it does not hit directly the water area. To perform a realistic scenario of activation, some strategic tasks are employed: first of all, for having the maximum number of secondary neutrons, the losses from the primary beam are stopped and minimized. In this way, the maximum production of radioactive particles is expected and assured for the radio-protection calculus. For this reason, the study is developed to face a case where the major number of secondaries are present.

3.3. Water activation at CNAO

Water activation is an important matter in radioprotection at CNAO: first of all, it is fundamental to know which radionuclides are formed, their quantities and in which point of the structure they are produced. This process is composed of a priori part, which consists of studying the physical process that takes to the generation of that particle and comparing them with the results of the program.

Knowing these data, workers can operate safely in case of leaks and perform a better maintenance of the pipeline. Moreover, this evaluation can assure a safe structure and environment.

In the actual synchrotron, ordinary maintenance takes places normally four times a year and lasts a couple of days: the beam is stopped, the radioprotection group measures the

radioactivity levels of the accelerator, in order to provide safety of the structure to all the workers and researchers, who can enter and proceed with their tasks.

In addition, it can be useful for a future decommission to know which parts and components are activated in that investigated period, for being handled with all the required precautions and transported to the waste facility.

On the other hand, talking about which parent nuclides are involved and how much quantities, it depends from the water characteristics. Generally, two kind of water circuits are present: the first one is characterized by demineralized water and it is located in the water synchrotron circuit of the actual accelerator, in the cooling system of the synchrotron of the protontheraphy and of the BNCT target; the second type is composed of softened water and it represents the cooling system of the utilities, which is present in the three facilities.

For studying a conservative scenario, water with more impurities is investigated and simulated. In this way, the obtained result is the worst conditions that can be supposed for the water activation of that facility. This hypothesis is chosen to perform a complete radioprotection analysis, that remains solid in case of the presence of impurities. To simulate realistic data, the analysis of similar scenarios are employed:

- the demineralized water is simulated with the composition of the analysis of DAFNE accelerator from INFN, National Laboratory of Frascati:

Table 3.1: Water analysis of DAFNE from INFN

Element	$[\mu g/l]$
Cu	2-5
Fe	< 5
Cr	< 0.2
Ni	< 0.2
Mo	< 0.2

- the softened water is simulated with the potable water from the water supply of Pavia:

Table 3.2: Analysis of water supply of Pavia

Element	$[mg/l]$
Fluorides	1.30E-01
Chlorides	3.00E+00
Nitrites	5.00E-02
Bromides	5.00E-02
Nitrates	1.00E+00
Phosphates	2.00E-01
Sulphates	4.00E+00
Ammonia	1.00E-01
Calcium	4.20E+01
Magnesium	8.40E+00
Potassium	1.40E+00
Sodium	1.10E+01
Cadmium	5.00E-04
Chromium	5.00E-04
Copper	5.00E-03
Iron	1.70E-03
Manganese	5.00E-03
Nickel	1.00E-03
Lead	5.00E-04
Antimony	5.00E-04
Uranium	1.00E-03
Vanadium	1.00E-03
Zinc	5.00E-03

Here, as a comparison, the composition of the CNAO demineralized water is listed:

Parameter	result	unit of measurement
colony count at 36 °C	<1	UFC/ml
colony count at 22 °C	<1	UFC/ml
coliform bacteria at 37 °C	0	UFC/100ml
escherichia coli	0	UFC/100ml
enterocci	0	UFC/100ml

Table 3.3: CNAO demineralized water analysis

Thanks to these tables, it is possible to know which are the parent nuclides that can react to give other particles. Anyway, it is important to keep in consideration the isotopic abundance of the father radionuclide to foresee if the reaction products are possible to happen.

In addition, in FLUKA particles are investigated with a detector after $1\,s$ to see the immediate particles production and after $900\,s$, to highlight the decays of short lived radionuclides and the constant activity of the long ones.

The expected produced radionuclides can be differentiated for their half lives, if it is higher then a couples of hours in long lived radionuclides and otherwise in short lived radionuclides [18].

3.3.1. Long lived radionuclides

Some radionuclides posses a longer life time, so they have a particular relevance for calculus of dose, for ordinary maintenance and decommissioning.

Some of the main protagonists of this analysis are:

- ^{3}H production derives from the reaction of a neutron and ^{2}H, as a natural isotope of hydrogen with an abundance of $0.015\,\%$. The half life is 12.32 years and is characterized by $\beta-$ decay in ^{3}He with maximum energy $18.6\,keV$. It follows the cross section of the reaction 3.2.

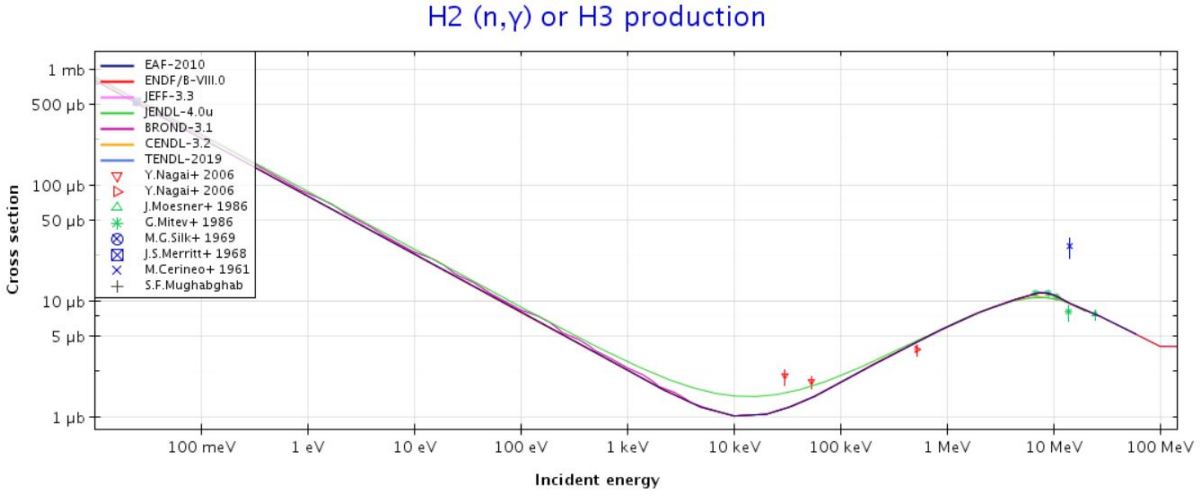

Figure 3.2: Deuterium cross section for ^{3}H generation

- ^{7}Be has an half life of 55.22 days and is followed by the electronic capture with the production of ^{7}Li . ^{7}Be is produced from the following reactions: $^{16}O\,(p, d{+}2\alpha)\,^{7}Be$,

where d stands for deuterium, and $^{16}O\,(n, 2n + 2\alpha)\,^{7}Be$.

Here, it is placed the cross section of the two reactions:

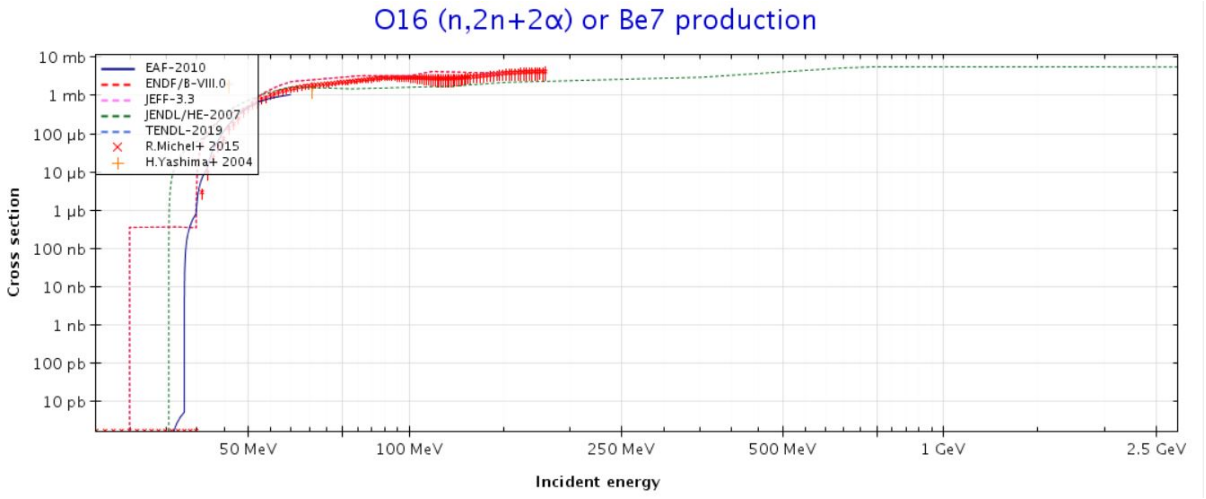

Figure 3.3: Cross section plot of $^{16}O\ (n, 2n + 2\alpha)\ ^{7}Be$

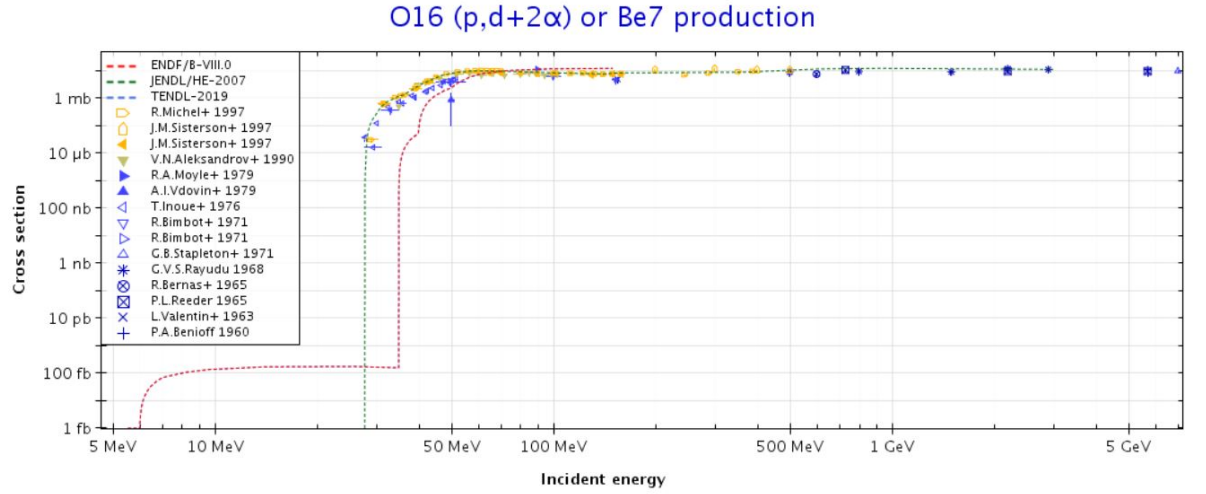

Figure 3.4: Cross section plot of $^{16}O\ (p, d + 2\alpha)\ ^{7}Be$

- ^{14}C possesses an half life 5730 years characterized by $\beta-$ decay in ^{14}N with an energy value of $156.476\,keV$. The reactions and their cross sections, that explains its generation, are the following:
  - $^{14}N(n, p)^{14}C$

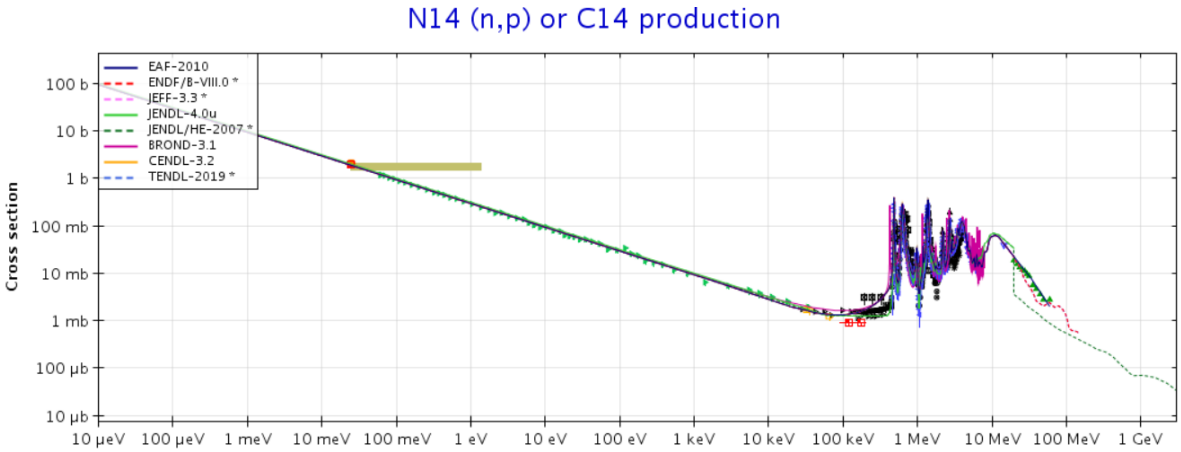

Figure 3.5: Cross section of $^{14}N(n,p)^{14}C$

– $^{16}O\,(n,p+d)\,^{14}C$, where d stands for ^{2}H

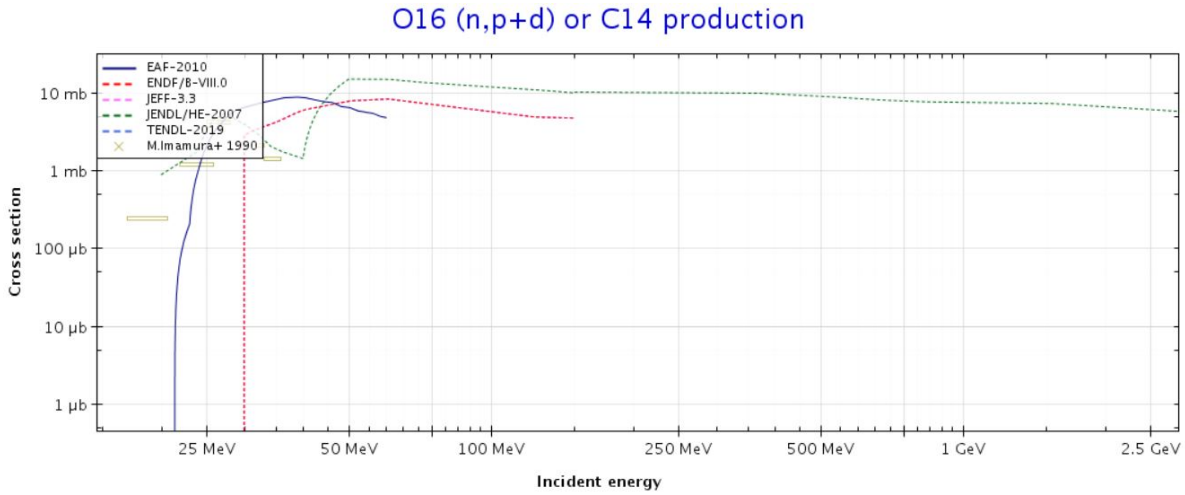

Figure 3.6: Cross section of ^{16}O(n,p+d)^{14}C

– $^{16}O\,(n,n+2p)\,^{14}C$

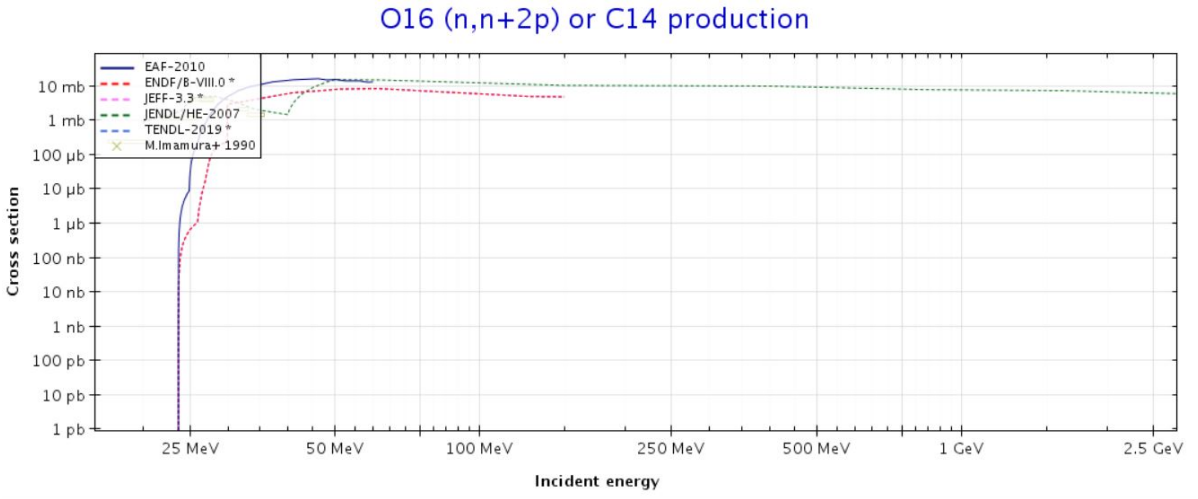

Figure 3.7: Cross section of ^{16}O (n,n+2p) ^{14}C

– $^{16}_{8}O\,(n,\,^{3}He)\,^{14}C$

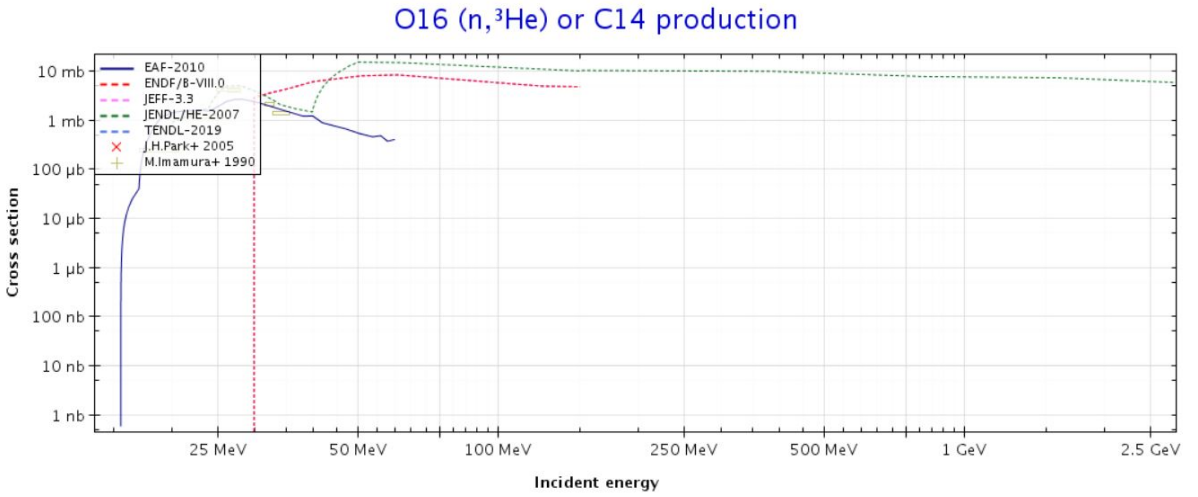

Figure 3.8: Cross section of ^{16}O $(n,\,^{3}He)$ ^{14}C

– $^{17}O\,(n,\,\alpha)\,^{14}C$

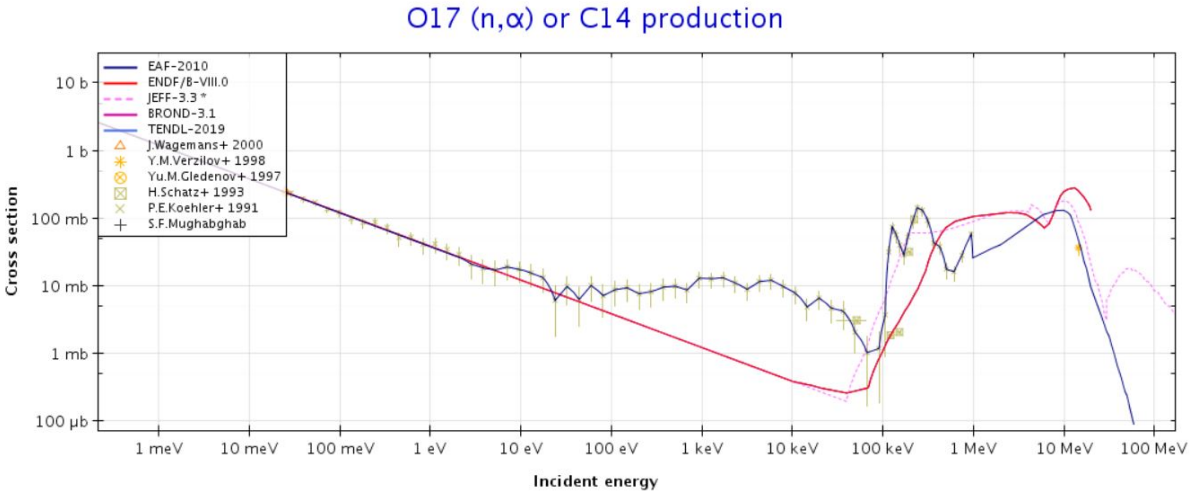

Figure 3.9: Cross section of $^{17}O\ (n,\,\alpha)\ ^{14}C$

The last reaction has a particular relevance for BNCT, while the others principally for synchrotron.

- ^{36}Cl has an half life of 301000 years and characterized by $\beta-$ decay. It is formed with the reaction $^{35}Cl\,(n,\,\gamma)\,^{36}Cl$, where ^{35}Cl has an natural abundance of 75.77%, and is present in water when is used the 3.2 analysis. The reaction cross section is the following:

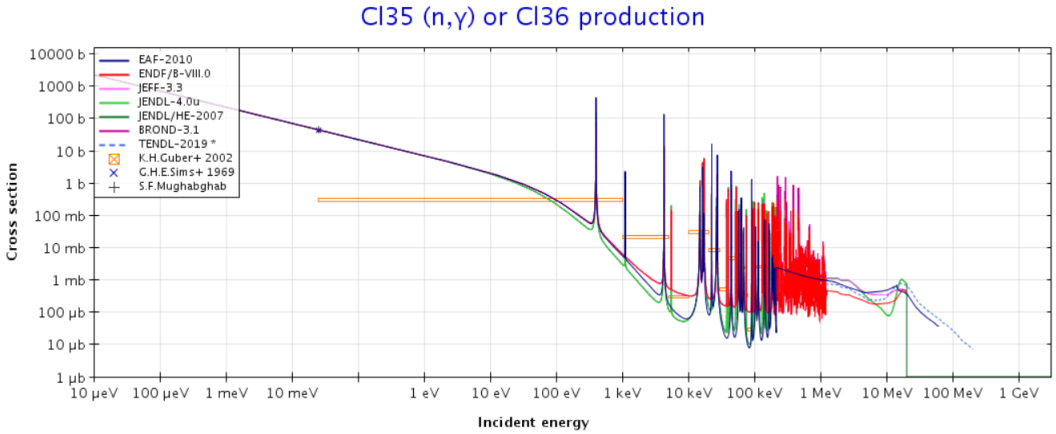

Figure 3.10: Cross section of $^{35}Cl\ (n,\,\gamma)\ ^{36}Cl$

- ^{41}Ca has a long half life, which is equal to $9.94 \cdot 10^4$ years, and characterized by electronic capture. It is produced by the reaction $^{40}Ca\,(n,\,\gamma)\,^{41}Ca$. ^{40}Ca has a

natural abundance of 97% and is present when the 3.2 analysis is employed. The reaction cross section is the following:

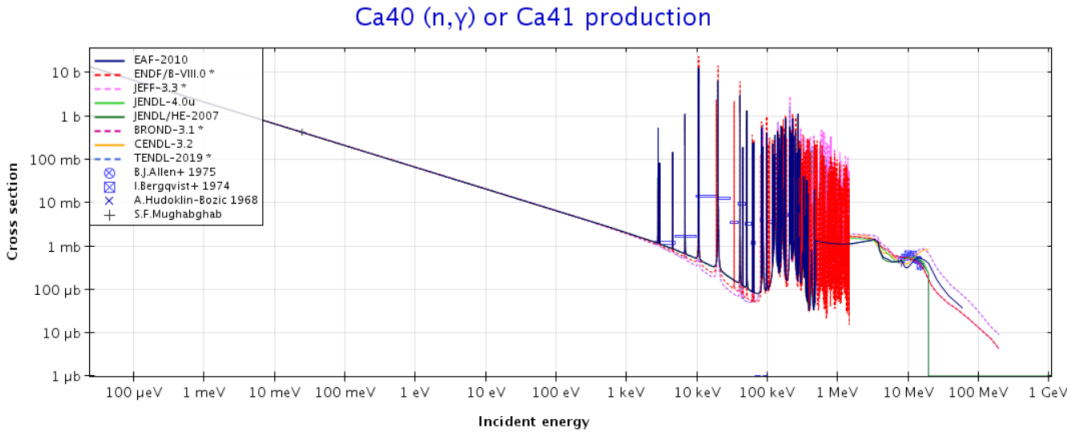

Figure 3.11: Cross section of $^{40}Ca\ (n,\ \gamma)\ ^{41}Ca$

In addition, an other particle has to be kept in consideration: ^{10}Be with half life equals to $1.39 \cdot 10^6$ years and characterized by β- decay with the production of ^{10}B. However, just traces of ^{10}Be are formed and the total activity is not comparable to others. The production is mostly due to spallation reaction on oxygen.

3.3.2. Short lived radionuclides

Short lived particles are produced and detect 1 s after the stopping of the irradiation. They have a minor importance as regards the water activation, because considering a realistic path of the water passing through the pipes in the synchrotron room they decays before. Even though this fact, it is important to know how much quantity is produced to keep them monitored.

Furthermore considering an emergency situation, is important to know their presence and activity for operating in safety and awareness.

A list of the most frequent and how they react here it is presented.

Radion	Half life	Decay	Produced particle
$^{24}_{11}Na$	14.957 h	$\beta-$	$^{24}_{12}Mg$
$^{16}_{7}N$	7.13 s	$\beta-$	$^{16}_{8}O$
$^{15}_{6}C$	2.45 s	$\beta+$	$^{15}_{5}B$
$^{15}_{8}O$	122.24 s	$\beta+$	$^{15}_{7}N$
$^{14}_{8}O$	70.62 s	$\beta+$	$^{14}_{7}N$
$^{17}_{7}N$	4.17 s	$\beta-$	$^{17}_{8}O$
$^{13}_{7}N$	9.96 min	$\beta+$	$^{13}_{6}C$
$^{11}_{6}C$	20.00 min	$\beta+$	$^{11}_{5}B$
$^{10}_{6}C$	19.30 s	$\beta+$	$^{10}_{5}B$

Table 3.4: List of the main short lived particles

These radionuclides are mainly produced by the reaction of a neutron or a proton that interacts with ^{16}O, ^{17}O and ^{18}O, which have a natural abundance of 99.762%, 0.038% and 0.2% respectively.

Moreover, ^{24}Na, ^{15}O, ^{13}N, ^{11}C and ^{7}Be possess a slightly longer life and are formed in bigger quantity. For these reasons, it is important to examine how they can be formed.

In addition, ^{15}O, ^{13}N and ^{11}C have a fundamental role in air activation in the synchrotron room.

^{24}Na is formed through a neutron absorption described with this reaction $^{23}Na\,(n,\,\gamma)\,^{24}Na$, considering the fact that ^{23}Na is present when the 3.2 analysis is employed. The reaction cross section is the following:

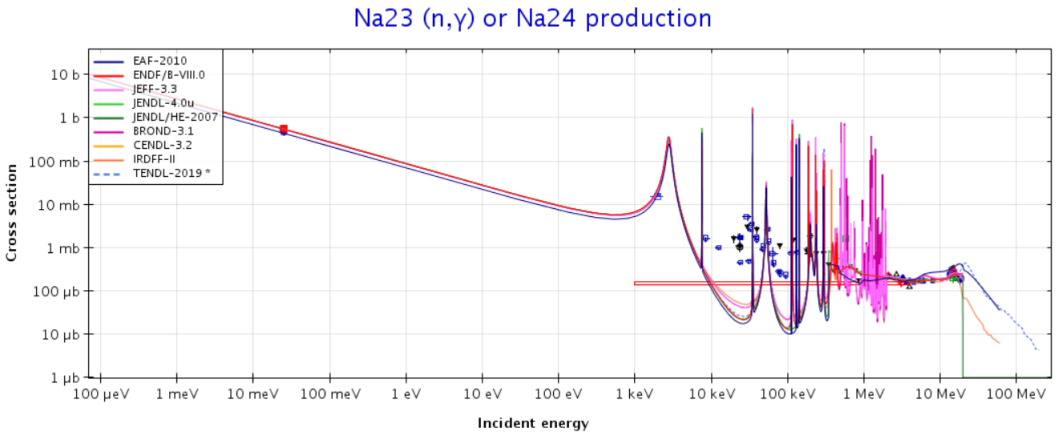

Figure 3.12: Cross section of $^{23}Na\ (n,\,\gamma)\ ^{24}Na$

^{15}O is produced thanks to the absorption of a neutron, followed by the expulsion of two neutrons. The graphic explains how this reaction is possible by showing the reaction cross section:

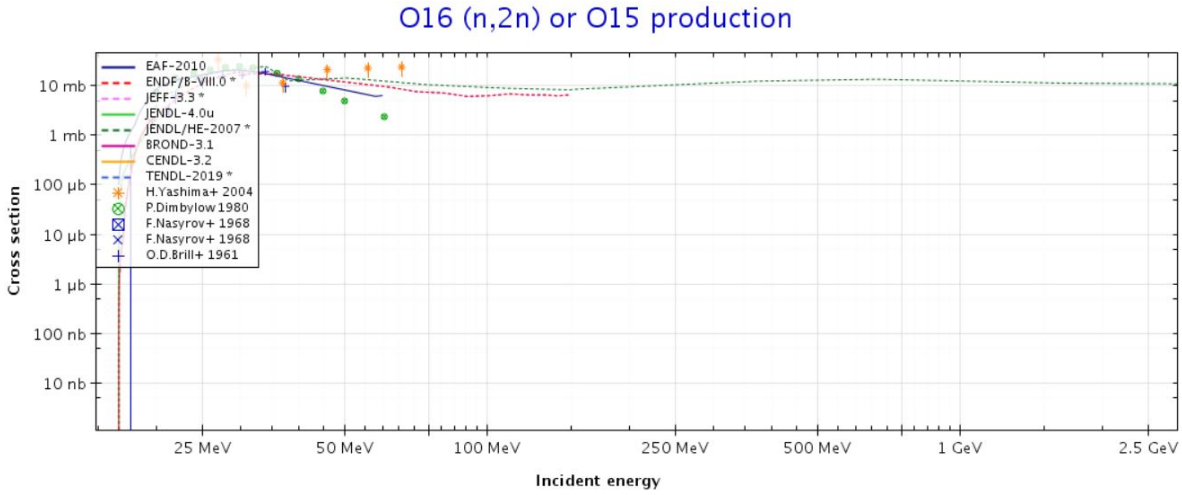

Figure 3.13: Cross section of $^{16}O(n, 2n)^{15}O$

^{13}N is generated by the following reactions with the correspondence cross section:

- $^{16}O(n, n+t)^{13}N$, where t is ^{3}H

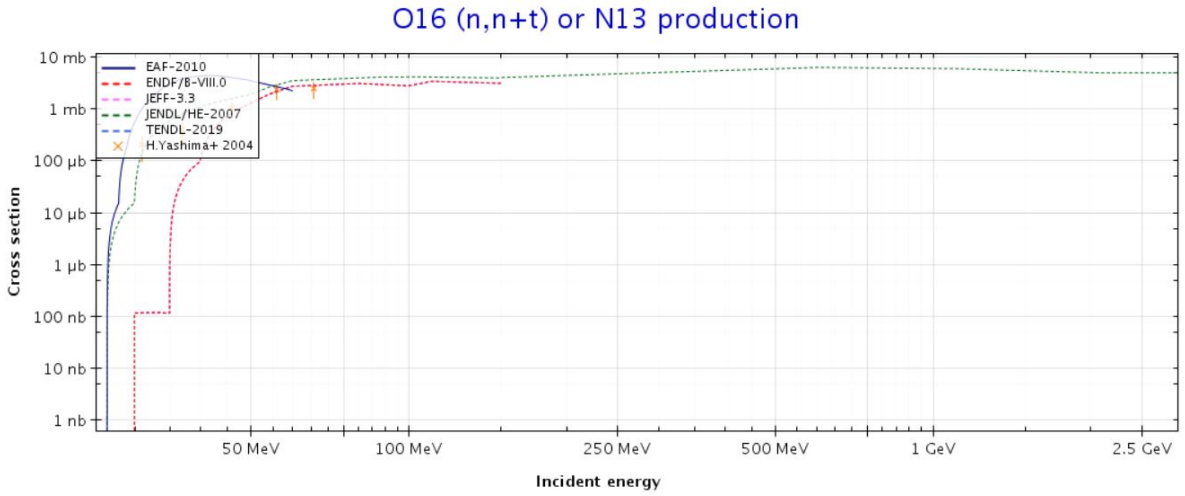

Figure 3.14: Cross section of $^{16}O(n, n+t)^{13}N$

- $^{16}O(n, 3n+p)^{13}N$

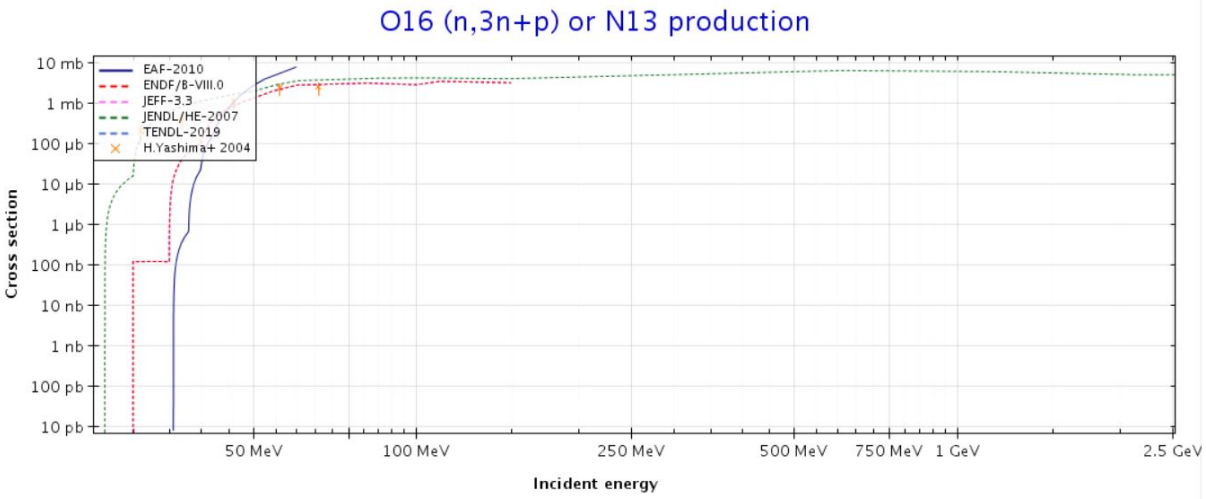

Figure 3.15: Cross section of $^{16}O(n, 3n+p)^{13}N$

As regards ^{11}C, its formation can take place thanks to these three reactions:

- $^{16}O(n, 3n +^3 He)^{11}C$

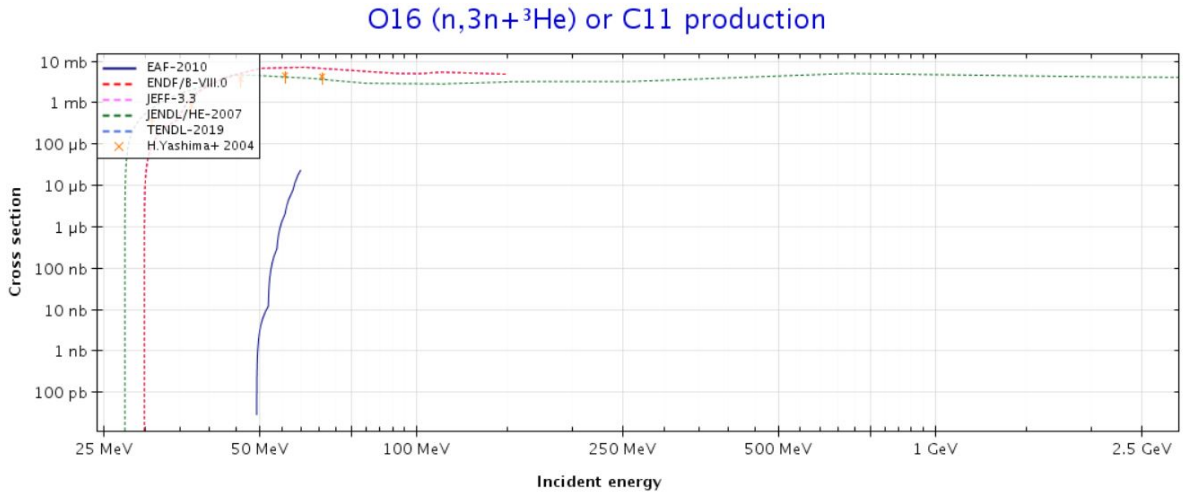

Figure 3.16: Cross section of $^{16}O(n, 3n +^3 He)^{11}C$

- $^{16}O(n, n + d + t)^{11}C$, where d stands for ^2H and t for ^3H

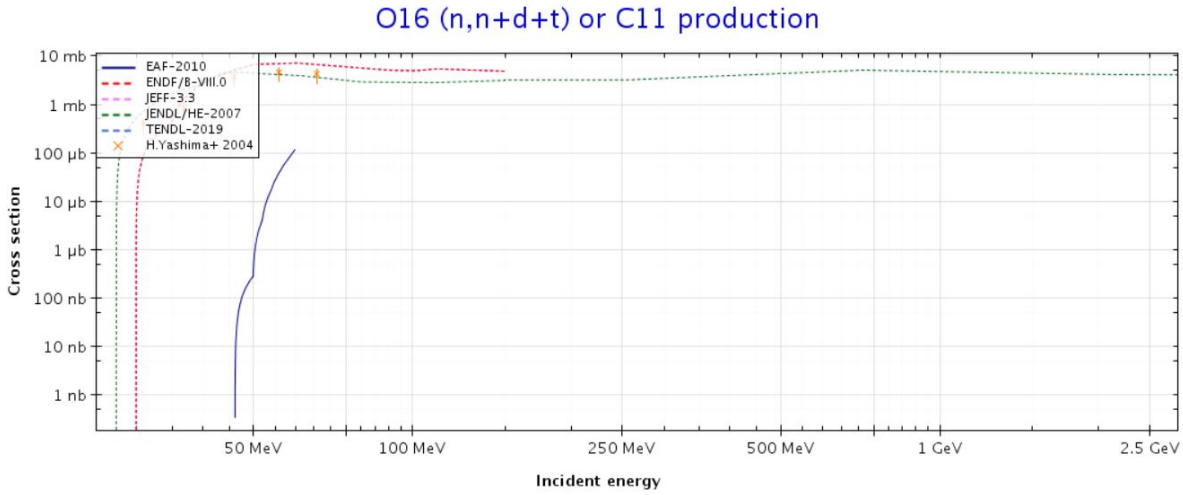

Figure 3.17: Cross section of $^{16}O(n, n + d + t)^{11}C$

- $^{16}O(n, 4n + 2p)^{11}C$

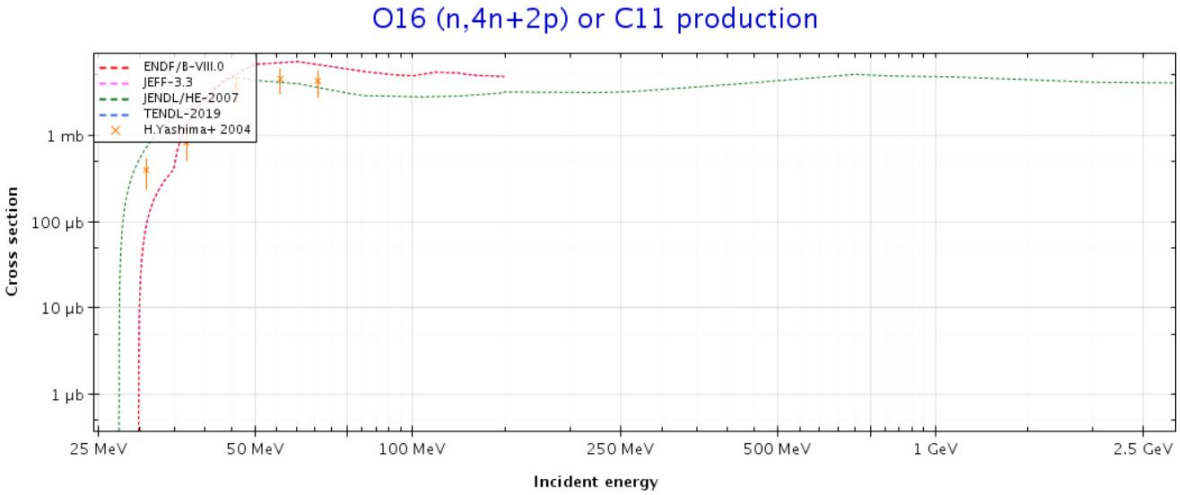

Figure 3.18: Cross section of $^{16}O(n, 4n + 2p)^{11}C$

4 | Synchrotron simulation

In this chapter, a detailed analysis of water activation of the synchrotron circuit is developed: staring from previous analysis, that dates back to the CNAO Foundation, an implementation is designed with a more realistic structure and a more complex pipeline.

Moreover, simulations and analysis are performed not only for carbon ions and protons, the actual therapies, but also for the ions projected for the expansion. In the table 4.1 all the accelerated particles are listed with their energies and their maximum allowed particles per seconds, when the synchrotron is on.

Table 4.1: Data for the employment of new ions

Particles	Energy [MeV/u]	[particles/seconds]
^{4}He	320	5.0 E+08
^{7}Li	306	4.5 E+08
^{16}O	400	7.3 E+07
^{56}Fe	306	3.6 E+07

4.1. Water activation in the cooling system

The goal is to describe all the radionuclides that can be formed in the water cooling system. To develop it, FLUKA is employed as a simulator of the global system, comprehending the structure with its physic.

A fundamental part of the simulation is composed of the beam loss model developed by the CNAO radioprotection office, that is analyzed in the first paragraph, followed by the global design of the simulations with their results.

4.2. Beam losses hypothesis

The beam transport is ideally perfect, while in fact it is complex and not all the particles are able to reach the maximum energy or to follow the designed path. These phenomena are due to the fact that in local points such as injection and deviation, leakages of particles

are affecting the transport. In this way, a secondary field is generated and has to keep monitored for radioprotection reasons, particularly to calculate the activation levels of material, air and water.

Three kind of leakages are observed:

1. the accidental losses are difficult to be detected and are generated mainly by the interactions of primaries with structural components or with residual gasses in the void chamber;
2. the losses that are generated by hitting a target or a structural component;
3. the losses due to the way of working of the synchrotron, that is to say the beam has to hit a damp to be stopped.

The transport of the synchrotron was analyzed in detail when the facility was built by the Doc. Michele Ferrarini [12] to provide the correct wall shielding. In the following photo, it appears a scheme for the description of the points of loss in the synchrotron room and then, thanks to the table 4.2, an evaluation of the lost quantity in that point is provided.

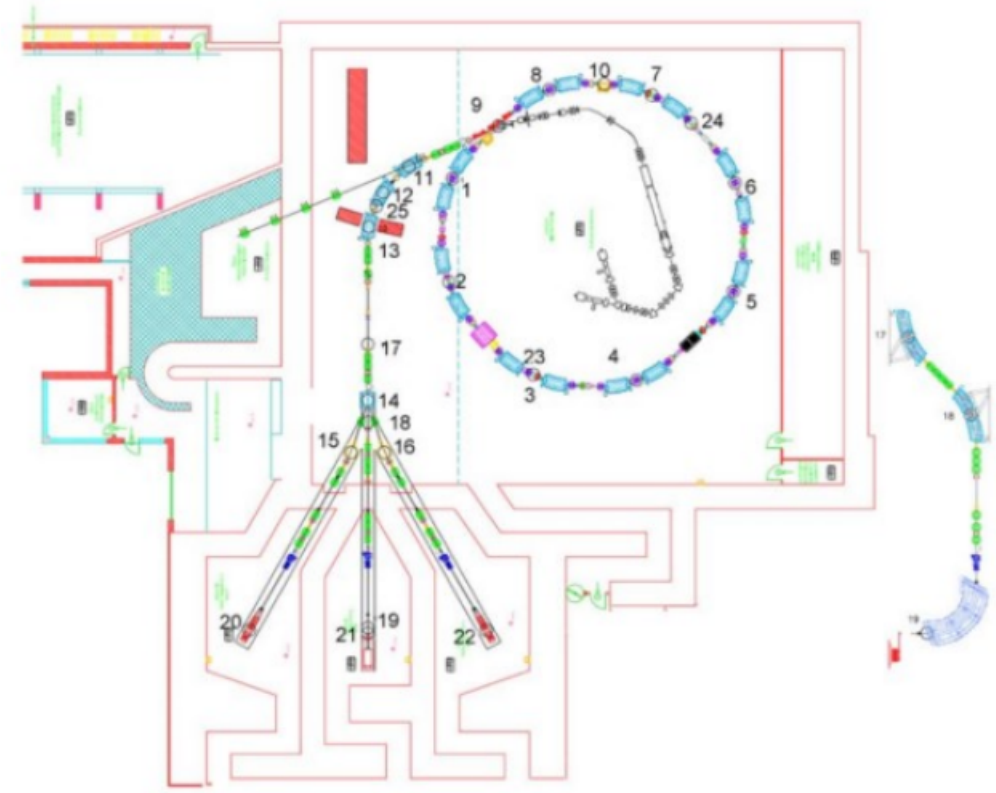

Figure 4.1: Points of loss in the synchrotron room [12]

Table 4.2: Estimation of the losses in the synchrotron beam

Zone	number position in 4.1	percentage of loss [%]
Synchrotron ring	from 1 to 8	3.7
Magnetic septum	9	3.7
Electrostatic septum	10	3.7
Extraction dipole 1	11	0.385
Extraction dipole 2	12	0.113
Extraction dipole 3	13	0.09
Switching dipole	14	0.0744
Matching dipole 1	15	0.0296
Matching dipole 2	16	0.0296
Vertical line dipole 1	17	0.015
Vertical line dipole 2	18	0.0149
Dipole 90°	19	0.0148
Iso ST1	22	4.72
Iso ST2	21	4.72
Iso ST3	20	4.72
Horizontal damp	24	37
Vertical damp	23	2.22
Damp chopper HEBT	25	3.6
Isocenter XPR 1	S1	7.8
Isocenter XPR 2	S2	7.8
Isocenter XPR 3	S3	7.8
Isocenter XPR 4	S4	7.8

As it is notable from the table, the major losses are coming from the beam damp and other parts of the accelerator designed to stop or to tailor the beam. In fact, in the horizontal damp, the 37% of losses are registered. On the other hand, the vertical damp, used to stop the beam in emergency condition, and the damp chopper, used in ordinary condition, represent the 2.2% and 3.6% respectively. Moreover, in the circumference there are 8 loss-points, as it appears in the photo 4.1, with the 3.7% of value in total. They are simulated like one uniformly distributed loss along the synchrotron ring. Other important components, that are causing remarkable losses, are the electrostatic and magnetic septum, with a 3.7% for each.

4.3. FLUKA synchrotron model

4.3.1. Geometry

The idea of the simulated structure comes from the original planimetry and from visual inspection, adapted to FLUKA, in order to make it the most similar to reality.

Furthermore, all the pipelines are designed to be located in strategic positions to estimate the worst condition as regarding activation. For the same purpose, these pipes are placed at the same height as the beam.

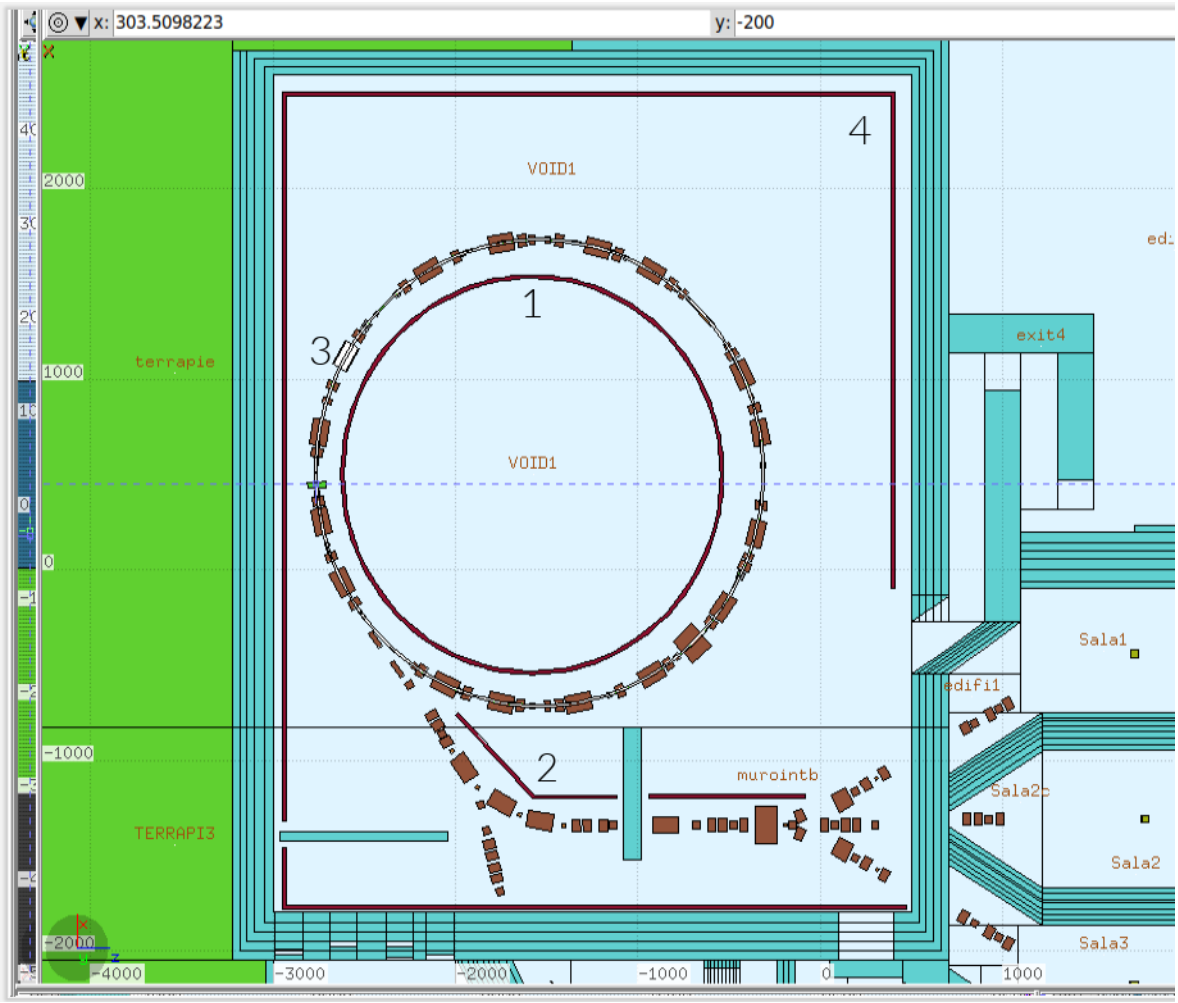

Figure 4.2: Simulated pipeline in the Synchrotron room, top view at beam height

The simulated water regions consist of two different parts: one for the cooling system of the utilities, pointed out in the figure 4.2 with the number 4, and the other one for the synchrotron pipelines. The synchrtron circuit is composed of three areas comprehending

the pipes at the centre of the ring indicated with the number 1, along the HEBT line, highlighted with number 2, and inside the magnets with the number 3.

Synchrotron pipelines

The analysis starts with the cooling system of the synchrotron: it is composed of a complex circuit, that is subdivided in zone to realize the activation of each area.

Here the simulated pipeline of the cooling circuits with their dimension are listed.

First of all, a pipe inside the ring, indicated in the 4.2 figure with the number 1, is placed. Its dimension are the same as developed by previous simulation with the following characteristics:

- radius = 10.4 m
- distance to magnets = 1.5 m
- pipe diameter = 0.2 m
- total volume = 2612.5 l

From this point, all the added pipes are for implementing the previous simulation and furthermore to perform them with all the future particles.

A pipe is placed next to the HEBT line of the synchrotron, where the beam is extracted and directed to the treatment rooms. It is highlighted in the 4.2 picture, with the number 2 and has these dimensions:

- pipe diameter = 0.2 m
- length = 17.5 m
- total volume = 549.19 l

Magnet pipes

Then, inside the magnets, a cooling system is present. The major quantity of water is present in the dipoles compared to the quadrupoles and sestupoles, because the last two are more compact. In fact, the total volume of water in a quadrupole is 0.19 l, respect to a dipole with 1.5 l. For this reason, in the simulation it is outlined the structure of a dipole with its principal elements, as it appears in the following picture 4.3. It is noticeable that the water is inside two layers of copper surrounded by iron, which is the frame of the magnet.

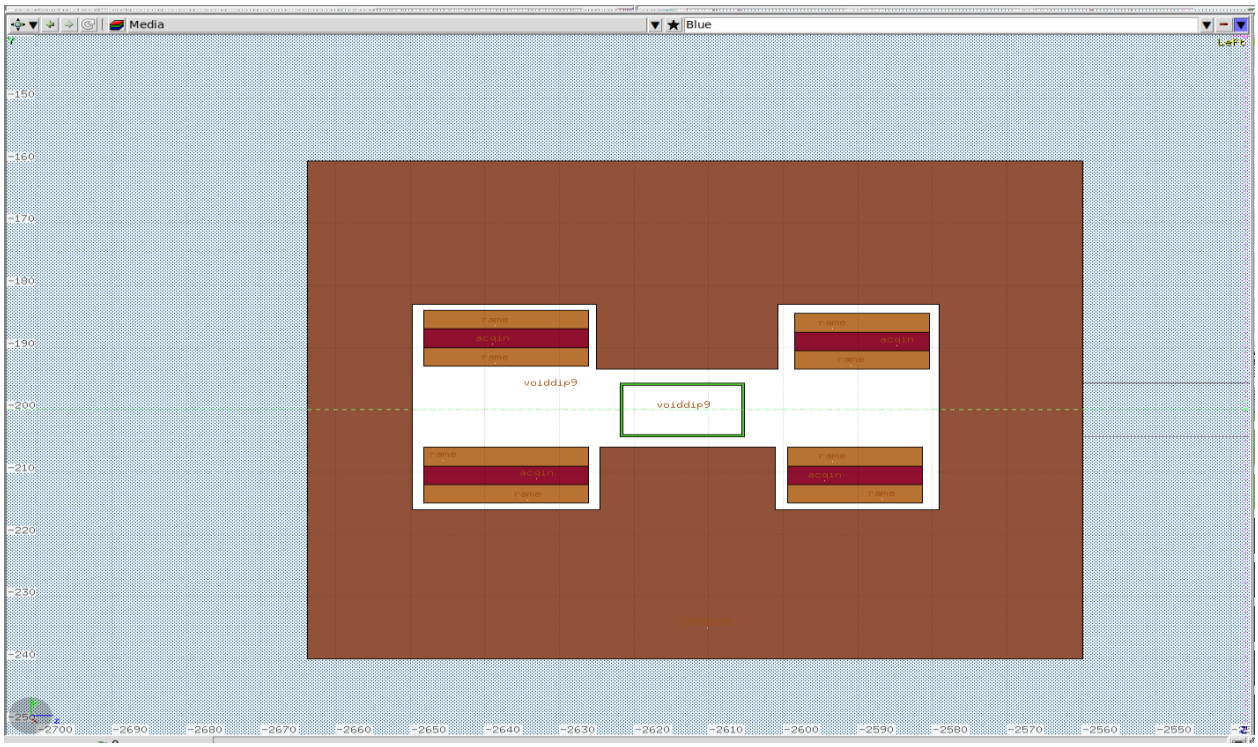

Figure 4.3: Inside a dipole. The principal brown block is made of iron, while the 4 parallepipeds are composed of water, that appears red, surrounded by two layers of copper

The sizes of the simulated water region are:

- height = 3 cm
- width in the right side = 15.6 cm
- width in the left side = 19.1 cm
- total volume = 29.2 l

The water volume of the designed dipole is bigger than the real one, because it was chosen to represent the water of all the dipoles, that are present in the ring, in one. This dipole is selected because of its strategic position, as it appears in the 4.2 figure, with the number 3, where the beam losses have bigger rate.

Utilities pipelines

The cooling system of the utilities is designed with a perimetric pipe to simulate all the cooling water presence against the wall, as it appears in the 4.2 figure, with the number 4 with the following dimensions:

- pipe diameter = 0.2 m

- length according to the facing wall= 34.2 m; 33.6 m; 38.1 m; 29m
- total volume = 4235.86 l

4.3.2. Water characteristics

In the cooling system of the syncrothron, demineralized water is present, but for a conservative reason, it is simulated with the composition of water coming from the analysis of DAFNE accelerator from INFN, National Laboratory of Frascati. For keeping in consideration the worst scenario the maximum values of the 3.1 table are used in the simulation.

The region of the cooling system appears red in the pictures 4.2 and 4.3, because of the added impurities, as shown in the table 3.1. So, instead of using the standard water present in the program, a new material can be created and assigned to a region. This is possible thanks to the Compound card.

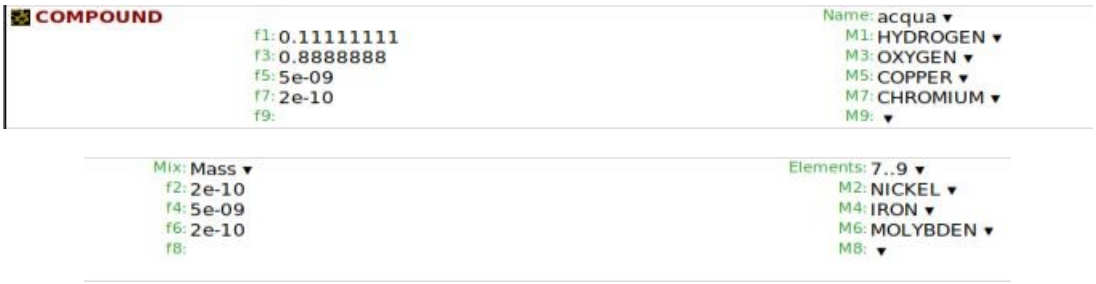

Figure 4.4: Compound card employed for Synchrotron cooling system

On the other hand, in the cooling system of the utilities softened water is placed. This is performed employing the analysis of potable water from the water supply of Pavia. These values are available at the table 3.2 of the previous chapter.

These values are placed in FLUKA through the use of the card compound, as it appears in 4.5, and then are allocated in the proper region.

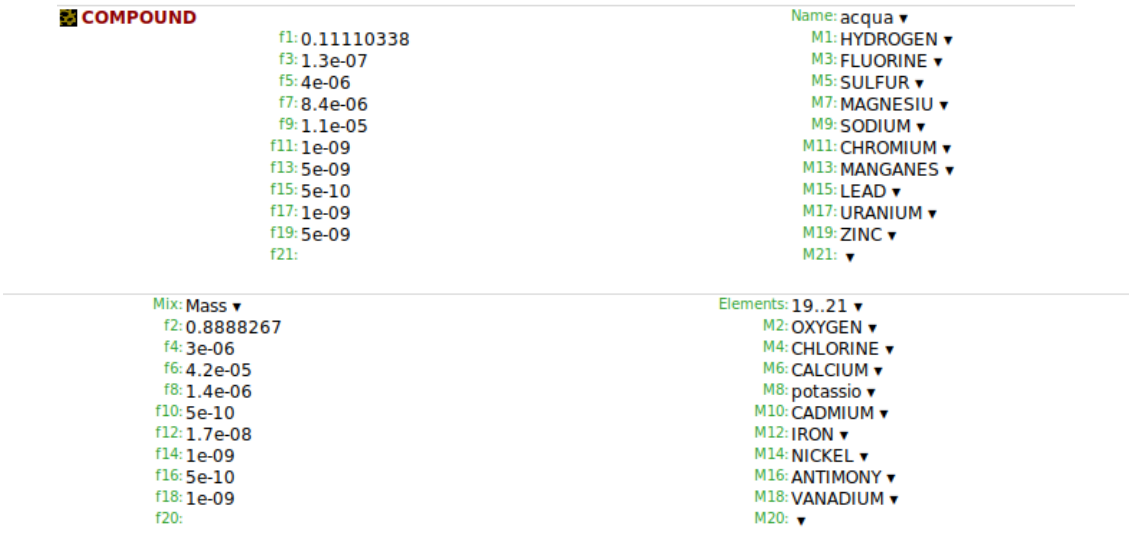

Figure 4.5: Compound card employed for for the cooling system of the utilities

In addition, the activation of the cooling system is evaluated considered all the present water as static for the period of the simulation.

4.3.3. Beam loss model in FLUKA

In the FLUKA simulation, the transport of the beam is described in a routine *source.f*: it is a code written in Fortran77, that is compiled and an executable file is created. Therefore, the generation of a primary beam is the results of the code instruction. Instead the losses are the result of a comparison from a sequence of IF blocks, where for each iteration a loss is performed according to the their percentages.

In the computational code, the 8 loss-points of the ring are simulated like a primary beam, but tangential to the circumference of the accelerator. Following a similar method, the other leakages are described as primaries accelerated tangent to the ring. The main difference is that these primaries are hitting a block of copper, iron or lead of dimension $10x10x10cm^3$ to create a realistic loss with its physics.

Studying and employing the routine that describes the beam losses and the track of the primary particles, a problem came out: the primary beam was hitting directly the water area. This situation is not describing the reality, because structural parts and other elements, such as controlling and measuring monitors, are present and stopping a great part of the losses. Moreover, as described in the 3.2 paragraph, the goal of this project is describing the worst scenario for the radioprotection, so the water activation is evaluated with the maximum number of secondary neutrons.

To reach a proper water activation result for radioprotection reason, some procedures are employed. First of all, the ring with all the magnets is implemented by increasing the dimensions of the magnets. The expansion of the structure of some centimeters represents the structural components that are stopping or attenuating the beam in reality. This technique is performed gradually for not creating a total different structure: analyzing where the major losses are, it is possible to increase proportionally the lengths of some magnets. This choice is employed because the elements that interfere consist of iron, the same material as the magnets.

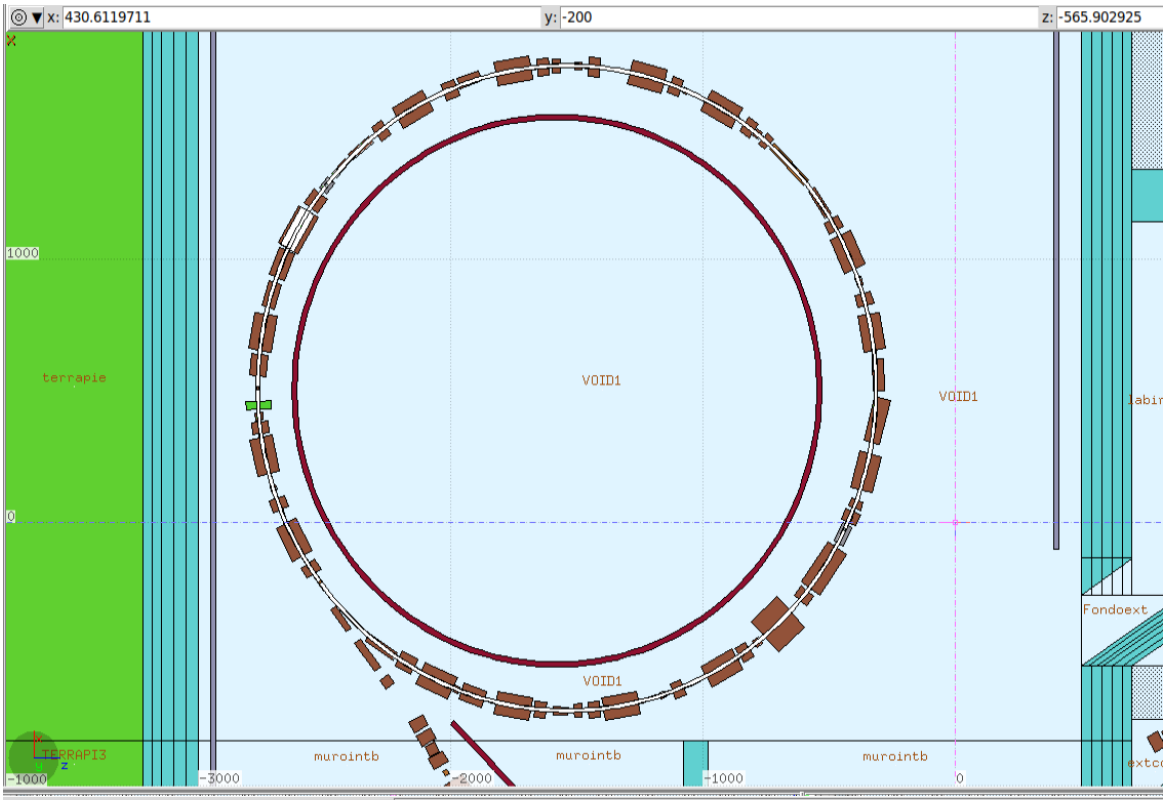

Figure 4.6: Detail of the enlarged magnets, top view at beam height

The proposed solution for solving all the losses of the primary beam is not enough in the case of protons. The obtained result is not solid, showing high errors and great variability for little changes in the structure or number of primary. This statistical problem is due to the fact that the activity is very low, so the program finds difficulty to detect some radionuclides.

The solution to have a realistic primary particles track is to design a thicker void chamber. In particular, before the void chamber had uniform walls with $0.3\,cm$ of thickness and for this simulation their are extended of $0.7\,cm$ towards the inner side of the ring and $1.7\,cm$ towards the outside. This approach provides stable and constant results.

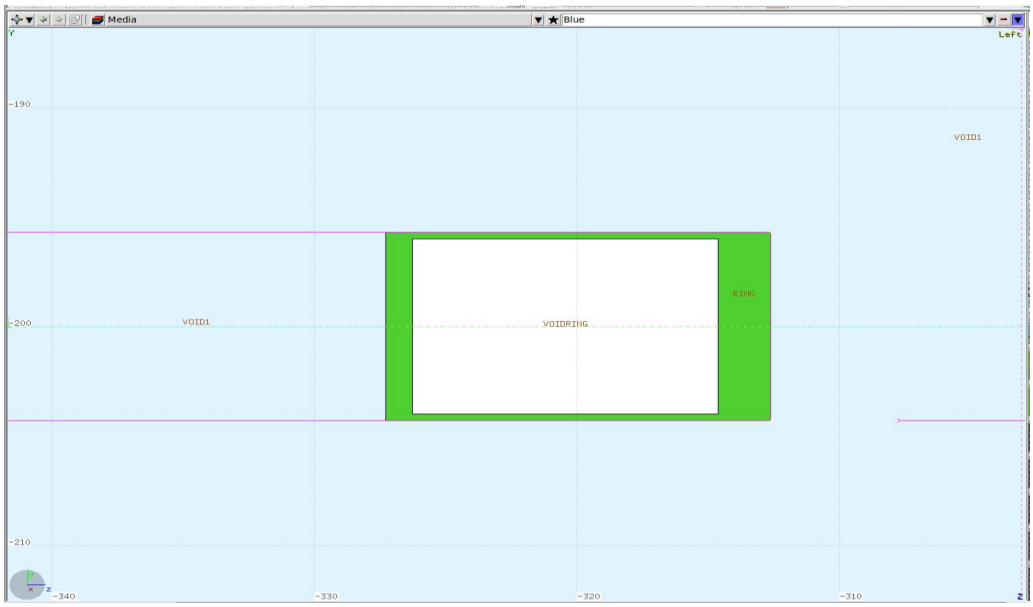

Figure 4.7: Void chamber designed for protons

Protons have a higher range, less weight and also a lower energy than heavy ions. For all these reasons, the protons are mostly stopped before reaching the water region.

A solution, to increase the performance of the statistic, is to place bigger volumes in a point where losses from the beam are present. So, in the perimetric pipeline, the detector is a new region composed of two new parallelepipeds. The sum of their volumes is equal to $123930\,l$, respect to $4235.9\,l$. After having evaluated the water activation in the bigger volume, the next step is to re-scale it through the specific activity. Thanks to this mechanism, the statistic is implemented detecting a bigger volume and because of the strategic position, the program provides an higher number of Becquerel respect to the reality, but it is employed for a conservative evaluation.

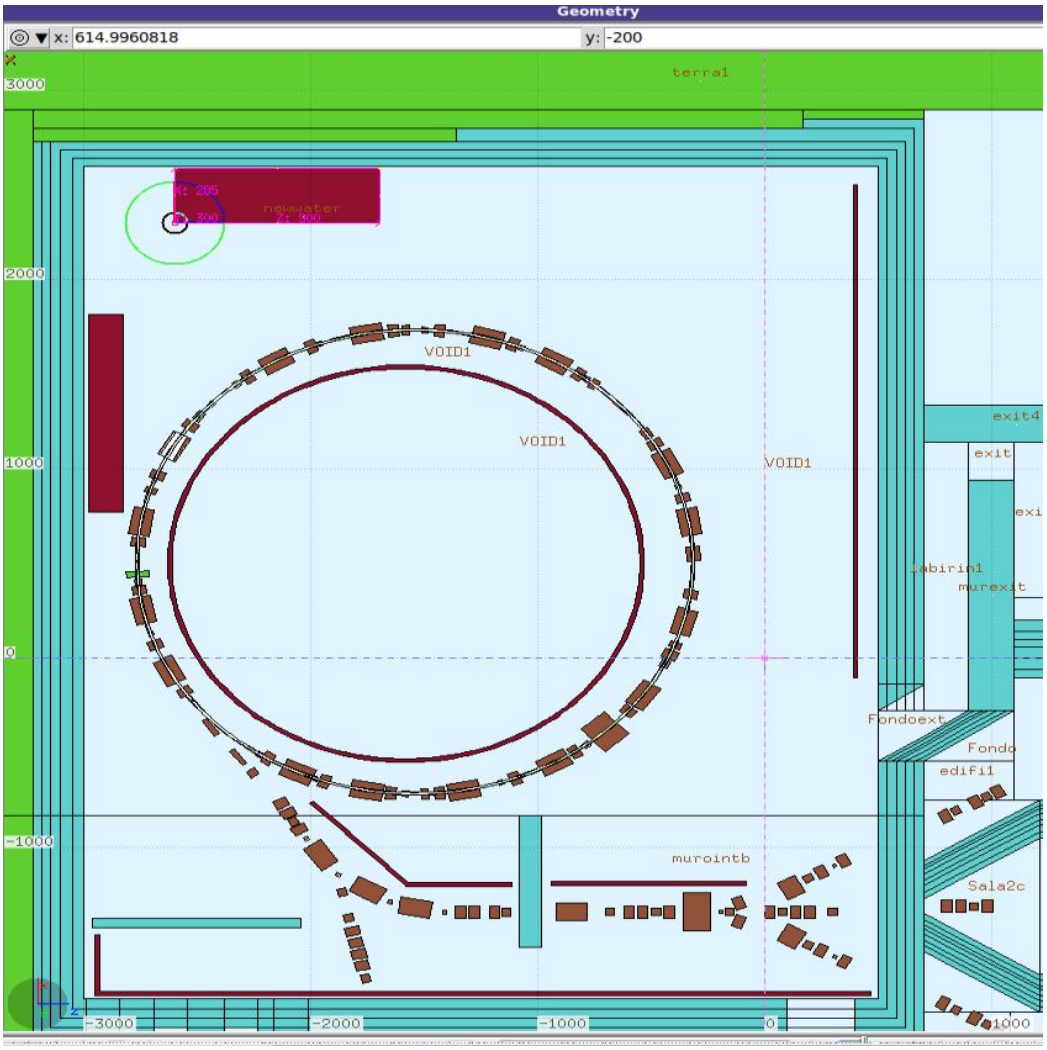

Figure 4.8: Water bodies added for implementing the results

4.3.4. Activation cards

The activation process on FLUKA is design from the selection of particular cards:

- IRRPROFIle allows the description of a particular profile of irradiation in particles per seconds that can vary during time. In fact, a step function is possible by choosing a value of particles per seconds for each time intervals.
- RADDECAY is a card that makes the simulation keep in consideration about not only the radioactive decays that are happening, but also their transport and biasing.
- COALESCEnce permit to consider all the phenomena concerning the physics of the coalescence.
- EVAPORATation allows to count all the nuclear evaporation processes that can

happen.

4.3.5. Scoring cards

The scoring of water activation is performed by the employment of different cards:

- DCYTIMES sets up times to perform a radioactive scoring.
- DCYSCORE questions the detector after an eligible amount of time to score the results.
- RESNUCLEi performs the scoring of all the produced nuclei through inelastic reactions in the questioned region.

4.4. Results

In this section the results from the performed simulation are listed. The produced particles are the expected ones as shown in the previous chapter. The activity changes among the different accelerated particles. This phenomenon is mainly due to the different neutron yields, that depends on several factors as the geometry, the beam energy and the atomic number of the parent nuclide [4].

4.4.1. Carbon ions: Beam data and results

The beam composed of carbon ions has an energy of 400 MeV/u and particles per seconds equals to $3E + 08$. It was performed for a year, that is to say 31536000 s. These data are the maximum allowed for the structure of the accelerator and shielding, but for an everyday use they can be lower according to the need for the required therapy.

The results are detected after 1 and 900 seconds for loosing the short-lived particles. Analyzing the questioned detector after 1 s, lots of radionuclides with a short half life are present as they are listed in the 3.3.2 paragraph.

Table 4.3: ^{12}C ions - Ring pipeline results after 1 s

A	Z	A [Bq]	A_s [Bq/g]	Statistical error
16	7	3.45E+04	1.32E-02	8
15	6	1.88E+03	7.21E-04	22
15	8	5.67E+04	2.17E-02	6
14	6	3.95E+00	1.51E-06	14
14	8	4.95E+02	1.90E-04	29
13	7	3.00E+03	1.15E-03	21
11	6	2.55E+04	9.76E-03	25
10	4	4.82E-03	1.84E-09	23
10	6	1.93E+03	7.39E-04	17
7	4	7.93E+03	3.04E-03	12
3	1	2.76E+03	1.06E-03	6

Table 4.4: ^{12}C ions - Ring pipeline results after 900 s

A	Z	A [Bq]	A_s [Bq/g]	Statistical error
15	8	3.46E+02	1.33E-04	6
14	6	3.95E+00	1.51E-06	14
14	8	7.27E-02	2.78E-08	29
13	7	1.06E+03	4.05E-04	21
11	6	1.53E+04	5.86E-03	25
10	4	4.82E-03	1.84E-09	23
7	4	7.93E+03	3.04E-03	12
3	1	2.76E+03	1.06E-03	6

Table 4.5: ^{12}C ions -Pipeline next to HEBT line, results after 1 s

A	Z	A [Bq]	A_s [Bq/g]	Statistical error
16	7	1.82E+03	3.30E-03	17
15	6	3.77E+02	6.86E-04	19
15	8	1.24E+04	2.26E-02	22
14	6	5.47E-01	9.96E-07	27
13	7	9.99E+02	1.82E-03	31
11	6	6.00E+03	1.09E-02	21
10	4	6.88E-04	1.25E-09	27
8	3	4.38E+02	7.98E-04	21
7	4	1.49E+03	2.71E-03	17
3	1	7.11E+02	1.29E-03	15

Table 4.6: ^{12}C ions - Pipeline next to HEBT line, results after 900 s

A	Z	A [Bq]	A_s [Bq/g]	Statistical error
15	8	7.60E+01	1.38E-04	22
14	6	5.47E-01	9.96E-07	27
13	7	3.52E+02	6.42E-04	31
11	6	3.60E+03	6.56E-03	21
10	4	6.88E-04	1.25E-09	27
7	4	1.49E+03	2.71E-03	17
3	1	7.11E+02	1.29E-03	15

Table 4.7: ^{12}C ions - Inside the dipole pipeline results after 1 s

A	Z	A [Bq]	A_s [Bq/g]	Statistical error
16	7	1.82E+03	6.22E-02	47
15	8	6.46E+03	2.22E-01	15
14	6	4.86E-01	1.67E-05	32
13	7	9.99E+02	3.42E-02	29
11	6	3.00E+03	1.03E-01	39
10	4	2.29E-04	7.86E-09	29
7	4	9.91E+02	3.40E-02	21
3	1	5.19E+02	1.78E-02	14

Table 4.8: ^{12}C ions - Inside the dipole pipeline results after 900 s

A	Z	A [Bq]	A_s [Bq/g]	Statistical error
15	8	3.95E+01	1.35E-03	15
14	6	4.86E-01	1.67E-05	32
13	7	3.52E+02	1.21E-02	29
11	6	1.80E+03	6.17E-02	39
10	4	2.29E-04	7.86E-09	29
7	4	9.91E+02	3.40E-02	21
3	1	5.19E+02	1.78E-02	14

Table 4.9: ^{12}C ions - Perimetrical pipeline results after 1 s

A	Z	A [Bq]	A_s [Bq/g]	Statistical error
41	20	5.98E-03	1.41E-09	19
36	17	1.27E-02	3.00E-09	10
24	11	4.29E+02	1.01E-04	33
19	8	1.20E+02	2.82E-05	26
17	7	5.20E+01	1.23E-05	35
16	7	1.63E+04	3.85E-03	7
15	6	5.08E+02	1.20E-04	21
15	8	3.77E+04	8.90E-03	5
14	6	2.68E+00	6.33E-07	5
14	8	2.43E+02	5.74E-05	36
13	7	2.45E+03	5.78E-04	15
11	4	3.50E+02	8.26E-05	44
11	6	1.75E+04	4.14E-03	6
10	4	2.17E-03	5.11E-10	13
10	6	1.12E+03	2.65E-04	24
7	4	6.63E+03	1.56E-03	10
3	1	1.45E+03	3.42E-04	6

Table 4.10: ^{12}C ions - Perimetrical pipeline results after 900 s

A	Z	A [Bq]	A_s [Bq/g]	Statistical error
41	20	5.98E-03	1.41E-09	19
36	17	1.27E-02	3.00E-09	10
24	11	4.24E+02	1.00E-04	33
19	8	1.02E-08	2.41E-15	26
15	8	2.30E+02	5.44E-05	5
14	6	2.68E+00	6.33E-07	5
14	8	3.57E-02	8.43E-09	46
13	7	8.64E+02	2.04E-04	15
11	6	1.05E+04	2.49E-03	6
10	4	2.17E-03	5.11E-10	13
7	4	6.63E+03	1.56E-03	10
3	1	1.45E+03	3.42E-04	6

Reading the tables of the results coming from the perimetrical pipeline, it is remarkable the presence of impurities from the analysis of potable water of Pavia, that lead to the formation of these radioisotopes: ^{41}Ca, ^{36}Cl and ^{24}Na. They are produced from neutron capture reaction as shown in the 3. In addiction, ^{41}Ca and ^{36}Cl have a long half life so it is important to keep them monitored.

The production of ^{7}Be and ^{3}H is salient against all the other particles: in the zone at the centre, that is the closest one to the beam, the production of some kBq is seen. In addition, ^{14}C has a production of some Becquerel, but it has to be kept in consideration for the long half life. As listed in chapter 3, in the detector after 1 s it is noticeable the short lived particles that mostly disappear in the detector after 900 s. Only ^{15}O, ^{14}O, ^{13}N and ^{11}C are still present because, in first place, they are produced in bigger quantity and it is remarkable how their activity is decreasing with time.

Moreover, the listed reaction in the chapter 3 are the most frequent and probable: for them it is possible to reach a good statistic and a trustful error. On the other hand, the presence of high errors is due to exotic reactions that barely happens or common reactions that have very slow frequency. In the previous tables this phenomenon happens with: ^{14}O, ^{8}B and ^{13}N are short lived radionuclides so it can happen that the program does not reach a stability; on the contrary, just traces of ^{10}Be are produced that are difficult to follow for FLUKA. ^{8}B and ^{6}He are not placed in the tables because of their half life is in the order of some milliseconds.

In fact, if the statistical error associated to the most frequent reaction as described int the previous chapter is acceptable, even though increasing the number of simulated primaries, the error of the exotic reaction would not decrease in a substantial way. For having a complete description, these radionuclides are reported here, but they are not relevant for the radioprotection analysis.

4.4.2. Oxygen ions: Beam data and results

Oxygen ions are accelerated with a maximum value of $400\,MeV/u$ and $3E+08$ particles per second and for a conservative analysis, to study the maximum activation data these value are employed.

Here, it follows the tables of the investigated detectors.

Table 4.11: ^{16}O ions -Ring pipeline results after 1 s

A	Z	A [Bq]	A_s [Bq/g]	Statistical error
17	7	2.59E+01	9.91E-06	21
16	7	4.13E+03	1.58E-03	3
15	6	1.24E+02	4.76E-05	20
15	8	1.00E+04	3.84E-03	3
14	6	5.73E-01	2.19E-07	5
14	8	9.69E+01	3.71E-05	25
13	7	5.74E+02	2.20E-04	13
11	4	1.74E+01	6.68E-06	26
11	6	4.74E+03	1.81E-03	3
10	4	6.03E-04	2.31E-10	6
10	6	1.89E+02	7.23E-05	16
7	4	1.92E+03	7.33E-04	5
3	1	4.17E+02	1.60E-04	3

Table 4.12: ^{16}O ions - Ring pipeline results after 900 s

A	Z	A [Bq]	A_s [Bq/g]	Statistical error
15	8	6.13E+01	2.35E-05	3
14	6	5.73E-01	2.19E-07	5
14	8	1.42E-02	5.45E-09	25
13	7	2.03E+02	7.75E-05	13
11	6	2.84E+03	1.09E-03	3
10	4	6.03E-04	2.31E-10	6
7	4	1.92E+03	7.33E-04	5
3	1	4.17E+02	1.60E-04	3

Table 4.13: ^{16}O ions - Pipeline next to HEBT line, results after 1 s

A	Z	A [Bq]	A_s [Bq/g]	Statistical error
16	7	6.49E+02	1.18E-03	11
15	6	2.76E+01	5.03E-05	20
15	8	2.22E+03	4.04E-03	5
14	6	9.29E-02	1.69E-07	8
13	7	1.04E+02	1.89E-04	22
11	6	9.05E+02	1.65E-03	8
10	4	1.26E-04	2.30E-10	13
10	6	4.72E+01	8.60E-05	34
7	4	3.70E+02	6.73E-04	11
3	1	9.80E+01	1.78E-04	7

Table 4.14: ^{16}O ions - Pipeline next to HEBT line, results after 900 s

A	Z	A [Bq]	A_s [Bq/g]	Statistical error
15	8	1.36E+01	2.47E-05	5
14	6	9.29E-02	1.69E-07	8
13	7	3.66E+01	6.67E-05	22
11	6	5.43E+02	9.89E-04	8
10	4	1.26E-04	2.30E-10	13
7	4	3.70E+02	6.73E-04	11
3	1	9.80E+01	1.78E-04	7

Table 4.15: ^{16}O ions - Inside the dipole pipeline results after 1 s

A	Z	A [Bq]	A_s [Bq/g]	Statistical error
16	7	2.72E+02	9.33E-03	15
15	6	1.84E+01	6.32E-04	19
15	8	1.39E+03	4.78E-02	6
14	6	5.80E-02	1.99E-06	10
14	8	1.82E+01	6.23E-04	23
13	7	9.77E+01	3.35E-03	27
11	4	1.16E+01	3.99E-04	19
11	6	7.15E+02	2.45E-02	11
10	4	8.70E-05	2.98E-09	10
10	6	3.54E+01	1.21E-03	17
7	4	3.28E+02	1.12E-02	11
3	1	5.55E+01	1.90E-03	8

Table 4.16: ^{16}O ions - Inside the dipole pipeline results after 900 s

A	Z	A [Bq]	A_s [Bq/g]	Statistical error
15	8	8.51E+00	2.92E-04	6
14	6	5.80E-02	1.06E-07	10
14	8	2.67E-03	4.86E-09	23
13	7	3.45E+01	6.28E-05	27
11	6	4.29E+02	7.82E-04	11
10	4	8.70E-05	1.58E-10	10
7	4	3.27E+02	5.96E-04	11
3	1	5.55E+01	1.01E-04	8

Table 4.17: ^{16}O ions - Perimetrical pipeline results after 1 s

A	Z	A [Bq]	A_s [Bq/g]	Statistical error
41	20	1.27E-03	3.00E-10	28
36	17	1.62E-03	3.82E-10	20
24	11	2.61E+01	6.15E-06	29
17	7	4.42E+01	1.04E-05	68
15	6	1.18E+02	2.78E-05	32
15	8	5.39E+03	1.27E-03	7
14	6	3.58E-01	8.45E-08	11
14	8	7.75E+01	1.83E-05	23
13	7	3.91E+02	9.22E-05	30
11	6	2.42E+03	5.72E-04	6
10	4	4.43E-04	1.04E-10	16
10	6	1.01E+02	2.37E-05	27
7	4	8.27E+02	1.95E-04	17
3	1	2.28E+02	5.38E-05	6

Table 4.18: ^{16}O ions - Perimetrical pipeline results after 900 s

A	Z	A [Bq]	A_s [Bq/g]	Statistical error
41	20	1.27E-03	3.00E-10	28
36	17	1.62E-03	3.82E-10	20
24	11	2.58E+01	6.08E-06	29
15	8	3.30E+01	7.78E-06	7
14	6	3.58E-01	8.45E-08	11
14	8	1.14E-02	2.69E-09	23
13	7	1.38E+02	3.25E-05	30
11	6	1.46E+03	3.43E-04	6
10	4	4.43E-04	1.04E-10	16
7	4	8.27E+02	1.95E-04	17
3	1	2.28E+02	5.38E-05	6

Results are comparable to carbon ions: it is noticeable a similar activity produced in a year with a very slightly less activation of ^{7}Be and ^{3}H. This result is expected, because ^{12}C and ^{16}O have similar weights and energies, so the number of generated secondary neutrons, that induce the reactions, are similar. It is remarkable noting that the presence

of higher statistical errors is due to rare or exotic reaction, while, on the other hand the expected particles 3 have a reasonable error. Although increasing the number of primaries, their error would not decrease.

Moreover, particles with half life minor than 1 s generates high error because the program is not capable to evaluate them correctly. For this reason, ^{16}C, ^{9}Li, ^{8}He and ^{8}Be are not present in the previous tables.

As regards the tables 4.17 and 4.18, it is salient the presence of ^{41}Ca, ^{36}Cl and ^{24}Na due to the fact of employing the analysis from the potable water of Pavia, that has more impurities and they are produced through neutron capture as shown in the 3 chapter.

4.4.3. Lithium ions: Beam data and results

Lithium ions are accelerated with the following data: energy of 306 MeV/u and 2.67E+08 particles per second. As commented before, for simulated the worst scenario the highest values are simulated.

Results from the simulation are listed in the following tables.

Table 4.19: ^{7}Li ions - Centre pipeline results after 1 s

A	Z	A [Bq]	A_s [Bq/g]	Statistical error
16	7	1.96E+04	7.50E-03	7
15	6	6.78E+02	2.59E-04	35
15	8	3.60E+04	1.38E-02	5
14	6	2.41E+00	9.21E-07	9
14	8	6.36E+02	2.44E-04	18
13	7	1.67E+03	6.39E-04	25
11	6	1.54E+04	5.90E-03	8
10	4	2.71E-03	1.04E-09	11
10	6	4.96E+02	1.90E-04	45
7	4	7.90E+03	3.02E-03	11
3	1	1.78E+03	6.81E-04	7

Table 4.20: ^{7}Li ions - Centre pipeline results after 900 s

A	Z	A [Bq]	A_s [Bq/g]	Statistical error
15	8	2.20E+02	8.43E-05	5
14	6	2.41E+00	9.21E-07	9
13	7	5.89E+02	2.25E-04	25
11	6	9.26E+03	3.54E-03	8
10	4	2.85E-03	1.09E-09	11
7	4	7.90E+03	3.02E-03	11
3	1	1.78E+03	6.81E-04	7

Table 4.21: ^{7}Li ions - Pipeline next to HEBT, results after 1 s

A	Z	A [Bq]	A_s[Bq/g]	Statistical error
16	7	2.92E+03	5.31E-03	17
15	8	9.46E+03	1.72E-02	10
14	6	3.59E-01	6.54E-07	15
13	7	2.57E+02	4.67E-04	28
11	6	3.08E+03	5.61E-03	17
10	4	4.72E-04	8.59E-10	20
10	6	2.48E+02	4.51E-04	68
7	4	1.02E+03	1.86E-03	14
3	1	2.88E+02	5.24E-04	9

Table 4.22: ^{7}Li ions - Pipeline next to HEBT, results after 900 s

A	Z	A [Bq]	A_s [Bq/g]	Statistical error
15	8	5.78E+01	1.05E-04	10
14	6	3.59E-01	6.54E-07	15
13	7	9.05E+01	1.65E-04	28
11	6	1.85E+03	3.37E-03	17
10	4	4.72E-04	8.59E-10	20
7	4	1.02E+03	1.86E-03	14
3	1	2.88E+02	5.24E-04	9

Table 4.23: ^{7}Li ions - Inside the dipole pipeline results after 1 s

A	Z	A [Bq]	A_s [Bq/g]	Statistical error
16	7	9.33E+02	3.20E-02	31
15	8	6.26E+03	2.15E-01	14
14	6	2.34E-01	8.03E-06	22
13	7	2.57E+02	8.80E-03	28
11	6	2.05E+03	7.04E-02	33
10	4	2.36E-04	8.09E-09	24
7	4	1.15E+03	3.93E-02	17
3	1	2.39E+02	8.19E-03	13

Table 4.24: ^{7}Li ions - Inside the dipole pipeline results after 900 s

A	Z	A [Bq]	A_s [Bq/g]	Statistical error
15	8	3.83E+01	1.31E-03	14
14	6	2.34E-01	8.03E-06	22
13	7	9.05E+01	3.10E-03	28
11	6	1.23E+03	4.23E-02	33
10	4	2.36E-04	8.09E-09	24
7	4	1.15E+03	3.93E-02	17
3	1	2.39E+02	8.19E-03	13

Table 4.25: ^{7}Li ions - Perimetrical pipeline results after 1 s

A	Z	A [Bq]	A_s [Bq/g]	Statistical error
41	20	3.36E-03	7.93E-10	25
36	17	6.65E-03	1.57E-09	15
24	11	6.43E+02	1.52E-04	24
16	7	9.33E+03	2.20E-03	12
15	8	2.24E+04	5.28E-03	9
14	6	1.39E+00	3.28E-07	17
14	8	4.77E+02	1.13E-04	25
13	7	1.28E+03	3.03E-04	25
11	6	7.87E+03	1.86E-03	14
10	4	1.18E-03	2.78E-10	17
10	6	3.10E+02	7.32E-05	28
7	4	4.30E+03	1.02E-03	15
3	1	8.08E+02	1.91E-04	12

Table 4.26: ^{7}Li ions - Perimetrical pipeline results after 900 s

A	Z	A [Bq]	A_s [Bq/g]	Statistical error
41	20	3.36E-03	7.93E-10	25
36	17	6.65E-03	1.57E-09	15
24	11	6.35E+02	1.50E-04	24
15	8	1.37E+02	3.23E-05	9
14	6	1.39E+00	3.28E-07	17
14	8	7.01E-02	1.66E-08	25
13	7	4.53E+02	1.07E-04	25
11	6	4.73E+03	1.12E-03	14
10	4	1.18E-03	2.78E-10	17
7	4	4.30E+03	1.02E-03	15
3	1	8.08E+02	1.91E-04	12

As it appears in the previous tables, the production of ^{3}H and ^{7}Be are the most consistent for radioactivity levels. The presence of ^{14}C, ^{41}Ca and ^{36}Cl is relevant for their long half life. These particles show a low less activity production respect to the previous because the lithium ions has less energy and weight.

On the other hands, radionuclides such as ^{8}He, ^{6}He, ^{8}B, ^{8}Li and ^{9}Li that have half life

less than 1s are not placed, because they do not reach stability and are characterized by a high error. It is remarkable the presence of ^{41}Ca, ^{36}Cl and ^{24}Na due to the water employed with impurities coming form the analysis of the potable water of Pavia. Their production is explained in the 3.3 chapter due to neutron capture.

4.4.4. Helium ions: Beam data and results

Helium ions has the following data: maximum energy value of 320 MeV/u and $8.00E+08$ particles per second. It comes after the results of the detected monitors.

Table 4.27: ^{4}He ions -Ring pipeline results after 1 s

A	Z	A [Bq]	A_s [Bq/g]	Statistical error
16	7	1.32E+04	4.13E-03	7
15	6	4.19E+02	1.31E-04	14
15	8	2.46E+04	7.70E-03	7
14	6	1.83E+00	5.75E-07	6
14	8	2.75E+02	8.62E-05	22
13	7	1.53E+03	4.78E-04	18
11	4	1.32E+02	4.14E-05	23
11	6	1.26E+04	3.94E-03	8
10	4	1.38E-03	4.33E-10	11
10	6	2.68E+02	8.40E-05	23
7	4	4.36E+03	1.37E-03	11
3	1	1.12E+03	3.51E-04	6

Table 4.28: ^{4}He ions - Ring pipeline results after 900 s

A	Z	A [Bq]	A_s [Bq/g]	Statistical error
15	8	1.50E+02	4.71E-05	7
14	6	1.83E+00	5.75E-07	6
14	8	4.04E-02	1.27E-08	22
13	7	5.38E+02	1.69E-04	18
11	6	7.56E+03	2.37E-03	8
10	4	1.38E-03	4.33E-10	11
7	4	4.36E+03	1.37E-03	11
3	1	1.12E+03	3.51E-04	6

Table 4.29: ^4He ions - Pipeline next to HEBT, results after 1 s

A	Z	A [Bq]	A_s [Bq/g]	Statistical error
16	7	2.06E+03	3.75E-03	13
15	8	5.48E+03	9.97E-03	9
14	6	3.15E-01	5.74E-07	15
13	7	6.01E+02	1.09E-03	33
11	6	2.31E+03	4.21E-03	14
7	4	7.34E+02	1.34E-03	25
3	1	2.48E+02	4.52E-04	11

Table 4.30: ^4He ions - Pipeline next to HEBT, results after 900 s

A	Z	A [Bq]	A_s [Bq/g]	Statistical error
15	8	3.35E+01	6.10E-05	9
14	6	3.15E-01	5.74E-07	15
11	6	1.39E+03	2.53E-03	14
10	4	1.70E-04	3.09E-10	38
7	4	7.34E+02	1.34E-03	25
3	1	2.48E+02	4.52E-04	11

Table 4.31: ^4He ions - Inside the dipole pipeline results after 1s

A	Z	A [Bq]	A_s [Bq/g]	Statistical error
16	7	1.05E+03	3.60E-02	20
15	8	3.36E+03	1.15E-01	13
14	6	1.86E-01	6.37E-06	16
13	7	2.78E+02	9.51E-03	32
11	6	1.99E+03	6.82E-02	17
10	4	3.40E-04	1.17E-08	18
7	4	5.51E+02	1.89E-02	25
3	1	1.06E+02	3.64E-03	16

Table 4.32: ^4He ions - Inside the dipole pipeline results after 900 s

A	Z	A [Bq]	A_s [Bq/g]	Statistical error
15	8	2.05E+01	7.04E-04	13
14	6	1.86E-01	6.37E-06	16
13	7	9.79E+02	3.35E-03	32
11	6	1.19E+03	4.10E-02	17
10	4	3.40E-04	1.17E-08	18
7	4	5.51E+02	1.89E-02	25
3	1	1.06E+02	3.64E-03	16

Table 4.33: ^4He ions - Perimetrical pipeline results after 1 s

A	Z	A [Bq]	A_s [Bq/g]	Statistical error
41	20	1.94E-03	4.57E-10	15
37	18	4.63E+01	1.09E-05	27
36	17	5.11E-03	1.21E-09	15
16	7	7.35E+03	1.74E-03	9
15	6	3.49E+02	8.23E-05	20
15	8	1.75E+04	4.13E-03	8
14	6	1.39E+00	3.28E-07	8
13	7	1.16E+03	2.73E-04	21
11	6	8.75E+03	2.06E-03	8
10	4	1.10E-03	2.61E-10	16
10	6	3.13E+02	7.38E-05	22
7	4	3.35E+03	7.91E-04	13
3	1	7.80E+02	1.84E-04	8

Table 4.34: ^{4}He ions - Perimetrical pipeline results after 900 s

A	Z	A [Bq]	A_s [Bq/g]	Statistical error
41	20	1.94E-03	4.57E-10	15
37	18	4.63E+01	1.09E-05	27
36	17	5.11E-03	1.21E-09	15
15	8	1.07E+02	2.52E-05	8
14	6	1.39E+00	3.28E-07	8
13	7	4.08E+02	9.62E-05	21
11	6	5.25E+03	1.24E-03	8
10	4	1.10E-03	2.61E-10	16
7	4	3.35E+03	7.91E-04	13
3	1	7.80E+02	1.84E-04	8

The most relevant radionuclides are ^{3}H, ^{7}Be and ^{14}C, that provide the highest values of radioactivity.

On the other hands, radionucled such as ^{8}He and ^{8}B that have half life less than 1 s are not reported, because they do not reach stability and are characterized by a high error.

As regards the perimetric pipeline, the production of ^{41}Ca, ^{36}Cl and ^{24}Na is due to the different composition of water employed for the cooling system of the utilities. Their production is due to neutron capture reaction as shown in the 3 chapter.

4.4.5. Iron ions: Beam data and results

Iron ions are accelerated with a maximum value of $306\,MeV/u$ and $3E+08$ particles per second. These values are employed for the simulation and here, the results of the investigated circuits are reported.

Table 4.35: ^{56}Fe ions - Ring pipeline results after 1 s

A	Z	A [Bq]	A_s[Bq/g]	Statistical error
16	7	2.18E+03	8.36E-04	4
15	6	1.10E+02	4.22E-05	11
15	8	5.02E+03	1.92E-03	4
14	6	3.01E-01	1.15E-07	7
13	7	3.15E+02	1.20E-04	18
11	6	2.42E+03	9.25E-04	3
10	4	3.35E-04	1.28E-10	10
10	6	6.51E+01	2.49E-05	33
7	4	1.00E+03	3.84E-04	9
3	1	2.06E+02	7.89E-05	7

Table 4.36: ^{56}Fe ions - Ring pipeline results after 900 s

A	Z	A [Bq]	A_s [Bq/g]	Statistical error
15	8	3.07E+01	1.17E-05	4
14	6	3.01E-01	1.15E-07	7
13	7	1.11E+02	4.25E-05	18
11	6	1.45E+03	5.56E-04	3
10	4	3.35E-04	1.28E-10	10
7	4	1.00E+03	3.84E-04	9
3	1	2.06E+02	7.89E-05	7

Table 4.37: ^{56}Fe ions - Pipeline next to HEBT, results after 1 s

A	Z	A [Bq]	A_s [Bq/g]	Statistical error
16	7	2.96E+02	5.39E-04	16
15	8	1.01E+03	1.83E-03	11
14	6	3.96E-02	7.22E-08	16
13	7	8.99E+01	1.64E-04	27
11	6	4.05E+02	7.37E-04	15
10	4	6.19E-05	1.13E-10	22
7	4	1.67E+02	3.05E-04	21
3	1	4.67E+01	8.51E-05	10

Table 4.38: ^{56}Fe ions - Pipeline next to HEBT, results after 900 s

A	Z	A [Bq]	A_s [Bq/g]	Statistical error
15	8	6.15E+00	1.12E-05	11
14	6	3.96E-02	7.22E-08	16
13	7	3.17E+01	5.77E-05	27
11	6	2.43E+02	4.43E-04	15
10	4	6.19E-05	1.13E-10	22
7	4	1.67E+02	3.05E-04	21
3	1	4.67E+01	8.51E-05	10

Table 4.39: ^{56}Fe ions - Inside the dipole pipeline results after 1 s

A	Z	A [Bq]	A_s [Bq/g]	Statistical error
16	7	1.23E+02	4.20E-03	28
15	8	7.50E+02	2.57E-02	12
14	6	2.73E-02	9.37E-07	20
13	7	3.37E+01	1.16E-03	70
11	6	2.70E+02	9.25E-03	13
10	4	3.61E-05	1.24E-09	40
7	4	1.45E+02	4.97E-03	28
3	1	2.71E+01	9.28E-04	10

Table 4.40: ^{56}Fe ions - Inside the dipole pipeline results after 900 s

A	Z	A [Bq]	A_s [Bq/g]	Statistical error
15	8	4.58E+00	1.57E-04	12
14	6	2.73E-02	9.37E-07	20
13	7	1.19E+01	4.08E-04	70
11	6	1.62E+02	5.55E-03	13
10	4	3.61E-05	1.24E-09	40
7	4	1.45E+02	4.97E-03	28
3	1	2.71E+01	9.28E-04	10

Table 4.41: ^{56}Fe ions - Perimetrical pipeline results after 1 s

A	Z	A [Bq]	A_s [Bq/g]	Statistical error
41	20	3.09E-04	7.30E-11	48
38	17	1.48E+01	3.49E-06	93
36	17	6.46E-04	1.53E-10	20
35	16	1.40E+01	3.30E-06	93
24	11	4.44E+01	1.05E-05	48
17	7	1.25E+01	2.96E-06	93
16	7	6.85E+02	1.62E-04	12
15	6	4.46E+01	1.05E-05	40
15	8	2.21E+03	5.21E-04	6
14	6	1.33E-01	3.14E-08	13
13	7	7.39E+01	1.74E-05	33
11	6	9.02E+02	2.13E-04	15
10	4	8.15E-05	1.92E-11	23
7	4	4.11E+02	9.70E-05	16
3	1	7.44E+01	1.76E-05	8

Table 4.42: ^{56}Fe ions - Perimetrical pipeline results after 900 s

A	Z	A [Bq]	A_s [Bq/g]	Statistical error
41	20	3,09E-04	7,30E-11	48
38	17	1,12E+01	2,64E-06	93
36	17	6,46E-04	1,53E-10	20
35	16	1,40E+01	3,30E-06	93
24	11	4,39E+01	1,04E-05	48
15	8	1,35E+01	3,18E-06	6
14	6	1,33E-01	3,14E-08	13
13	7	2,61E+01	6,15E-06	33
11	6	5,42E+02	1,28E-04	15
10	4	8,15E-05	1,92E-11	23
7	4	4,11E+02	9,70E-05	16
3	1	7,44E+01	1,76E-05	8

As analyzed for the previous particles the most significant activity are ^{3}H and ^{7}Be, with a special highlight to ^{14}C for its long half life. For having a more comprehensive lecture

for the tables the particles with half life minor than 1s, for example ^{16}C and ^{6}He are not listed.

Moreover, the production of ^{41}Ca, ^{36}Cl and ^{24}Na is recorded only in the perimetric pipeline because in this circuit water from the analysis of potable water of Pavia is employed. Their production is due to neutron capture as described in the 3 chapter.

4.4.6. Protons: Beam data and results

The proton beam possesses an energy of 250 MeV and particles per seconds equals to $2E + 10$. These are the maximum allowed values for the synchrotron structure and this irradiation was simulated for a year, that is to say 31536000 s.

As said in the 4.3.3, for improving the statistic the water activation of the cooling system of the utilities is evaluated in bigger volume and then is re-scaled at the actual volume, through the specific activity.

The following tables show the results for the investigated circuits.

Table 4.43: ^{1}H ions - Water activation along the perimeter, results after 1 s

A	Z	A [Bq]	$A_s[Bq/g]$	Real A [Bq]	Statistical error
41	20	1.38E-09	1.11E-17	4.72E-11	15
36	17	9.35E-09	7.54E-17	3.19E-10	18
24	11	4.01E-02	3.24E-10	1.37E-03	30
16	7	3.02E+04	2.44E-04	1.03E+03	9
15	8	4.92E+03	3.97E-05	1.68E+02	6
14	6	2.04E-06	1.64E-14	6.96E-08	10
13	7	3.26E+01	2.63E-07	1.11E+00	30
11	6	2.69E+02	2.17E-06	9.20E+00	8
10	4	1.91E-09	1.54E-17	6.52E-11	18
7	4	3.01E-02	2.43E-10	1.03E-03	11
3	1	1.19E-03	9.58E-12	4.06E-05	9

Table 4.44: ^{1}H ions - Water activation along the perimeter, results after 900 s

A	Z	A [Bq]	$A_s[Bq/g]$	Real A [Bq]	Statistical error
41	20	1.38E-09	1.11E-17	4.72E-11	18
36	17	9.35E-09	7.54E-17	3.19E-10	15
24	11	3.96E-02	3.20E-10	1.35E-03	30
15	8	3.01E+01	2.43E-07	1.03E+00	6
14	6	2.04E-06	1.64E-14	6.96E-08	10
13	7	1.15E+01	9.26E-08	3.92E-01	30
11	6	1.62E+02	1.30E-06	5.53E+00	8
10	4	1.91E-09	1.54E-17	6.52E-11	18
7	4	3.01E-02	2.43E-10	1.03E-03	11
3	1	1.19E-03	9.58E-12	4.06E-05	9

Table 4.45: ^{1}H ions - Pipeline next to HEBT line, results after 1 s

A	Z	A [Bq]	$A_s[Bq/g]$	Statistical error
16	7	2.10E+02	3.83E-04	24
15	8	2.41E+01	4.39E-05	7
14	6	1.93E-08	3.51E-14	15
13	7	5.36E-01	9.76E-07	27
11	6	2.25E+00	4.10E-06	9
7	4	3.01E-04	5.49E-10	17
3	1	1.03E-05	1.87E-11	7

Table 4.46: ^{1}H ions - Pipeline next to HEBT line, results after 900 s

A	Z	A [Bq]	$A_s[Bq/g]$	Statistical error
15	8	3.51E-01	6.39E-07	7
13	7	2.21E-01	4.03E-07	27
11	6	1.62E+00	2.94E-06	9
7	4	3.01E-04	5.49E-10	17
3	1	1.31E-05	2.38E-11	7

Table 4.47: ^{1}H ions - Ring pipeline results after 1 s

A	Z	A [Bq]	$A_s[Bq/g]$	Statistical error
16	7	3.11E+03	1.19E-03	7
15	8	2.46E+02	9.41E-05	8
14	6	1.59E-07	6.08E-14	7
13	7	2.89E+00	1.11E-06	20
11	6	1.47E+01	5.64E-06	10
10	4	7.27E-11	2.78E-17	14
7	4	8.67E-04	3.32E-10	11
3	1	7.58E-05	2.90E-11	7

Table 4.48: ^{1}H ions - Ring pipeline results after 900 s

A	Z	A [Bq]	$A_s[Bq/g]$	Statistical error
15	8	1.50E+00	5.75E-07	8
14	6	1.59E-07	6.08E-14	7
13	7	1.02E+00	3.91E-07	20
11	6	8.85E+00	3.39E-06	10
10	4	7.27E-11	2.78E-17	14
7	4	8.67E-04	3.32E-10	11
3	1	7.58E-05	2.90E-11	7

Table 4.49: ^{1}H ions - Inside the dipole pipeline results after 1 s

A	Z	A [Bq]	$A_s[Bq/g]$	Statistical error
16	7	5.25E+01	1.80E-03	44
15	8	1.55E+01	5.32E-04	19
14	6	1.25E-08	4.29E-13	15
13	7	3.40E-01	1.17E-05	17
11	6	1.30E+00	4.47E-05	21
7	4	5.65E-05	1.94E-09	27
3	1	7.58E-06	2.60E-10	10

Table 4.50: ^{1}H ions - Inside the dipole pipeline results after 900 s

A	Z	A [Bq]	$A_s[Bq/g]$	Statistical error
15	8	1.58E-01	5.40E-06	9
14	6	9.95E-09	3.41E-13	14
13	7	1.19E-01	4.08E-06	17
11	6	8.51E-01	2.92E-05	14
7	4	8.16E-05	2.80E-09	27
3	1	8.84E-06	3.03E-10	10

These tables represent less activation respect to heavy ions, because protons have less energies and generate less secondary neutrons.

The most relevant radionuclides are ^{7}Be and ^{3}H for their high activity and long half life. The production of ^{14}C decreases, because protons have lower energy levels so they can generate less secondary neutrons. Moreover, it is remarkable the presence of short lived particles, such as ^{11}C and ^{15}O, also in the detector after 900s.

As regard the perimetric pipeline, the production of ^{41}Ca, ^{36}Cl and ^{24}Na is due to neutron capture for the presence of impurities from the analysis of potable water of Pavia.

The fact that high errors are sometimes still shown is not so relevant, because they are present in the detector investigated after 1s, but they decays and not revealed after 900s.

4.4.7. Comparison among the main produced radionuclides

This part is dedicated to visual plots of the results to provide a fast comparisons among the different accelerated ions. The main produced radionuclides are ^{3}H, ^{7}Be, ^{11}C and ^{13}N. Therefore, their histograms are placed for the synchrotron cooling water circuit and the utilities. Furthermore, it is pointed out that the carbon ions are able to produce more activities. Other important radionuclides as ^{14}C, ^{10}Be and ^{36}Cl are produced in traces, for these reasons they are not reported.

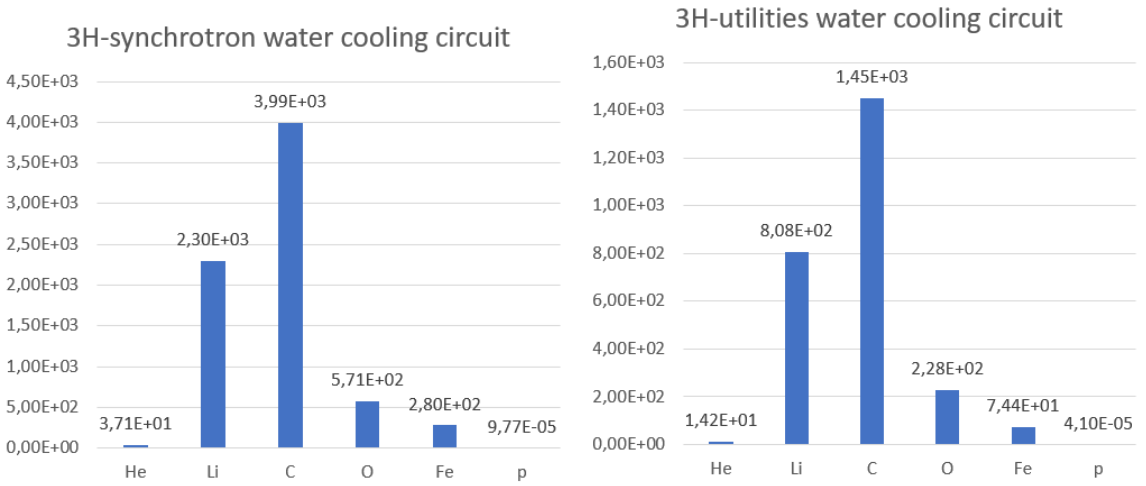

Figure 4.9: ^{3}H activity [Bq] per year

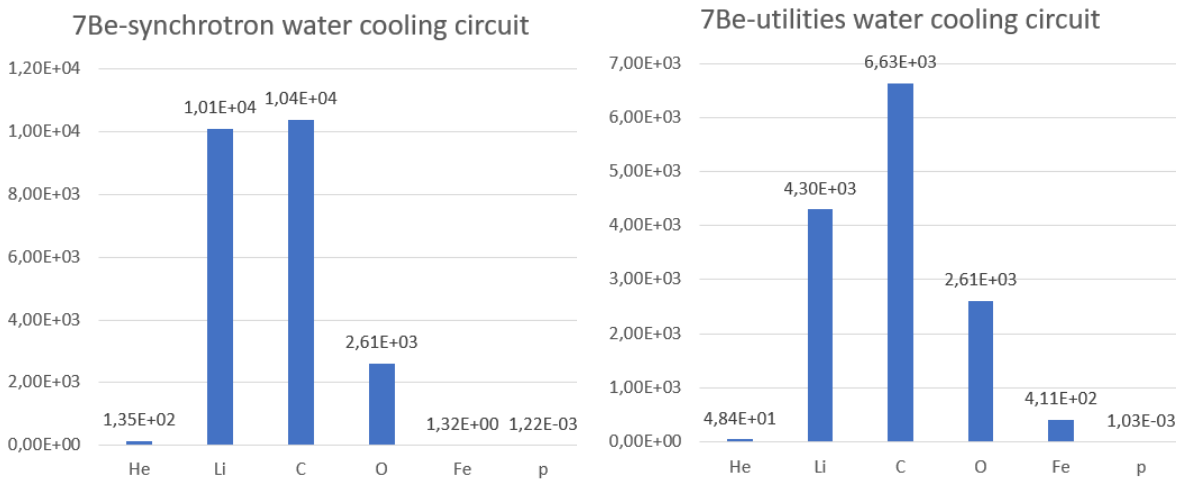

Figure 4.10: ^{7}Be activity [Bq] per year

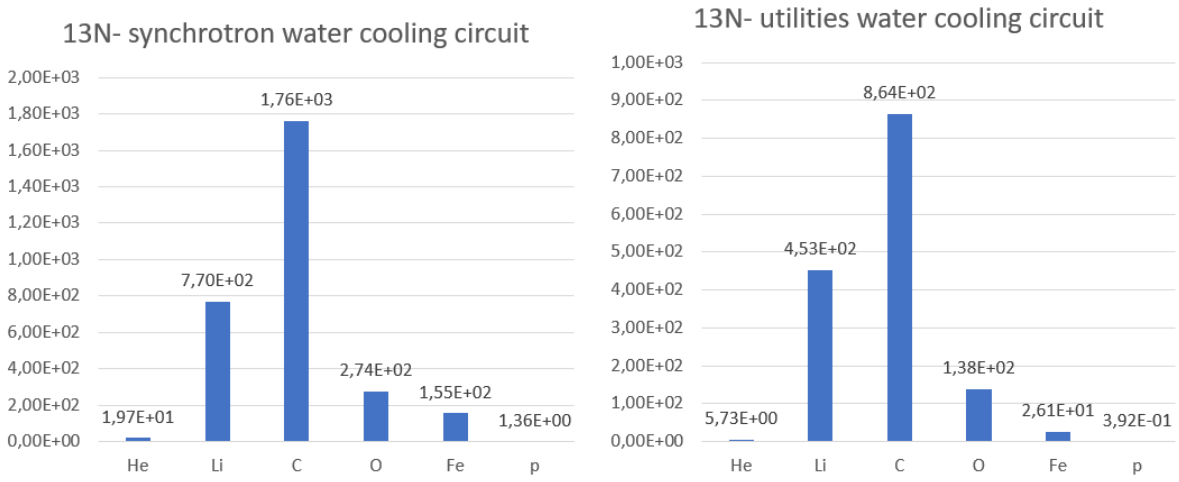

Figure 4.11: ^{13}N activity [Bq] per year

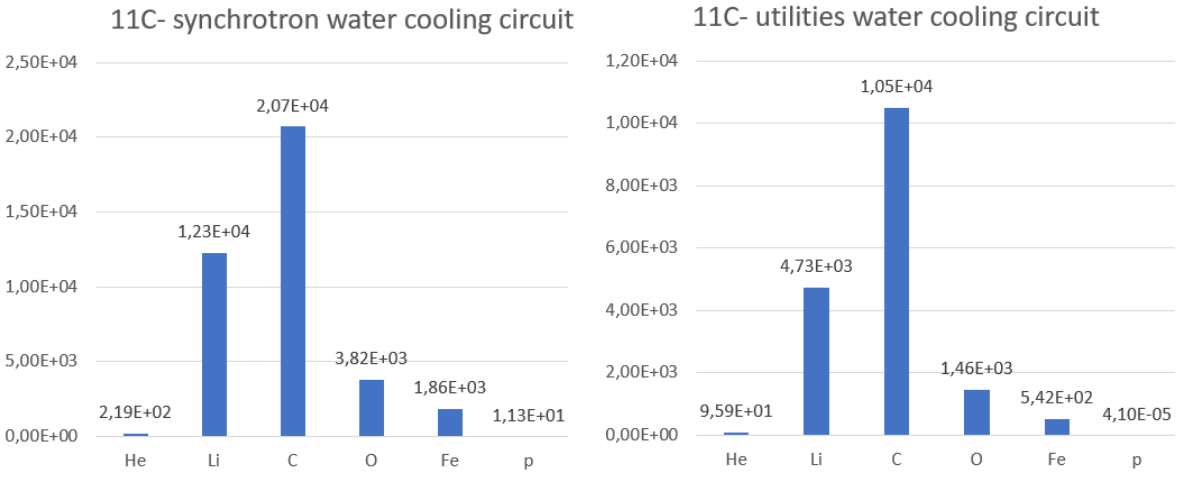

Figure 4.12: ^{11}C activity [Bq] per year

5 | Hitachi simulation

This chapter is dedicated to the analysis of water activation as regards the Hitachi facility. As already discussed in the second chapter, a new synchrotron dedicated only to prototherapy will be built, thanks to a collaboration between CNAO Foundation and Hitachi.

5.1. Water activation in Hitachi

The water activation study is developed to evaluate the decommissioning of the facility: to perform a proper disposal is necessary to know the produced particles with their activity for radioprotection reasons.

To evaluate the decommissioning it is important to know the irradiation fields and for how much time they are performed. In order to estimate the water activation, the beam transport of the protontherapy has been studied by the radioprotection office at CNAO and it is discussed in the first paragraph, followed by the design of the simulation and its results.

5.2. Transport Model

The transport model developed by the radioprotection group at CNAO consists of a similar model of loss respect to the actual synchrotron: the main loss-points are located in correspondence with the four magnets of the ring and along the transport beam line. This line has two loss-points: the Beam Damper and the Faraday cup. The beam operates according to the request of the therapy, so it has to switch on and off instantly, thanks to the employment of the beam Damper. Additionally, the Faraday cup is an instrument able to measure the exact number of charged particles that hit the cup through the resulting current.

The main difference with the actual synchrotron is the presence of a gantry at the end of the line. This element deflects the beam of 270° and permits to rotate 360° around

the patient, to provide the most accurate dose to the lesion, but, on the other hand, the distribution of losses are following the whole circumference of the beam. Therefore, the gantry contributes widely to the losses, as it appears in the table with four isocenter points 5.1.

Table 5.1: Percentages of loss-points in the synchrotron

Zone	percentage of loss [%]
Magnet 1	5.9
Magnet 2	5.9
Magnet 3	5.9
Magnet 4	5.9
ESD	7.7
Faraday Cup	8.6
Beam Damper	6.0
Profile monitor	2.5
Isocenter 8a	12.9
Isocenter 8b	12.9
Isocenter 8c	12.9
Isocenter 8d	12.9

5.3. Hitachi model on FLUKA

5.3.1. Geometry

The Hitachi synchrotron has a less complex layout, thanks to the fact that only protons will be accelerated and at lower energies than the heavy ions.

The simulation consists of an investigation of the water of the cooling system of the utilities. Similar to the present synchrotron, the circuit of the utilities is composed of pipes along all the walls of the accelerator. Therefore, this circuit is recreated with a pipeline along all the perimeter of the synchrotron room and also the treatment room, respecting the original layout. This area has a particular interest, because of the presence of the gantry, that can generate beam losses and secondary particles, that can travel around the room and activate the water.

In addition, the project of the cooling system of the synchrotron is not clear yet: it is probable that a pipeline inside the ring is placed and, in that case, the calculus of specific

activity caused by the acceleration of protons developed for the actual synchrotron 4.4.6 are reliable.

As it appears in the following picture 5.1, the wall pipeline is placed at the same height as the beam and water is considered static, for simulating the worst scenario.

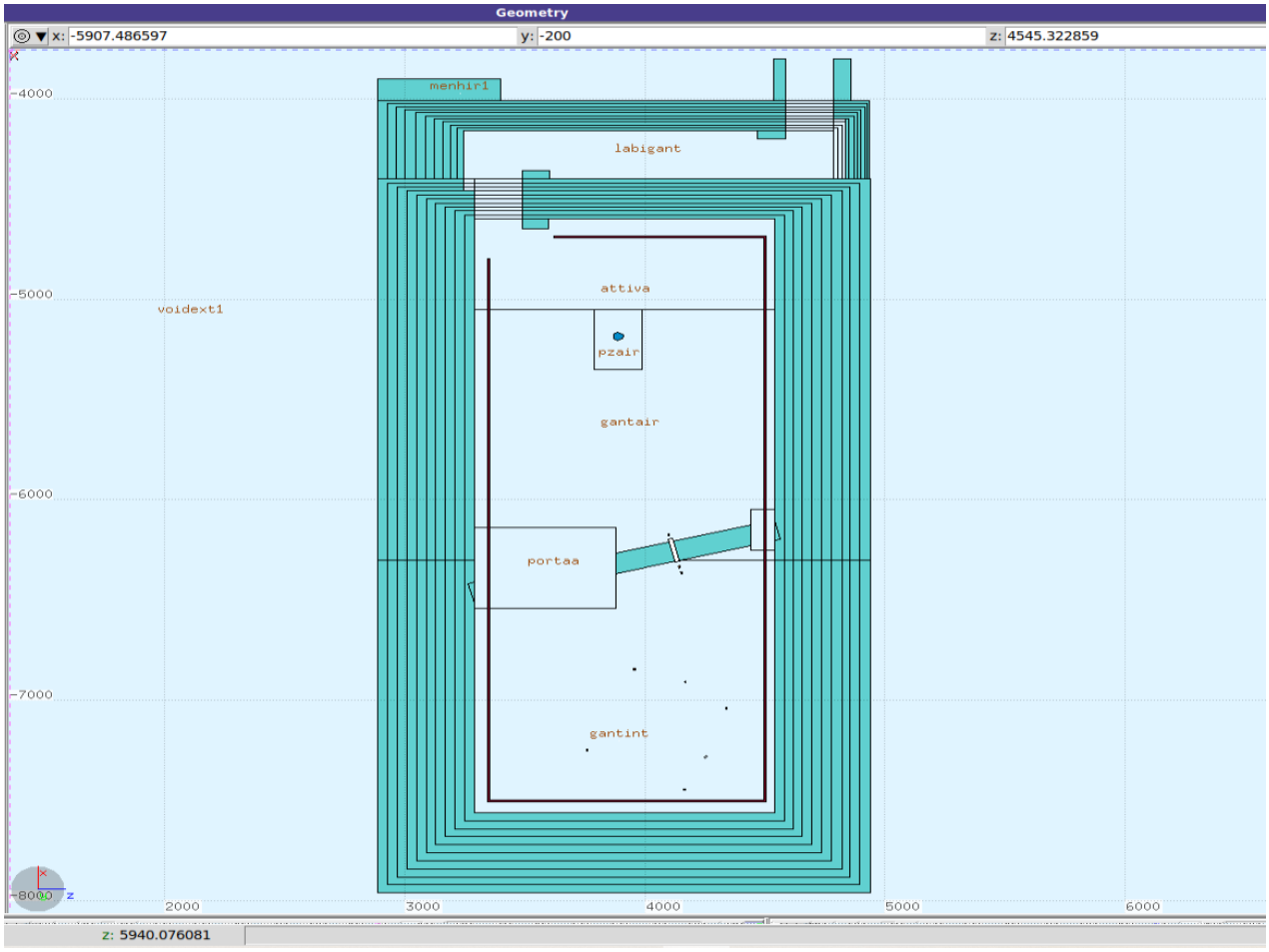

Figure 5.1: Hitachi simulated structure, top view at beam height. The water pipes are perimetrical and appears red.

The dimension of the pipes are the following:

- diameter= 10.2 cm
- length according to the facing wall= 27 m, 28 m, 8.8 m and 11.6 m
- total volume= 611.7 l

5.3.2. Water characteristics

In the cooling system of the utilities of Hitachi, softened water is present, but it is simulated the composition of water coming from the analysis of potable water from the water supply of Pavia. This choice is done to foresee the worst water activation and the table 3.2 shows the used values.

This table is simulated on FLUKA through the creation of a new material through the use of the COMPOUND card and then it is possible to allocate it to a particular region, like the perimetric pipeline.

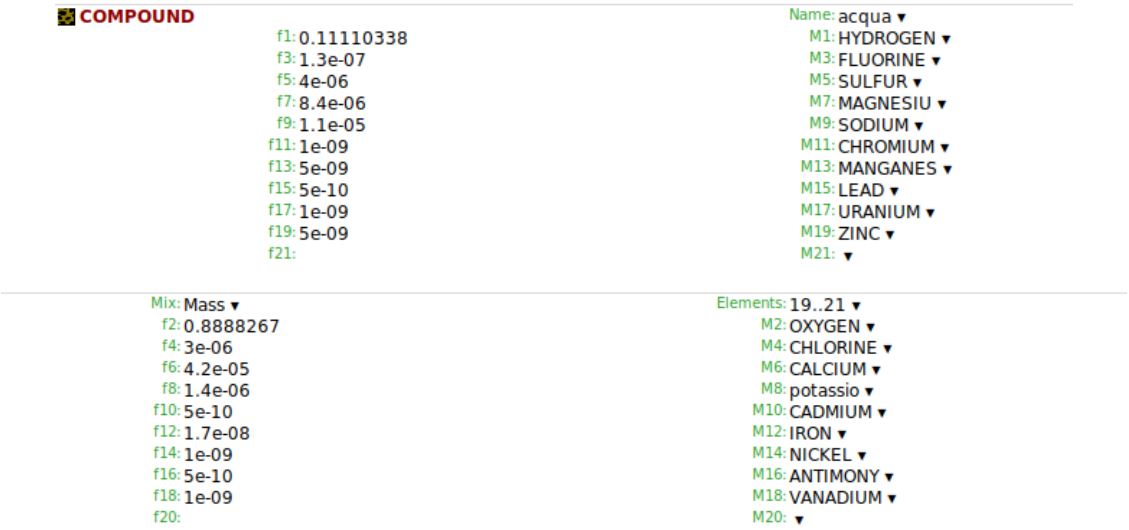

Figure 5.2: Compound card employed for Hitachi simulation

5.3.3. Beam loss model in FLUKA

The transport of the beam is simulated in FLUKA thanks to a routine called *Source.f*. The complete routine is written in Fortran77. The losses are the results of the instruction generated by the code, that is composed of IF blocks of the loss with its percentage.

The model here described is simulated in an analogous way to the actual synchrotron: in the ring the losses are four in correspondence of the four magnets and are created as a primary beam, but tangential to the circumference. The Faraday cup and the Beam Dumper losses are placed tangential to the transport beam line. All these loss-points are simulated through the employment of a primary beam hitting a block of iron or copper, to be more realistic as possible.

The innovative part of the routine is the simulation of the gantry: the losses are following the 360° of rotation, so the idea is to approximate the geometry through four isocenters

distant at 90° from each other and their losses split equally, with a percentage of $12,9\%$ each.

5.3.4. Activation and Scoring Cards

The used card for describing the activation process and scoring are the same as said in the 4.3.4 4.3.5 paragraphs.

The only difference is the values employed: here the simulation consists of protons with energy of $230\,MeV$ and profile of irradiation of $2.13E+10$ particles per second simulated for 20 years, described in the card IRPROFIle.

5.4. Protontherapy: water activation results

In this paragraph the tables with water activation results are reported. The investigated area is detected after $1\,s$ and after $900\,s$, as it is shown in the following tables.

Table 5.2: Wall pipeline results after 1 s

A	Z	A [Bq]	A_s [Bq/g]	Statistical error
41	20	5.87E-02	9.59E-08	26
36	17	9.93E-02	1.62E-07	25
24	11	1.68E+02	2.75E-04	28
16	7	3.05E+04	4.98E-02	10
15	6	3.48E+02	5.69E-04	91
15	8	8.60E+04	1.41E-01	7
14	6	8.99E+01	1.47E-04	13
14	8	8.32E+02	1.36E-03	20
13	7	2.94E+03	4.80E-03	35
11	6	4.83E+04	7.89E-02	12
10	4	1.43E-01	2.33E-07	26
10	6	2.84E+03	4.64E-03	21
7	4	1.26E+04	2.06E-02	15
3	1	4.48E+04	7.32E-02	11

Table 5.3: Wall pipeline results after 900 s

A	Z	A [Bq]	A_s [Bq/g]	Statistical error
41	20	5.87E-02	9.59E-08	26
36	17	9.93E-02	1.62E-07	25
24	11	1.66E+02	2.72E-04	28
15	8	5.26E+02	8.59E-04	7
14	6	8.99E+01	1.47E-04	13
14	8	1.22E-01	2.00E-07	20
13	7	1.04E+03	1.69E-03	35
11	6	2.90E+04	4.74E-02	12
10	4	1.43E-01	2.33E-07	26
7	4	1.26E+04	2.06E-02	15
3	1	4.48E+04	7.32E-02	11

Analyzing the results, the most relevant radionuclides are ^{41}Ca, ^{36}Cl, ^{7}Be, ^{3}H and ^{14}C, due to their major production and their long half life. ^{41}Ca, ^{36}Cl and ^{24}Na are present for the employment of the analysis of potable water of Pavia, showing that milligrams of the added impurities can conduce to the production of other radiactive elements. As listed in the 3 chapter, their formation is due to neutron capture.

Furthermore traces, of ^{10}Be are formed, an other long life radionuclide that can not be neglected.

^{15}C has an higher error, because for the program it is more difficult to provide a valid estimation when the half life is really short or for the occurrence of exotic reactions. In fact, even though some errors are higher, the most frequent reactions, listed in the 3 chapter, have a reliable and acceptable error. This means that the error of the exotic reactions cannot be improved in a significant way even if increasing the number of primaries.

6 | BNCT simulation

This chapter is dedicated to the water activation in the Boron Neutron Capture Therapy facility. The main difference respect to the previous analysis is the presence of a total different field: thanks to the reaction of accelerated protons on a target of ^{7}Li, that produces ^{7}Be and neutrons, as described in the 2 chapter. Followed by the Beam Shaping Assemblies, neutrons reach the epithermal energies, required for a proper therapy. A relevant and peculiar field is created, that is simulated through a routine provided by Neuboron Therapy System (NTS) and is not public available.

As regards the water activation, this facility has two circuits: the cooling system of the target area and the cooling circuit of the utilities, which is located in the HEBL room. The importance of their analysis stands for the fact that the cooling systems are placed under the presence of strong neutronic fields. Therefore, the first paragraph deals with the description of the field, the second studies the HEBL room and the third one the target area.

6.1. Source: field and approximation

The simulated source is an epithermal neutron source, that can be used in the BNCT treatments: it is characterized by a cosine angular distribution with an intensity of $2.4x10^{12}\, neutrons\, s^{-1}$.

This source is complex and it is composed of different spectra that are property of Neuboron Therapy System (NTS). No others features are publicly available.

It is employed in both simulations because the goal is to investigate the activation of the cooling system of the target and utilities during the daily work of Boron Neutron Capture Therapy.

6.2. HEBL room simulation in FLUKA

The HEBL room is the location of the High Energy Beam Line and the bending magnets to guide the beam from the tandem accelerator towards the treatment rooms. Before the treatment rooms are located the target to produce the proper neutronic field and they are located one at the right and one at the left of the HEBL room. For these reasons, the presence of an important neutronic field and the cooling pipeline of the utilities lead to the need of an accurate analysis of water activation.

In the next picture, it is noticeable the position of the HEBL room respect to the structure.

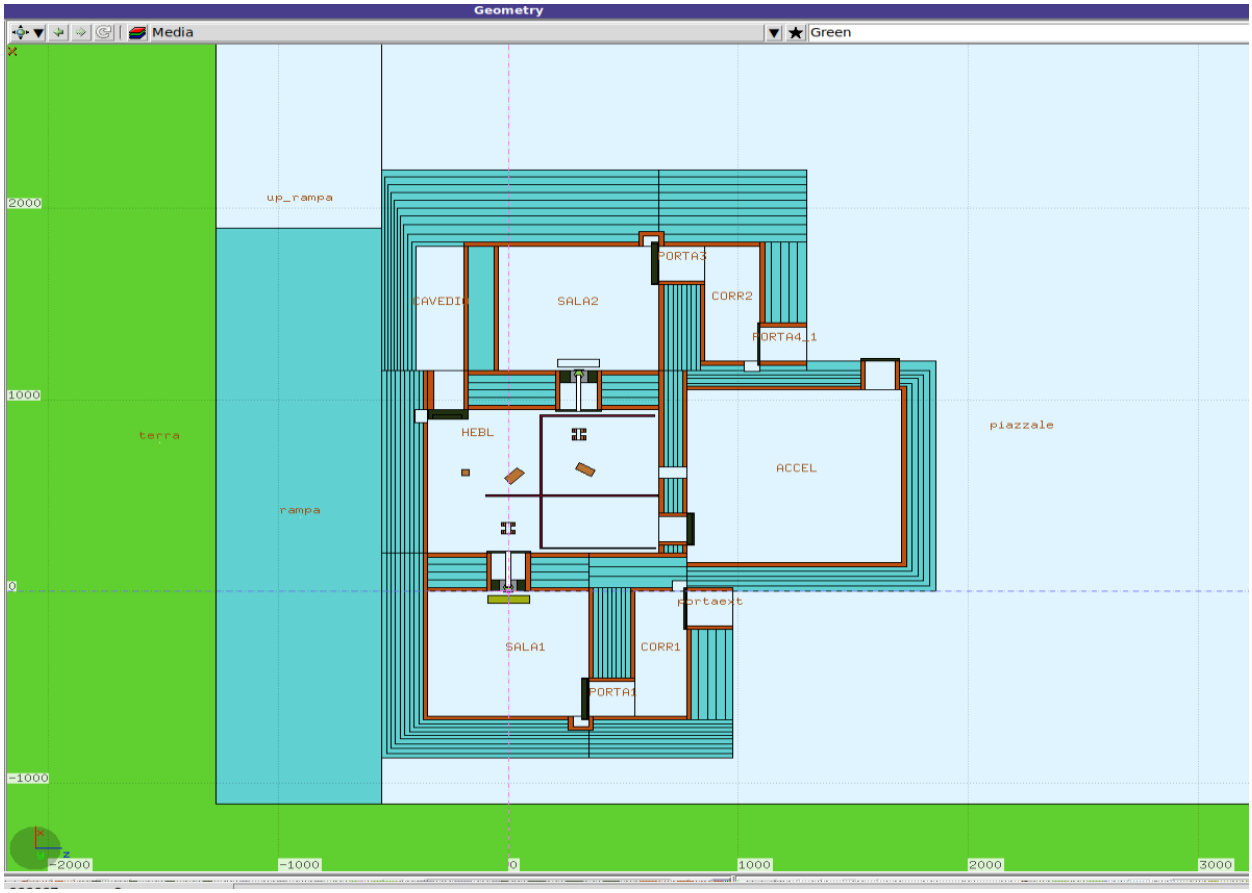

Figure 6.1: BNCT facility: layout from a top view. The HEBL is at the center of the facility: at its right it is located the accelerator room and in parallel the two treatment rooms.

Moreover, the water activation study is performed simulating 20 years of working life of the facility to evaluate the produced radionuclides for the decommissioning. The beam data are described by a routine that keeps in consideration the real spectrum from the neutrons formed by the reaction and the subsequent interactions.

6.2.1. Geometry

In the HEBL room the simulated pipes, as they appear in the figure 6.2, have the following size:

- diameter= 7.6 cm
- lengths of the parallel pipes= 5 m the external ones and 7.5 m the central pipe
- length of the perpendicular pipe= 6.85 m
- total volume= 111.05 l

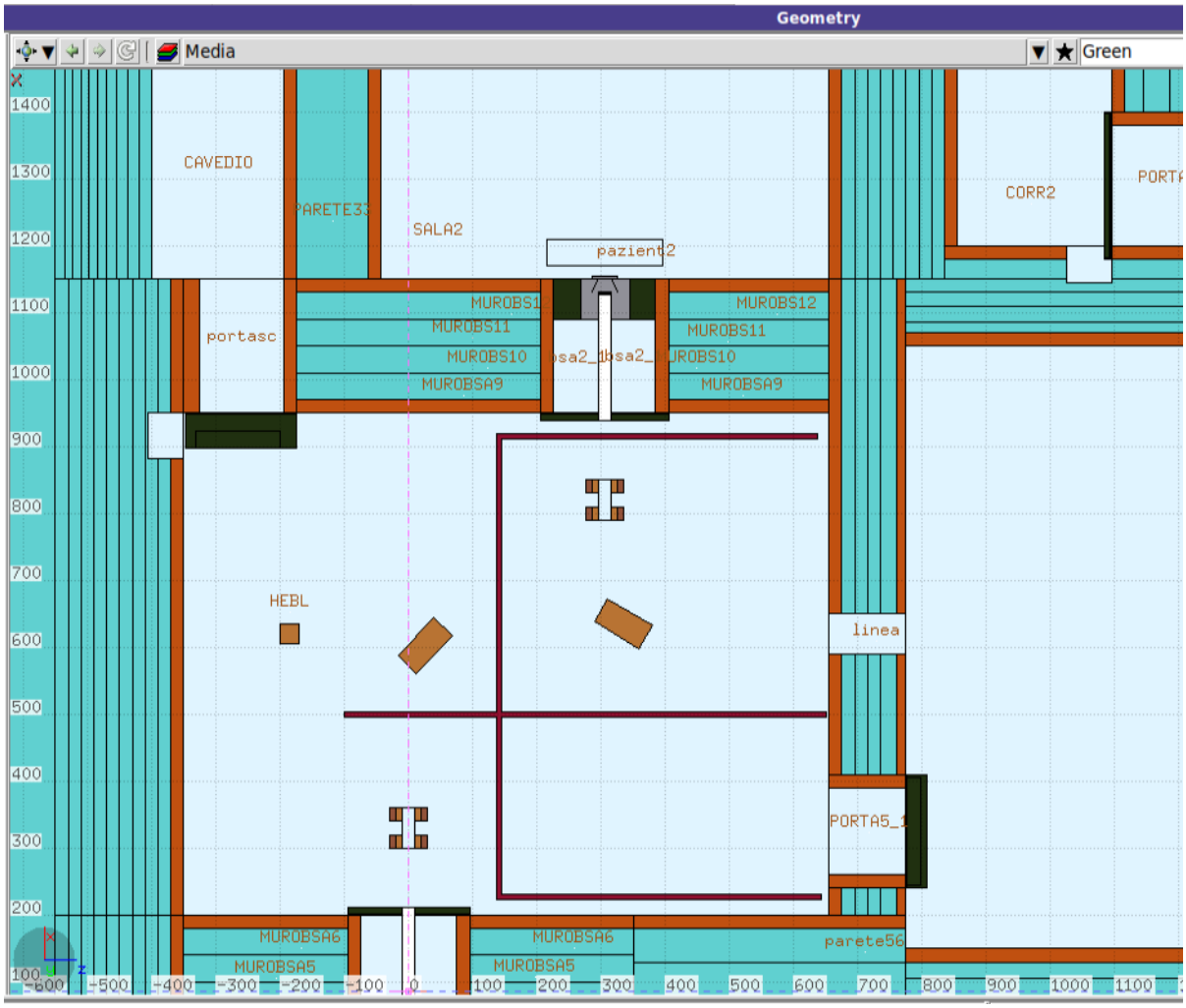

Figure 6.2: Pipeline in HEBL room, top view at beam height

6.2.2. Water characteristics

The pipeline of the utilities is characterized by softened water.

For studying the worst scenario, the potable water from Pavia water supply is simulated with the same properties and quantities of impurities as described in the table 3.2.

In FLUKA, this analysis is expressed through the compound card 6.3 and then the created material is associated to the region of the utilities pipes. Due to the added impurities, the created water appears red as in the 6.2 figure.

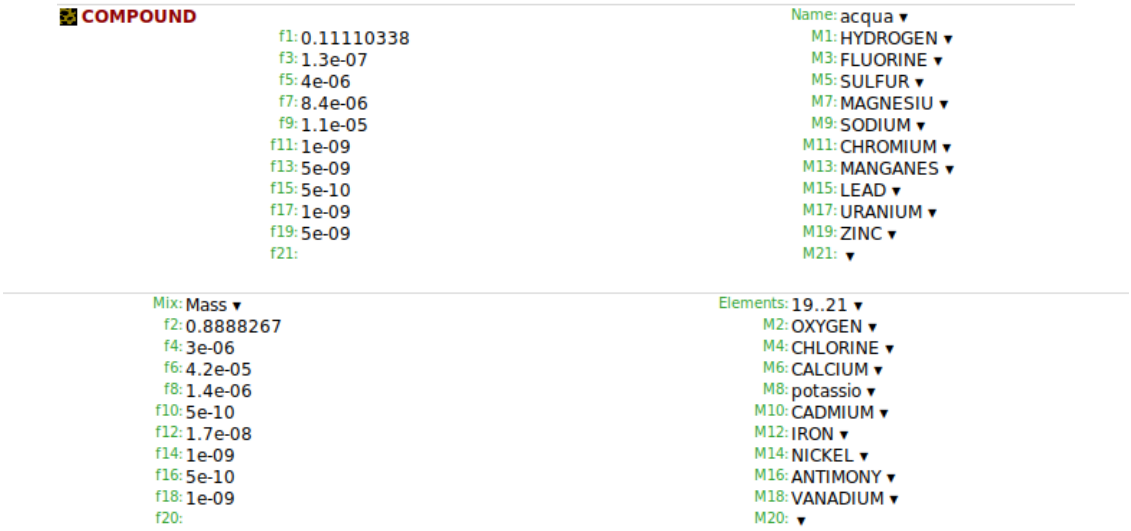

Figure 6.3: Compound card employed for BNCT utilities simulation

6.2.3. Routine

The simulation of the field is actualized by a subroutine Source.f, which is compiled by FLUKA and is different to the others described in the previous chapter. Due to the complexity of this field, the routine is implemented by particularly files that are user-defined and able to provide a complete description of the spectrum. Thanks to the employment of different files, a cumulative spectrum is created.

To assign the respective energy to a particle, a random number, between 0 and 1, is sampled and multiplied by a constant to cover all the energy bins of the spectrum. Through this procedure the interval of energies are determined.

Furthermore, the particles are allocated with a space distribution. This is described in the same subroutine and it is performed with an histogram of the angular bins from 0° to 90° with their relative yield. A random number selects the angular bin that is compared with the cumulative spectrum. After having defined properly the bin, the director cosine of the particles are allocated as the cos and sin of the minimum and maximum of the respective angular bin.

6.2.4. Activation and scoring cards

The selected cards for describing the activation process and scoring are the same as said in the 4.3.4 and 4.3.5 paragraphs.

6.2.5. Results

The results coming from FLUKA are detected after having stopped the beam for a time of 1 s and 900 s.

As a consequence that the formed radionuclides are only long lived particles, the two scoring volumes do not show differences in the produced quantities and in the statistical errors.

Table 6.1: Pipeline results from HEBL room

A	Z	A [Bq]	A_s [Bq/g]	Statistical error
36	17	1.58E+00	1.42E-05	14
14	6	2.30E+02	2.07E-03	28

In BNCT facility, it is present a total different field respect to the synchrotron: just ^{14}C and ^{36}Cl have a production that is detectable for FLUKA. These two particles are relevant for their long half life.

6.2.6. Offline results and comparison

This section is dedicated to the comparison between the results obtained with the simulation of the water cooling system of the utilities, reported in the 6.1 table, and the offline calculus of the water activation in the same circuit.

The investigated area has the same dimensions as the one listed in the 6.3.1 paragraph for a total volume of the pipes equal to 111 l. Furthermore, to provide a solid comparison, the studied water has the same impurities as the simulated water 3.2.

The goal is the estimation of the water activity in the pipeline of the cooling utilities of the HEBL room, which can be reach with the formula 1.2.7:

$$A = \frac{dN}{dt} = -\lambda \cdot N \tag{6.1}$$

The population of the produced radionuclide N is obtained through the reaction rate 3.1,

but in this evaluation the missing element is the flux. In the HEBL room, the neutronic flux depends on the fact that the source is located in the adjacent room, so the intensity of the beam is attenuated by the walls. The design of them is projected to protect the people and the environment. For this reason, the walls have a thickness of 200 cm, which is composed of of boron loaded concrete with 1 % of natural boron for the first 20 cm and followed by ordinary concrete. The employed solution exploits the natural B, that has a cross section of almost $10^3\,b$ for the capture of thermal neutrons and also a good one for the epithermals 6.4.

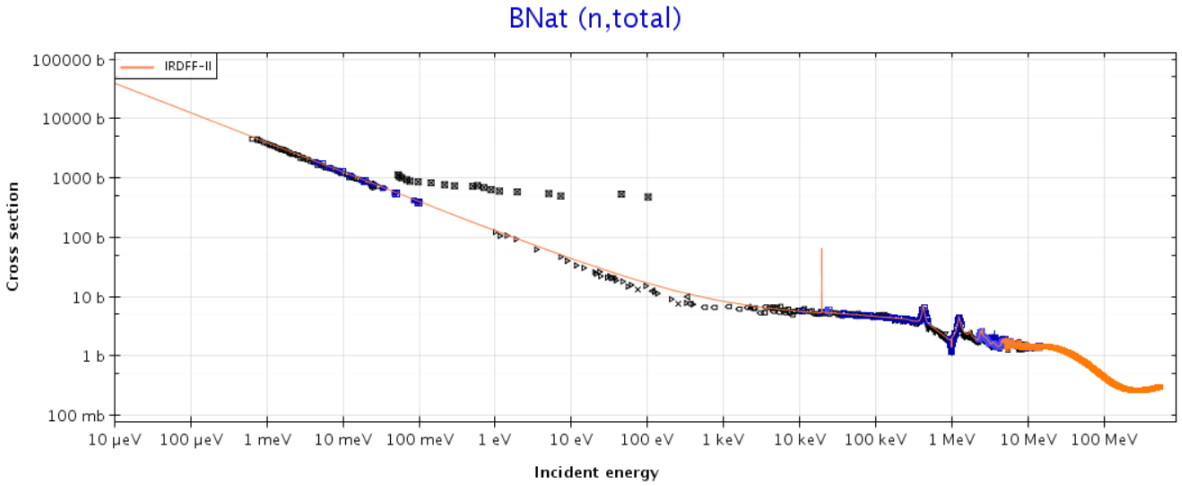

Figure 6.4: Cross section of natural B

To estimate the neutronic flux as a first approximation, the walls are considered to be composed of ordinary concrete for the entire thickness. In this way, the thermal neutron fluence rate ϕ_{th} can be calculated through the use of the formula of Patterson and Wallace (1958), as it is suggested in the NCRP 144 [25]:

$$\phi_{th} = \frac{c * Q_F}{S} \tag{6.2}$$

where Q_F is the yield of fast neutrons, S is the internal area of the considered room and c is a constant that depends on the thermalization process of the fast neutrons, they slow down with their interaction with the walls. The value proposed by Patterson and Wallace is 1.25, but in recent papers [22] [34] [35] the constant was studied more in detail discovering a dependence with the energy. For performing this estimation, the neutron beam was considered mono-energetic, while, on the other hand, in Boron Neutron Capture Therapy a more complex situation is present because the beam is described by different spectra. Nevertheless, a reliable approximation due to the thermalization events is to

consider the energy equal to $10\,keV$, in this particular situation by the Woo Lee [22] estimation the c constant is equal to 4.49.

Energy [MeV]	C	Energy [MeV]	C
~ 1.0E-5	6.20	~ 8	1.31
~ 1.0E-4	5.18	~ 9	1.29
~ 1.0E-3	4.87	~ 10	1.28
~ 1.0E-2	4.49	~ 14	1.12
~ 1.0E-1	4.07	~ 17	1.28
~ 1	3.68	~ 20	1.42
~ 2	3.13	~ 25	1.20
~ 3	2.43	~ 30	1.08
~ 4	2.05	~ 70	1.01
~ 5	2.12	~ 90	1.10
~ 6	1.69	~ 100	1.32
~ 7	1.62		

Figure 6.5: c constant values [22]

Subsequently, ϕ_{th} is multiplied by a $1/\eta$ factor for considering the B in the walls is added: a coefficient η equals to 10^4 is placed. This value is verified by the fact that the actual flux in the HEBL room is equal to $10^3\,n\,s^{-1}$.

The described procedure performs the activity per second. Moreover, to estimate the activity per year, the result is multiplied by $2000\,h$, that are the working hours per year, and then evaluated for 20 years to compare them with the performed simulations 6.1.

Reaction	cross section	isotopic aboundance	water analysis	mass	number of moles	Reaction Rate	λ	Activity per second	Activity per year	Acitivity per 20 years
	[barn]		[g/cm3]	[g]	[mol]	[particles/s]	[1/s]	[Bq/s]	[Bq/y]	[Bq]
H2(n,γ)H3	5,00E-04	1,50E-04		1,85E+00	1,85E+00	5,58E-01	1,78E-09	9,96E-10	7,17E-03	1,43E-01
O17(n,α)C14	2,50E-01	3,80E-04		4,70E+00	2,35E+00	3,54E+02	3,84E-12	1,36E-09	9,77E-03	1,95E-01
Ca40(n,γ)Ca41	4,00E-01	9,70E-01	4,20E-05	6,30E-03	1,53E-04	3,68E-02	3,08E-13	1,13E-14	8,15E-08	1,63E-06
Ca40(n,α)Ar37	2,00E-03	9,70E-01	4,20E-05	6,30E-03	1,53E-04	1,84E-04	2,29E-07	4,22E-11	3,04E-04	6,07E-03
Ca44(n,γ)Ca45	8,00E-01	2,09E-02	4,20E-05	6,30E-03	3,29E-06	1,58E-03	4,92E-08	7,79E-11	5,61E-04	1,12E-02
Ca46(n,γ)Ca47	7,00E-01	4,00E-05	4,20E-05	6,30E-03	6,30E-09	2,66E-06	1,77E-06	4,69E-12	3,38E-05	6,76E-04
Na23(n,γ)Na24	6,00E-01	1,00E+00	1,10E-05	1,65E-03	7,17E-05	2,59E-02	1,29E-05	3,34E-07	2,40E+00	4,80E+01
Cl35(n,γ)Cl36	5,00E+01	7,58E-01	3,00E-06	4,50E-04	9,62E-06	2,90E-01	7,30E-14	2,11E-14	1,52E-07	3,04E-06
Cl35(n,p)S35	5,00E-01	7,58E-01	3,00E-06	4,50E-04	9,62E-06	2,90E-03	9,17E-08	2,66E-10	1,91E-03	3,82E-02
Cl35(n,α)P32	7,00E-05	7,58E-01	3,00E-06	4,50E-04	9,62E-06	4,05E-07	5,61E-07	2,27E-13	1,64E-06	3,28E-05
Na23(n,γ)Na24	6,00E-01	1,00E+00	1,10E-05	1,65E-03	7,17E-05	2,59E-02	1,29E-05	3,34E-07	2,40E+00	4,80E+01
Cd108(n,γ)Cd109	9,00E-01	8,90E-03	5,00E-10	7,50E-08	5,96E-12	3,23E-09	1,77E-08	5,72E-17	4,12E-10	8,24E-09
Cd114(n,γ)Cd115	2,00E-01	2,87E-01	5,00E-10	7,50E-08	1,92E-10	2,32E-08	1,82E-07	4,22E-15	3,04E-08	6,08E-07
Cd116(n,γ)Cd117	7,00E-02	7,49E-02	5,00E-10	7,50E-08	5,02E-11	2,11E-09	5,82E-05	1,23E-13	8,86E-07	1,77E-05
Cr50(n,γ)Cr51	1,50E+01	4,35E-02	1,00E-09	1,50E-07	5,82E-11	5,26E-07	2,90E-07	1,52E-13	1,10E-06	2,19E-05
Cr54(n,γ)Cr55	6,00E-02	2,37E-02	1,00E-09	1,50E-07	6,82E-11	2,46E-09	3,30E-03	8,14E-12	5,86E-05	1,17E-03
Fe54(n,γ)Fe55	4,00E-01	5,85E-02	1,70E-08	2,55E-06	2,87E-09	6,91E-07	8,14E-09	5,63E-15	4,05E-08	8,10E-07
Fe58(n,γ)Fe59	1,00E-01	2,12E-02	1,70E-08	2,55E-06	9,68E-10	5,83E-08	4,87E-10	2,84E-17	2,05E-10	4,09E-09
Ni58(n,γ)Ni59	4,50E-01	6,81E-01	1,00E-09	1,50E-07	1,74E-09	4,71E-07	2,93E-13	1,38E-19	9,95E-13	1,99E-11
Ni62(n,γ)Ni63	2,00E+00	3,63E-02	1,00E-09	1,50E-07	9,29E-11	1,12E-07	2,20E-10	2,46E-17	1,77E-10	3,54E-09
Ni64(n,γ)Ni65	1,50E-01	9,26E-03	1,00E-09	1,50E-07	2,36E-11	2,14E-09	7,64E-05	1,63E-13	1,18E-06	2,35E-05
Pb204(n,γ)Pb205	7,00E-02	1,40E-02	5,00E-10	7,50E-08	5,07E-12	2,14E-10	1,47E-15	3,13E-25	2,25E-18	4,51E-17
Pb208(n,γ)Pb209	7,00E-05	5,24E-01	5,00E-10	7,50E-08	1,90E-10	8,00E-12	5,92E-05	4,74E-16	3,41E-09	6,82E-08

Figure 6.6: Water activation in HEBL room results

The offline calculus shows that no relevant productions of other radionuclides are present. On the other hand, some differences are observed: some radionuclides, as ^3H and ^{24}Na, show an increase of activity, at the same time ^{36}Cl and ^{14}C has a decrease. This phenomenon is due to the employed approximation in this calculus, while a Monte Carlo

method can consider all the phenomena and the statistic events at the same time. Nevertheless, this evaluation was needed to assure that no other radionuclides are produced with an important quantity.

6.3. Target simulation in FLUKA

The target simulation is a crucial point: it is where the production of neutrons takes place and the highest energies of the facility are focused. The study is performed to estimate which particles and their quantity are produced in a target lifetime, to assure the safety to all the workers and to execute the ordinary maintenance. The target lifetime is equal to $5000\,mA-h$ and the employed current is $10\,mA$, so the life of the target will be $500\,h$. Nevertheless, the supposed working time of the target is almost $4\,h$ so it means that can last for $655\,d$.

6.3.1. Geometry

The target zone is composed of an aluminium void chamber with a cylindrical shape, in which protons are accelerated, followed by a thin layer of lithium supported on a thicker part made of copper. After the core of the neutrons generation, a water region is present with the purpose of cooling the target and has the following dimensions:

- r= 7 cm
- h= 0.3 cm
- Total volume= 0.046 l

In addition, this water is collected by three pipes that are parallels to the cylindrical structure and provide a water circulation. This pipeline possesses a particular shape: the three pipes start from the cooling region in a parallel direction, followed by a vertical length and then a parallel part to the void chamber. Here, the real size are placed:

- r= 0.5 cm
- h= 4 cm
- Total volume= 0.0094 l
- r= 0.5 cm
- h= 8.7 cm
- Total volume= 0.02 l

- r= 0.5 cm
- h= 32 cm
- Total volume= 0.075 l

The total volume of the simulated pipeline is equal to 0.15 l.

The simulated structure is an exact reproduction of the original structure and it is not publicly available. For this reason, no figure of the target are placed.

6.3.2. Water characteristics

The cooling water in the target area is demineralized. For describing a conservative situation, where some impurities are present, the analysis of DAFNE accelerator from INFN, National Laboratory of Frascati, are employed as it was performed for the synchrotron circuit with 3.1 table. Moreover, for the same reason, the simulated water is considered static.

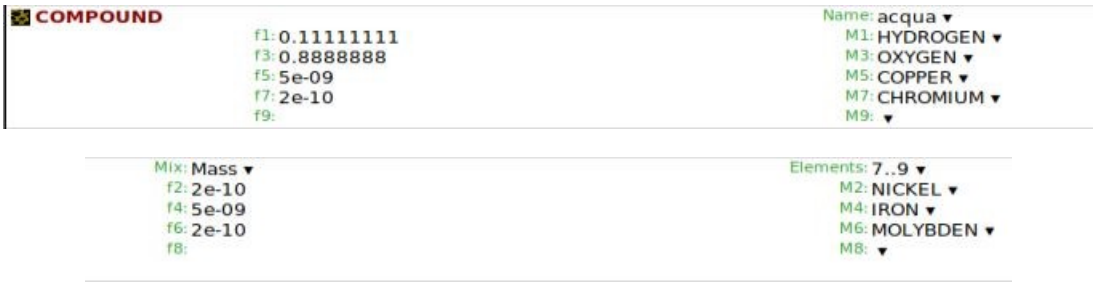

Figure 6.7: Compound card employed for BNCT target cooling system

6.3.3. Routine

The employed routine is the same as the one described in the 6.2.3 paragraph.

6.3.4. Activation cards

The employed cards for describing the activation process and scoring are the same as said in the 4.3.4 4.3.5 paragraphs.

The only difference is the employment of the USERTRACK card: if activated, it can provide the estimation of the fluence for a track-length detector. Thanks to this card, it is possible to know how many neutrons are passing in the selected region in the investigated time. In this case the region is starting from the support of the ^{7}Li target, that is made of Cu and ending with the water volume, in this way it is possible to consider

all the passing particles. Moreover, the obtained result is the distribution of fluence in double differential depending on the solid angle and the energy, with unit of measurement $[particles * cm^{-2} * GeV * primaries^{-}1]$. These data are used in the 6.3.6 paragraph.

6.3.5. Results

The beam data are simulated for $655\,d$, that is the supposed lifetime of the target with 1E+13 particles per second. The areas immediately after the target and the three pipes are investigated after 1 s and after 900 s, but due to the fact that only long half life radionuclides are present, only a time interval is represented:

Table 6.2: Pipeline results

A	Z	A [Bq]	A_s [Bq/g]	Statistical error
14	6	2,01E+02	1,91E+00	4

Table 6.3: Target area results

A	Z	A [Bq]	A_s [Bq/g]	Statistical error
14	6	3.60E+02	7.79E+00	20

Therefore, the water circulation forms a total activity of ^{14}C equal to $5.61E+02\,Bq$ and a specific activity of $3.74\,\frac{Bq}{g}$. These values are relevant due to the quantity of produced radionuclide and the long half life. It was surprising the absence of tritium, so this is investigated in the following section.

6.3.6. Offline analysis

The water region after the target is the one most invested by neutrons, therefore an offline calculus is performed to verify the activity of ^{3}H and ^{14}C.

The production of ^{3}H and ^{14}C is due to the following reactions: $^{2}H(n,\gamma)^{3}H$ and $^{17}O(n,\alpha)^{14}C$. Their quantities are estimated through the reaction rate and the activity through the formula employed in the 6.2.6 paragraph.

Once again, the missing element is the flux that is recovered through to the fluence. The FLUKA card USERTRACK allows to estimate the fluence of the neutrons passing through the region of ^{7}Li target in $[particles*cm^{-2}*GeV*primaries^{-}1]$. The investigated energy range is from $100\,\mu eV$ to $100\,keV$, after this energy value the fluence is equal to zero.

Janis Web [23] provides the neutron capture cross section of ^{2}H and ^{17}O [3.2, 3.9] and their correspondence energies. Therefore an accurate calculus of the total fluence can be obtained:

$$Total fluence = \Sigma_i \sigma_i E_i * primaries \tag{6.3}$$

where E_i stands for the average energy of the energy interval for that corresponding cross section.

Radionuclide	number of produced particles	λ $[s^{-1}]$	Activity [Bq]
^{3}H	2.84E+04	1,796E-09	4.42E-05
^{14}C	5.56E+06	3.836E-12	2.12E-05

Table 6.4: Results from the offline analysis

As it appears in the 6.4 table, the calculus of the activity shows a low value of activity for both particles. This can explain the absence of ^{3}H from the results obtained by FLUKA. At the same time, the ^{14}C does not fit the expectation. This phenomenon is explained by statistical evaluations: even though the simulation was performed with $4E+09$ particles, it could be difficult for the simulator to provide an accurate results in presence of low activity in a little volume. Moreover, the simulation could overestimate some resonance peaks in the epithermal energies.

7 | The Pavia Sewer case: dose estimation to workers

The CNAO water cooling system is composed of a closed loop in ordinary condition, thanks to the employment of ion exchange resin for the purification. On the other hand, in case of a failure or an accident in the circuit, an emergency pool is placed under the synchrotron room to collect its cooling water. After a proper measurement, the contained water in the emergency pool is released in the Pavia sewer. The same prototype is projected for the protontheraphy and BNCT.

This chapter is dedicated to the calculus of the accidental scenarios where some radionuclides are ending in the drainage system due to a failure of the system. The accidental situations here described are unlikely, because more than one safety system should fail. However, for a complete radioprotection analysis, two scenarios are studied with how much dose rate can provide to the workers of Pavia sewer and which risks are possible.

7.1. Sewer description

The nominal properties of the Pavia sewer are provided by the civil engineers and in this paragraph are discussed the needed characteristics to perform the dose estimation.

The CNAO drainage pipeline is linked to the sewerage of Pavia with a flow rate of $0.3\,ls^{-1}$, that can reach $5\,ls^{-1}$ as maximum.

The collection of all the waters in the principal basin is a phenomenon called corrivation. The average corrivation speed is equal to $0.3\,ms^{-1}$ and the corrivation time is $4\,h$, to reach the basin, that is $4\,km$ far away from CNAO foundation.

The estimation of water consumption per person are $220\,l$ a day, for a total of $15000\,m^3$ a day, considering the 70000 inhabitants of Pavia. The wastewater treatment plant is equipped with decanting tanks with a capacity of $3000\,m^3$, in ordinary circumstances they are partially filled in $3\,h$. The decanting tanks have a line dedicated to the collection

of the sludge, their extraction and purification. The sludge production per person is $1\,kg$ a day [19]. After the purification, the water can be released in the Ticino river with an average flow rate of $300\,m^3s^{-1}$.

7.2. Incident scenario hypothesis

The CNAO radioprotection group has studied the case in which the cooling water and other activated water, used by the departments of medical physicists and nuclear medicine, are ending in the drainage system. In that hypothesis, the following radionuclides are involved with their corresponding activity:

Table 7.1: List of radionuclides that could end in the sewerage

A	Z	A [Bq]	$T_{1/2}$
37	Ar	2.00E+04	35 d
55	Fe	2.00E+04	2.7 y
54	Mn	2.00E+04	312.2 d
51	Cr	1.00E+05	27.7 d
48	V	1.00E+05	15.97 d
49	V	2.00E+04	330 d
41	Ca	1.00E+03	9.94E+04 y
38	Cl	2.00E+06	37.18 m
36	Cl	1.00E+03	3.01E+05 y
35	S	1.00E+06	87.5 d
24	Na	1.00E+06	14.96 h
22	Na	3.00E+04	2.602 y
18	F	3.75E+08	109.7 m
19	O	1.00E+06	27.1 s
15	O	1.00E+06	122.24 s
14	C	1.00E+04	5730 y
14	O	1.00E+06	70.62 s
13	N	1.00E+06	9.96 m
11	C	1.00E+06	20 m
10	Be	1.00E+03	1.39E+06 y
10	C	1.00E+06	19.3 s
7	Be	1.00E+06	55.33 d
3	H	1.00E+06	12.32 y

Analyzing the possible scenarios among the CNAO residual water and the drainage system, the evaluation of the presence of a radioactive $\beta+$ or photons source as an incident scenario is considered.

Particularly, two possible risky situations are faced:

- a worker of the Pavia drainage system is near a pipeline and the radionuclides are passing at $1\,m$ of distance with the corrivation speed of $0.3\,ms^{-1}$;
- a person that is on the walkway over the depuration tanks or that is near the sludge for $200\,h$ per year.

7.2.1. Dose estimation to workers during corrivation

The dose estimation to workers during corrivation is performed under the following assumption: the exposed people are at a distance of $1\,m$ to the involved pipes and are affected by an external irradiation from the photons emitted from radionuclides decays.

The irradiation geometry can be designed as an infinite line, where a point-like source A is travelling at v speed, as it appears 7.1 figure.

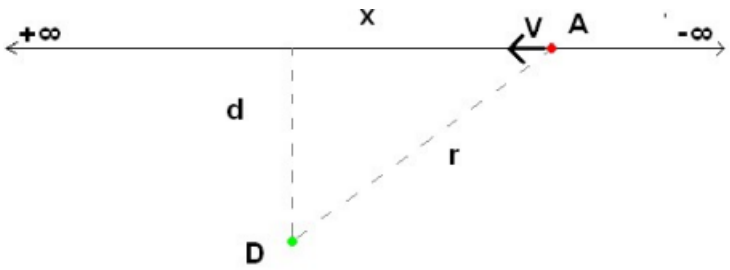

Figure 7.1: Sewer schematic model for dose estimation

The estimation of the ambient dose equivalent H*(10) in the point D at $1\,m$ of distance is performed along the path thanks to the integral:

$$H = \int_{-\infty}^{+\infty} \dot{H}(t)\,dt \tag{7.1}$$

where the following substitution can be performed according to the geometry $\dot{H}(t) = \frac{\dot{H}_0}{r^2}$ and $r^2(t) = d^2 + x^2$. Therefore, the equation becomes:

$$H(t) = \int_{-\infty}^{+\infty} \frac{\dot{H}_0}{(d^2 + x^2)}\,dt \tag{7.2}$$

and remembering that x=vt, the integral can be solved and the result is:

$$H = \frac{\dot{H}_0}{d\,v}\,\pi \tag{7.3}$$

$\dot{H}_0$ can be evaluated in $\frac{\mu Sv}{h}$ thanks to the employment of the specific Gamma-ray costant Γ multiplied by the activity at $1\,m$ and its values are:

- $\dot{H}_0$ for a point like source of $375\,MBq$ of ^{18}F is equal to $64.5\,\frac{\mu Sv}{h}$
- $\dot{H}_0$ for all the others radionuclides listed before is equal to $3\,\frac{\mu Sv}{h}$

At this point, knowing $\dot{H}_0$, $D = 1\,m$ and $v = 0.3ms^{-1}$, H*(10) is equal to $H = 202\,nSv$ in the case of ^{18}F and for all the rest of radionuclides $H = 9\,nSv$.

This evaluation is strongly conservative for the facts that usually the pipeline are placed underground and the radioactive decay is not considered during the corrivation. Therefore, no actual risk is present for the workers or any person that is close to the drain pipeline between CNAO and the dupuration facility.

7.2.2. Dose estimation to people from deputation tank and sludge line

To evaluate the received dose to a worker in the wastewater treatment plant, two subcases are distinct as regards the depuration tank and the sludge line. The first case is a situation where a worker is standing on a walkway over a depuration tank for a long time and an external irradiation can affect the personnel. The second situation involves a worker that stands close to the sludge tank, where the radionuclides are precipitated and absorbed.

To provide a proper estimation, the employment of FLUKA was required. Thanks to the simulation code, a dose map of the H*(10) is provide in $\frac{nSv}{primaries}$ and can be adapted to different activity.

Geometry simulation

The geometry of the investigated tank has a cylindrical shape with the following dimensions:

- radius= $20\,m$
- height= $3\,m$

- total volume= $3768\,m^3$

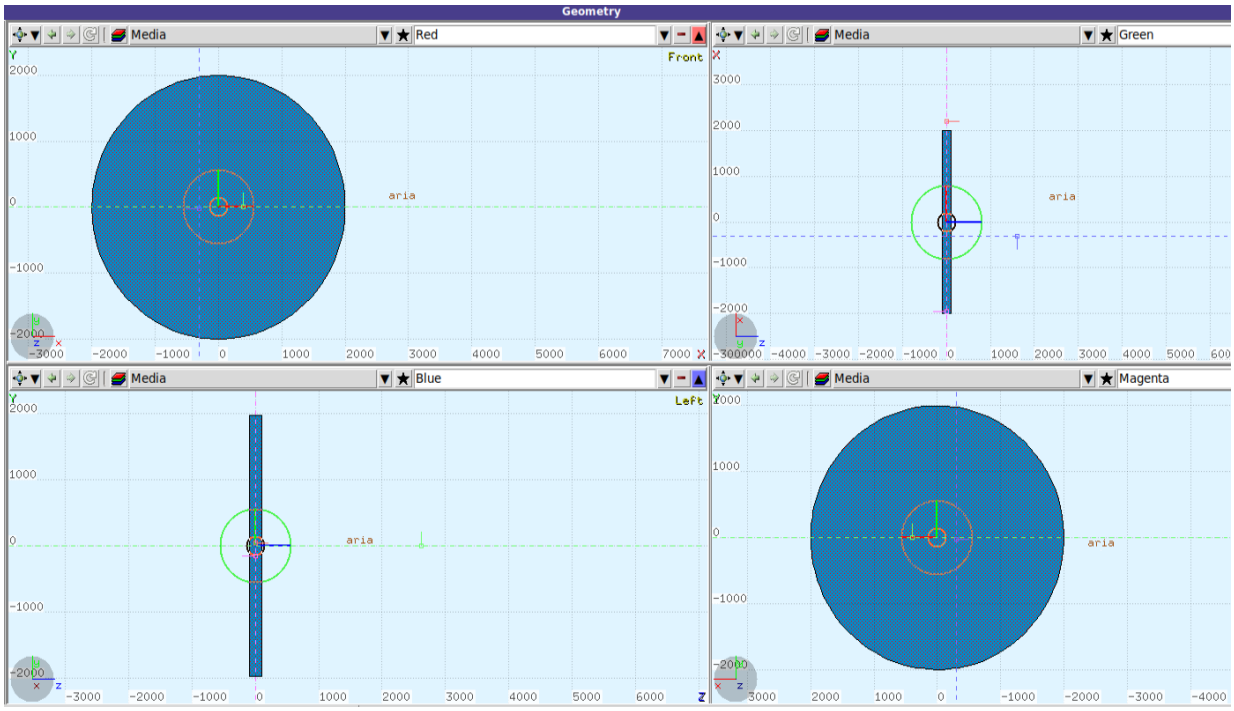

Figure 7.2: Depuration tank geometry in FLUKA

Source simulation

The simulated source is composed of an isotropic emitter uniformly distributed in the tank. The employed beams are $2\,MeV$ for the photons and $511\,KeV$ for $\beta+$ emitters.

In this particular case, the employment of a routine was not necessary, because the description of the source can be performed by the BEAM card with the BEAMPOSition cards. These last configuration are not only increasing the beam information of the position in space, but also here a particular shape is defined. Therefore, the option cylindrical shell is selected, but to define the source extended in the entire volume the internal cylinder is equal to zero and the external is equal to the total volume of the tank.

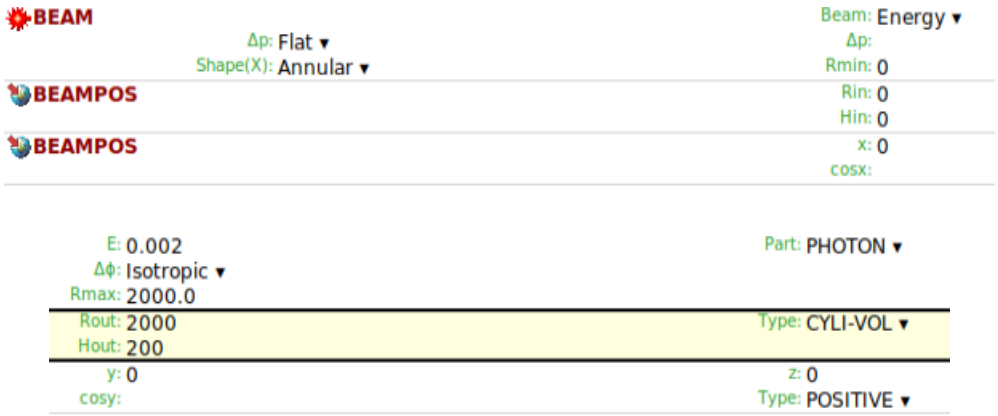

Figure 7.3: Source cards employed for depuration tank simulation

Scoring cards

The scoring is performed through the DOSE-EQ option in the USERBIN card. Thanks to the DOSE-EQ, a dose map can be generated with a desired mesh of proper dimension of the investigated area.

Results simulation

The results from the simulation are dose maps of H*(10) measured in $\frac{pSv}{primaries}$ multiplied by the normalization to reach the unit of measurement of $\frac{nSv}{h}$. In this case the primaries are $1\,MBq$, that is to say $10^6\,\frac{disintegrations}{s}$. This value is coming from the evaluation performed from FLUKA for the synchron water activation and it is representing the average activity of a radionuclide. Therefore, the resulting dose maps are the following 7.4 for the β emitters and 7.5 for $2\,MeV$ photons.

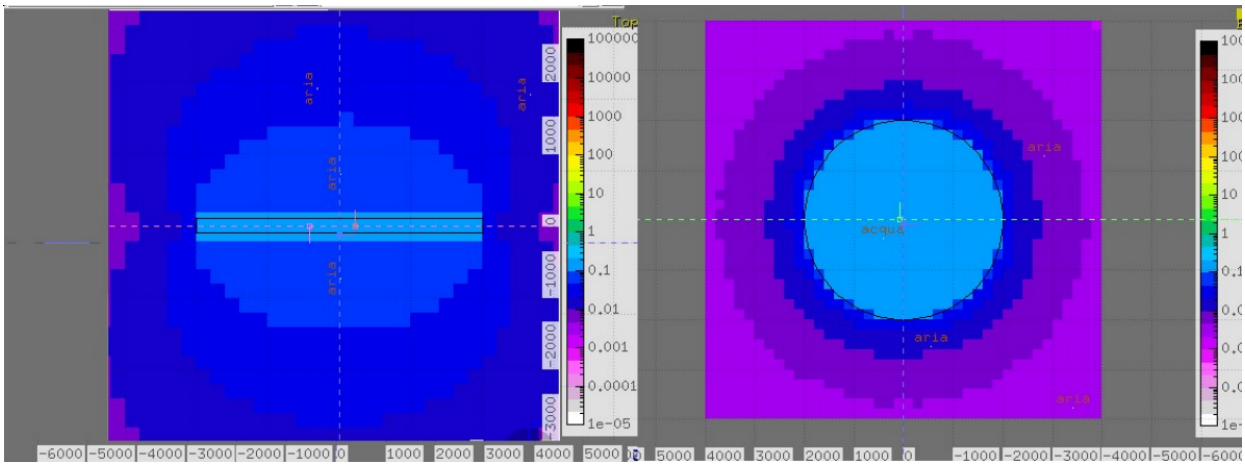

Figure 7.4: Equivalent dose map - $\beta+$ emitters

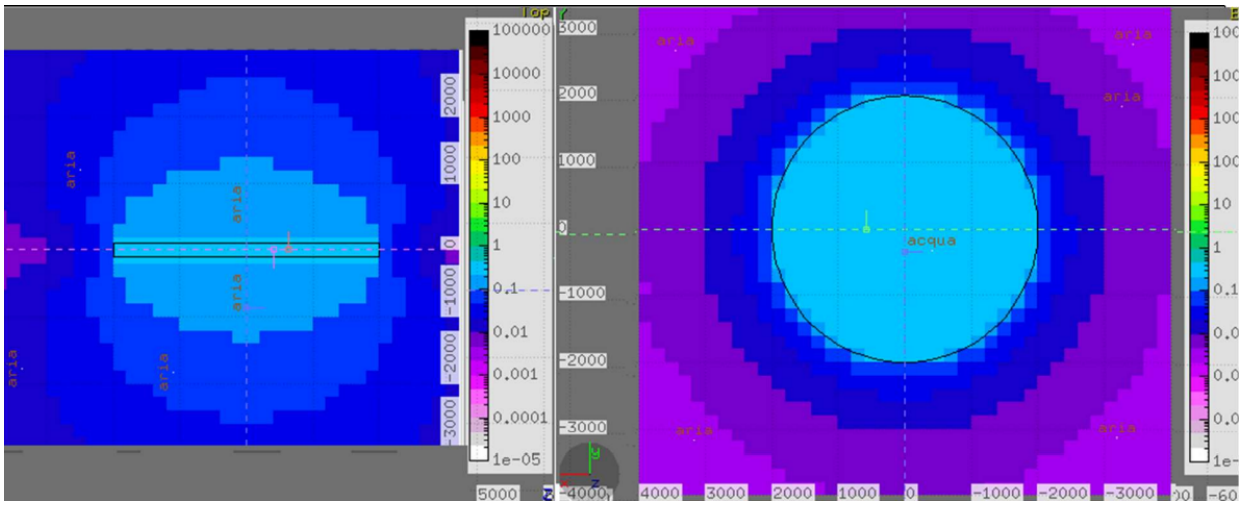

Figure 7.5: Equivalent dose map - 2 MeV

Dose evaluation from depuration tank

The H*(10) dose rate at 1 m from the water depuration tank are 0.2 $\frac{nSv}{h}$ for 1 MBq by a 2 MeV photons emitters and inferior to 0.1 $\frac{nSv}{h}$ for $\beta+$ emitters.

Moreover, performing an analysis that consider all the radionuclides from the 7.1 table, the γ emitters give a the total activity inferior to 5 Bq, excluding the short live $\beta+$ and the ^{18}F. The total dose of H*(10) for an exposition of 10 h would be inferior to 30 nSv.

A similar analysis for the ^{18}F with a released in the drain system of 1.5 Bq a day for 250 d/y would give 0.4 nSv a day and 100 nSv a year. Furthermore, ^{18}F is characterized by a short life and it is not assumable that is ending in the sludge line.

These estimations are conservative for radioprotection reasons and are overestimated, for example the exposition time of 10 h.

Dose evaluation from sludge tank

This section is dedicated to the evaluation of the case in which the radionuclides are absorbed in the sludge line after the wastewater treatment. The radionuclides are the same as in the 7.1 table, but the short lived particles are decayed, because all the collection and extraction of the drain lasts one day.

Every person produces in average produces 1 kg of sludges [19], so considering 70000 inhabitants for Pavia, the total production for a day is equal to 70 m^3. The real tank has the dimension of $5x5x3m^3$ for a total volume of 75 m^3.

Using the same dose map of H*(10) 7.5 7.4, at a distance 1 m from the sludge line a

H*(10) dose is equal to $10\,nSv/h$ almost entirely due to ^{24}Na. However, after a pair of days, the dose rate will be $2\,nSv/h$, provided by ^{48}V, ^{7}Be, ^{22}Na and ^{54}Mn.

Considering the shield of the tank wall and the fact that the workers stand there less time than $200\,h/year$ the total dose to the personnel will be less then $1\,\mu Sv$, that is under the radioprotection dose limit of $1\,mSv$ per year for the population.

8 | Liquid scintillation theory

In this chapter, the fundamental principles of scintillators are described, with a particular highlight to liquid scintillation counting, the technique employed in this work for the experimental evaluation.

Here, an introductory part to scintillation detectors is placed in the first paragraph with a focus on the organic one, followed by the paragraph of the theory of the liquid scintillation with its characterizing phenomena, such as the quenching and other interfering events.

8.1. Scintillation detectors

Scintillators are detectors used for investigating the presence of charged particles through the ability of transferring the kinetic energy in light with high efficiency. This process is happening in consequence of a partial collection of energy from the decay emission in the material medium of the detector. Furthermore, in the majority of cases, an electron of the medium is excited from the ground state to an upper level and its disexcitation is happening with the emission of a photon, which energy range is in the visible.

8.1.1. Scintillator Properties

The scintillator medium to transfer the energy in the most effective way, should have the following properties [21]:

- the produced luminescence should decay in a short time to generate a fast pulse
- the numbers of emitted photons should be proportional to the emitted energy with the decay
- having good optical property
- obtainable in different size
- to be transparent to the emission of its own wavelength
- to have an index of refraction, near to the glass ($\approx$ 1.5) to be coupled to the

photomultiplier tube

Unfortunately, among all the existing material, no one can conciliate all these characteristics. The fundamental property of a scintillator detector to be always respected is the ability to convert a reasonable quantity of energy in light, while minimizing all the interfering processes, such as noise, quenching and other physical phenomena.

The medium choice is performed according to the required measurement and field. For these reasons, different scintillators are available and are listed in the following paragraph.

8.1.2. Types of scintillators

The most common and used scintillators are:

- organic crystals, that are composed of aromatic hydrocarbon molecules, such as benzene and its derivatives. They are pure crystal and fast, in fact they decay in few seconds. On the other hand, it is difficult to develop them in big size, because of theirs fragility. The detection is anisotropic and the $20 - 30\%$ can be lost in resolution. Anthracene, that has the highest output of photons respect to the absorbed energy among any organic scintillators, and stilbene, that is used for a pulse shape discrimination between electrons and charged particles, are the most common organic scintillators.
- plastic scintillators, that are polymers composed of a solvent, typically styrene, with an organic scintillating material. Their pros stand in the fast response, approximately $2 - 4\,ns$ and they can be modelled both in thin layer as μm and large block, thanks to the fact that they can polymerized.
- gaseous scintillators, made of noble gasses such as He, Ar, Xe and Kr, characterized by very fast time of excitement, around $1\,ns$, because they excite one atom at time. Unfortunately, they usually emit wavelength for which most of the photomoltiplicator are inefficient. For this reason, they are mainly used in a mixture of gasses such as $90\%\,^3He$ and $10\%\,Xe$ at $200\,atm$ to increase their efficiency. They are used in astrophysics.
- glasses made of Ce activated with Li or boron silicates, used for detect slow or thermal neutrons, due to the fact that Li and B have large cross section in that energy range, but at the same time they are used also for detecting electrons and γ rays, thanks to their sensibility. They are resistant in different condition and their response time is around $10\,ns$.

- inorganic crystals, that are composed of alkali halide with added impurities to increase the efficiency of scintillation. The most common and used is NaI(Ti) doped with thallium with a time response of $500\,ns$, that is twice or three times bigger than the organic crystals but they own a better energy resolution and light emission.
- liquid scintillators, that are composed of a solvent and an organic scintillator. They are radioresistant, thanks to the fact that they have not a solid structure. This is the choice made for this project because of discussed in the 8.2 paragraph.

The light emission mechanism is different between organic and inorganic scintillator. Here, it follows the working principle of the organic one, because the analysis is performed with a liquid scintillator, that is based on the oscillation of the organic structure of the cocktail.

8.1.3. Working principle - organic detector

The scintillation phenomena of an organic detector are expressed through phosphorescence and fluorescence. Phosphorescence is a delayed emission with a range of time from microseconds to hours, because of the materials that compose the detector. Fluorescence is the element that allows the detection of a particle and is an immediate emission, that happens in $10^{-8}\,s$. Therefore, an efficient scintillator is able to emit almost all the absorbed energy in fluorescence; on the other hand, phosphorescence is considered white noise [9]. The light emission after an excitation is described by the following law:

$$I(t) = I_0\, exp(-\frac{\tau}{t}) \tag{8.1}$$

with τ is the fluorescence decay time.

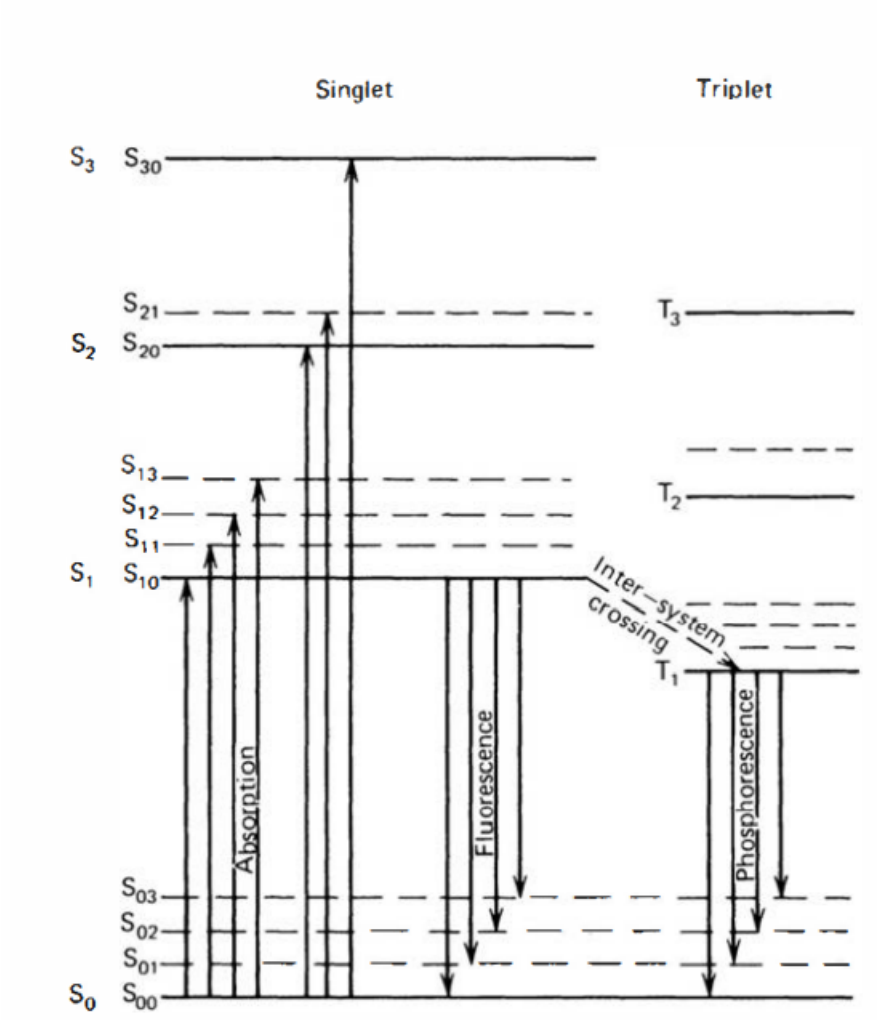

Figure 8.1: Energy levels of a π configuration molecule fig: [6]

As it appears in the figure 8.1, the fluorescence process takes place if the excitation is intrinsic to the same molecule. It exploits the π electronic configuration and internal resonances, typical of the aromatic molecules. S_1, S_2 and S_3 represent excited states of singlet and T_1, T_2 and T_3 the correspondence for a triplet. At room temperature, all the molecules are at the fundamental state S_{00}, because the energetic gap between S_0 and S_1 levels is $3 - 4\,eV$, while it tends to decrease if the atomic level is increasing and between two intermediate levels is equal to $0.15\,eV$.

The scintillation light is obtained when the excitement pass trough the S_{10}, the first exciting state, to S_{00} the fundamental state in $10^{-9}\,s$, while the higher excitation states need an intermediate passage, that is a disexcitation to S_{10} through internal conversion.

Moreover, some transition from triplet configuration can conduct to the formation of phosphorescence, due to a transition from T_1 to S_0 in $10^{-3}\,s$ and delayed fluorescence,

because of a primary excitement from T_1 to S_1 and de-exictement towards S_0.

Some photons with higher energy, in the figure 8.1 the ones with the longest arrow, are directly absorbed and have an higher energy respect to the fluorescence emission (except the transition between S_1 and S_0). Therefore, an organic scintillator can be trasparent to its own emission and it is valid also for the fluorescence. In fact, the minimal overlap between the optical absorption and emission is clearly represented in the figure 8.2 and is called the Stoke shift.

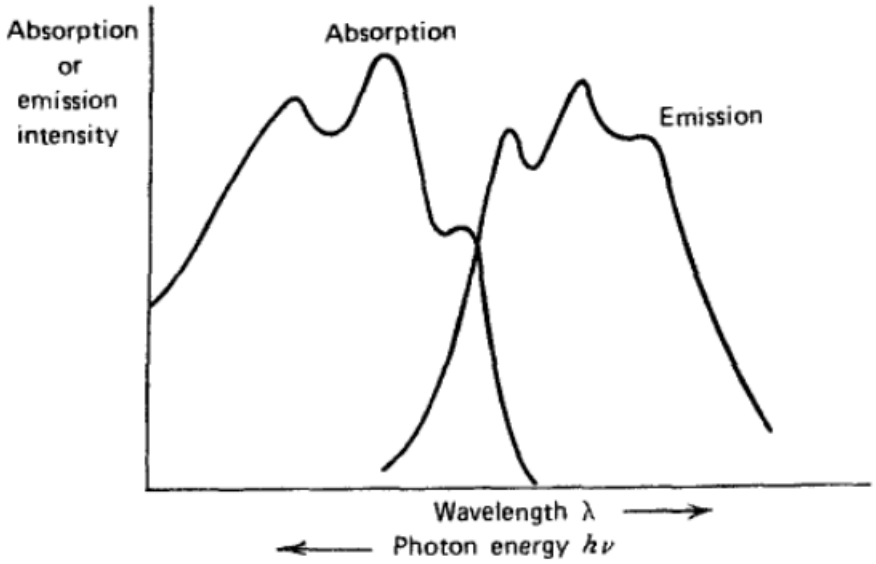

Figure 8.2: Absorption and emission spectra of an organic scintillator [21]

The response output is a portion of lost energy coming from the kinetic energy of the charged particle and it is converted in fluorescence. This fraction depends on the type and energy of the investigated particle. For the majority of organic scintillators, the answer is linear for energy higher than $125\,keV$ while for heavy particles a minor fraction of energy is converted and it becomes linear for higher energies.

8.2. Liquid scintillation theory

Liquid scintillation counting is an analysis that starts with the dissolution of the substance to study in a cocktail. It is better if the substance in study is liquid and compatible with the cocktail, for not creating third phases or particles that can not be dissolved. The cocktail is a liquid that allows to collect the kinetic energy coming from the decay and re emitting in light energy at different waves, more shifted to the blue one. This is important because the instrument is more sensible to blue length and in this way it is possible to

collect almost all the energy [[20],[24]].

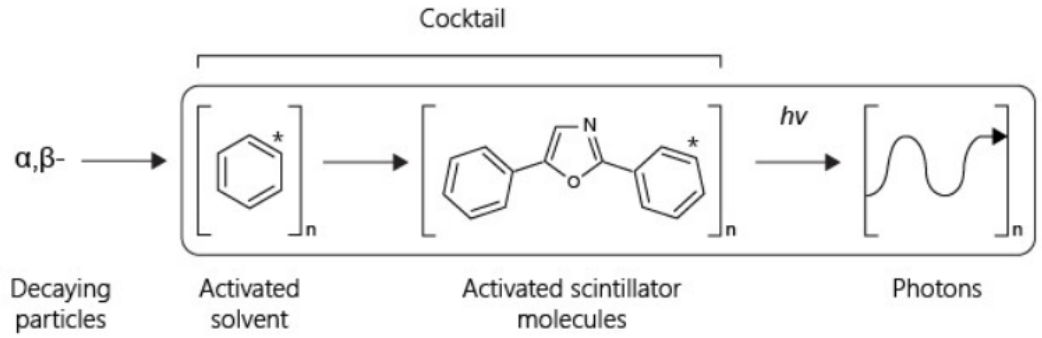

Figure 8.3: Liquid scintillation counting-schematic description [16]

Analyzing in detail the liquid scintillation cocktail, it is composed of a solvent and a scintillator. It is possible to summarize the mechanism in three steps [fig: 8.3]: first of all, the solvent is activated by the energies released by the decaying particles. Therefore, the main properties of the solvent are to provide solubility for scintillators and to transfer and to absorb energy efficiently. For example, good solvents are composed of alkylated organic aromatic molecules, due to the high electronic density, but on the contrary they can be toxic and dangerous for skin absorption and inhalation, such as toluene and xylene isomers. The second step is performed by the scintillator: its role is to absorb the energy from the solvent and emit it at higher wavelength in the visible light. The ideal properties of the scintillator are a fast decay time, to have a high yield for the florescent production and the resulting photons should be proportional to the beta particles. Moreover, some scintillators can be coupled to reach a particularly wavelength that is optimal for the PMT, in that way the scintillator part is made of a primary scintillator that transfer the energy to a secondary scintillator. Different cocktails are available to optimize the counting of specific samples, but all of them contain at least one organic solvent and one or more organic scintillator.

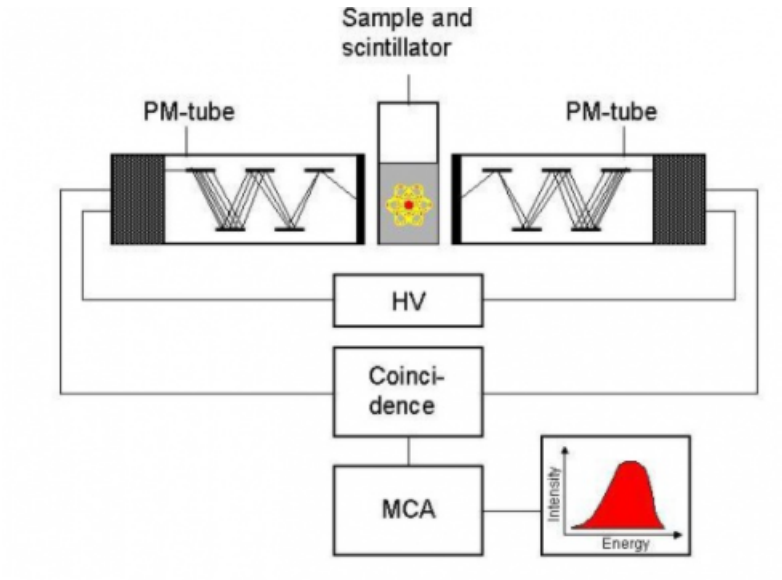

Figure 8.4: Acquisition chain for LSC

Photo Multiplier Tube PMT converts and amplifies the collected photons in an electric signal through the emission of secondary electrons. The first part of a PMT is composed of a photocathode, that is an absorbing material of the incoming photons and through photoelectric effect primary electrons are emitted. The second part is made of different dynodes, that are electrodes able to multiply in cascade the number of electrons, which ones are guided through potential difference. In the last part of a PMT, an anode is present and here a current pulse is detected with an electronic setup. The current pulse depends on the number of the generated primary photons, that in their turn depend on the photo-electrons. One photo-electron is produced from one photons, which are directly correlated to the energy of the incident particle in the scintillator. Therefore, analysing the current pulse, a data of the energy and the intensity of the incident nuclear particles is provided. The number of photomultipliers tubes depend on the type of instrument: if at least two PMT are present, they are followed by a coincidence unit, thanks to this element a clean signal is obtained, because if the two electrical pulses arrives simultaneously, the signal is counted as valid, otherwise the pulse is ignored. In the electronic chain, a multichannel analyzer is always present and provides the spectra of the investigated situation.

As regards β particle, the expected spectrum is similar to the figure 8.5 described in number of pulses versus the number of channel. The peak is at one third to the maximum energy and it is the most probable one and furthermore, β particles produce a continuum, visible in the plot with the long tail, due to the emission of the β particle and the antineutrino.

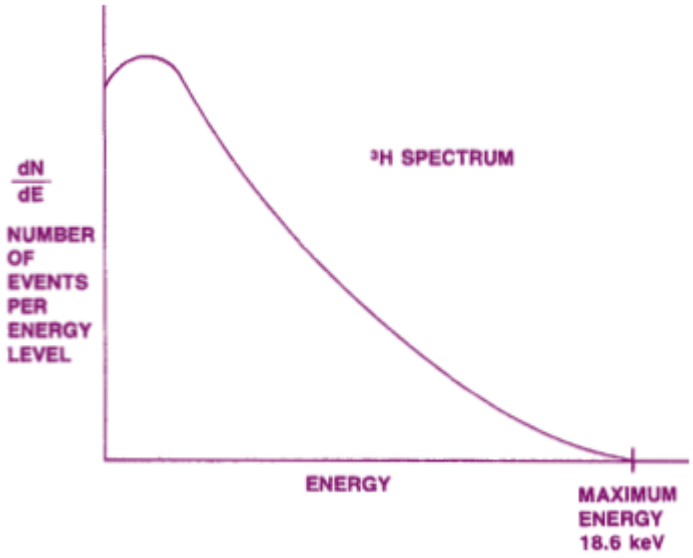

Figure 8.5: Spectrum of $\beta-$ ^3H [20]

After a general overview on the liquid scintillation theory, a detail analysis on the affecting events on the measurement is needed. In the experimental evaluation the most affecting phenomenon is the quenching that can reduce the number of counts drastically. For this reason, the following paragraph is dedicated to the quenching, that is followed by the description of other phenomena that can affect the measurement.

8.2.1. Quenching

Quenching is a phenomenon that affects the efficiency of the measure, it appears in the plot 8.6 as a signal reduction because it is a degradation of the energy released by the hitting particle. In fact, to measure the activity of the investigated sample it is needed to know the level of quenching to determine the counting efficiency [26].

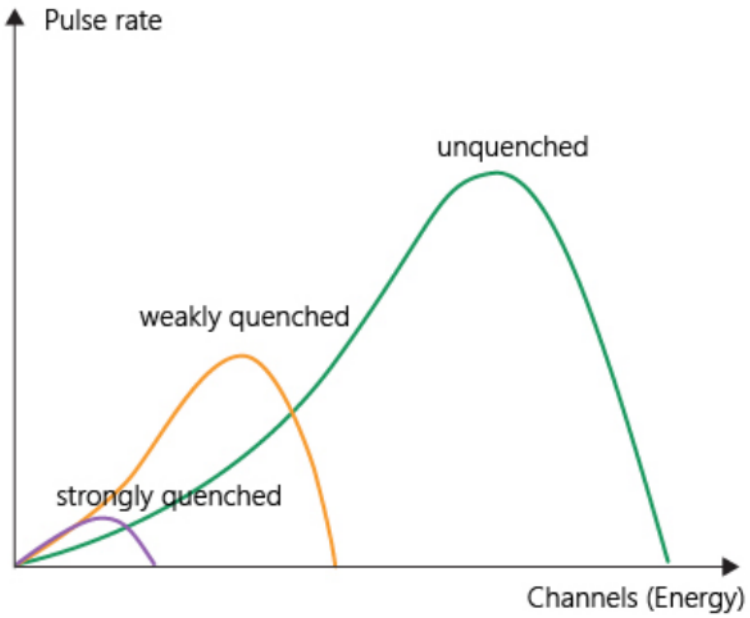

Figure 8.6: Quench plot [16]

As it appears in the figure, the quench can be divided in three types:

- physical quench is present if a physical separation affect the contact between the scintillator and the radioisotope or if some solid particles absorb the produced photons in the vial. It is common when different phases are present within the sample or when a disk or a support is present. It can be avoided by properly mixing and putting in contact the solution.
- chemical quench is the distortion of the emission of energy during the transfer to the solvent molecules. This interfering process is caused by the fact that the energy of the beta particle is not absorbed properly by the solvent, because some chemical elements with no aromatic structure are interfering. In this way no light will reach the detector.
- color quench occurs after the energy is transmitted to the photons, that are not able to be detected by the photomultiplier tube, because they are absorbed by color. Therefore, even though the fluorescence emission takes place, the signal process is interrupted. This is due to the fact that the fluorescent stage is performed in the blue part of the spectrum and if the spectrum color is altered the photons are absorbed. The colour quenching has an order of severity: it is worst from red $>$ orange $>$ yellow $>$ green $>$ blue.

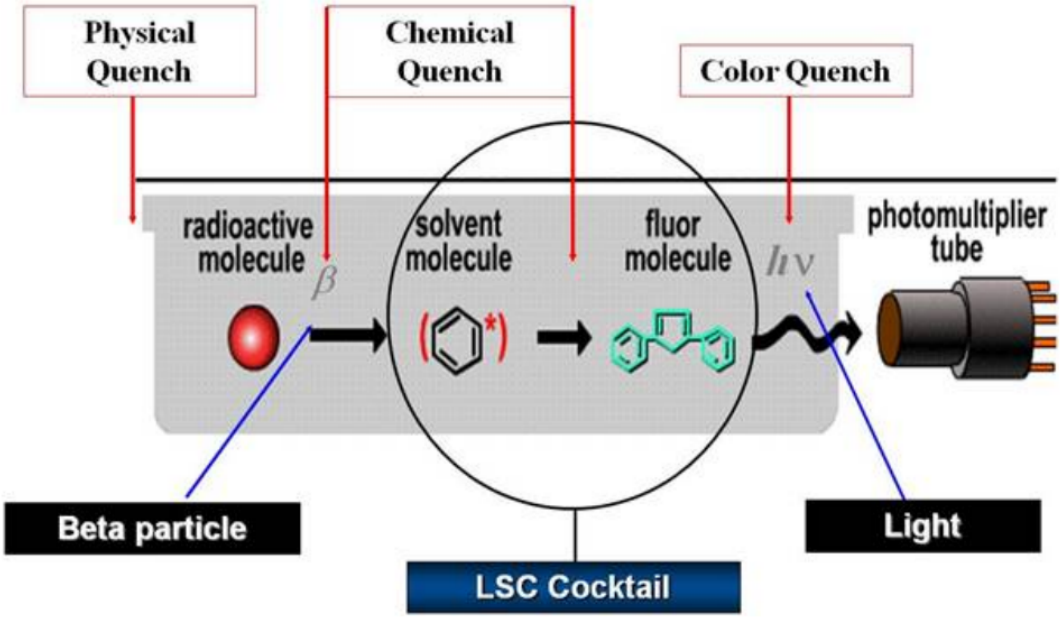

Figure 8.7: Physical, chemical and color quench [17]

Different solutions can be employed to correct the quench phenomenon. For this project, the internal standard method is applied. It consists of two phases:

1. a vial of an unknown activity is measured and its CPM_x are recorded.
2. a quantity of known activity $DPM_{standard}$ of the investigated radionuclide is added. Then the vial is measured and its CPM_{x+std} recorded.

Therefore, the efficiency can be estimate with the following formula:

$$efficiency = \frac{CPM_{x+std} - CPM_x}{DPM_{standard}} \tag{8.2}$$

and then the DPM_x of the unknown vial can be evaluated:

$$DPM_x = \frac{CPM_x}{efficiency} \tag{8.3}$$

This procedure is optimal when the investigated material keeps the same characteristics in provenience and composition as the sample used to determine the efficiency. In contrast, to ensure the same value of efficiency, the reproducibilty of samples has to be tested and a measurement with the internal standard has to be performed periodically. The other disadvantage is the constant production of radioactive waste to check the efficiency periodically.

An other method is the creation of the calibration curves with an internal standard: by plotting the quenching values printed by the instrument respect to the corresponding efficiency. In this way, the affecting efficiency can be corrected by to the counts can be estimated and obtain the real counts.

Therefore, the internal standard is a source of known activity, that is inserted in different samples with the proper cocktail. In this set of vials, a quantity of quench agent, for example CCl_4, is added increasing the quantity proportionally. The measurements are performed starting with the one with no quench agent to the one with the most quantity, to register how the quench is affecting the counting efficiency.

Both methods are valid, the calibration curves with an internal standard is tracking the quench, exploiting the sample isotope spectrum, while the internal standard is exploiting the efficiency of that vial with that features.

8.2.2. Other interfering phenomena

Some inferences can alter the counting in the liquid scintillation process and the principal are [6]:

- wall effect, a phenomenon occurring if the organic scintillator diffuses into the walls of the plastic vial and the wall itself behaves as a scintillator altering the spectrum, emitting improperly photons at lower energies. The wall effect can be correct through the use of glass vials and safer cocktail and solvent.
- static electricity, that can be generated accidentally during the preparation of the sample. A simple way to solve it is the employment of antistatic wipe or a humidification of the sample.
- luminescence, that is the production of light in the cocktail. In the case of photoluminescence, an activation of the scintillator or the vial is caused by ultraviolet light. It can be reduced by keeping the vial in the dark for $15 - 30\,minutes$. Instead, as regards chemiluminescence, the parasite light is produced by particular reaction, as such in presence of alkaline pH and peroxides. The employment of special cocktails or the neutralization of the solution can eliminate this phenomenon.
- radionuclides mixtures, that can appear in the resulting plot as the overlapping continuous spectra and it can be solved by radiochemical separation, in this way a single radionuclide is measured at a time or label counting.
- background, that can interfere with the measure providing false data. For example,

the electronic noise and the cosmic radiation has to be kept in consideration and they can be reduced by using coincidence circuit, passive or active shielding, such as the employment of Pi shields or an underground lab, low background vials and temperature control.

9 | Experimental measures: HPGe and LSC

Periodically, in correspondence with the ordinary maintenance, the radioprotection department performs an evaluation of the cooling water activity. The spills are taken directly from the demineralized water closed loop of the cooling system of the synchrotron and from the softened water closed loop of the cooling system of the linac. The collected water is conserved in time for further evaluation. The analysis was performed with a HPGe, a semiconductor detector for γ spectroscopy, that has the best resolution among all the detectors. However, the possibility to lose $\beta-$ counts is present. This can be a problem for performing a correct evaluation of ^3H, that can be present in the water cooling system.

In this chapter, a method is propose to perform an implementation to the water analysis: the HPGe can be applied as a first check and it is followed by a liquid scintillator counter. The available instrument at CNAO is the Triathler.

9.1. HPGe analysis

The analysis with the HPGe is the first step of the experimental part. The need to employ an accurate gamma spectroscopy is due to the possible presence of other radionuclides that can interfere with the liquid scintillation measurement. The gamma emitters can derive from the oxidation of the material that composed the pipes due to the water action. Then, the cooling water can transport these oxides, that can be activated. The HPGe is a semiconductor detector doped with high purity Ge and is characterized by the best resolution among all the detectors thanks to the following properties: its high efficiency, high atomic number and low average energy for the formation of electron hole pairs. On the other hand, the main disadvantage is the need to be cooled down to low temperature to obtain the spectroscopy.

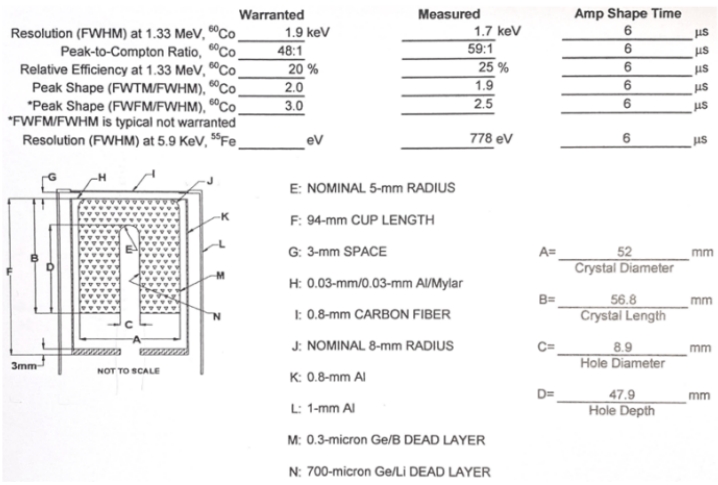

Figure 9.1: Technical features of HPGe at CNAO

For all the measurements the same kind of cylindrical container is used, called "*marinelli*" because it has the optimal shape for the HPGe. The first performed measurement is the background: the container was filled with water and it was measured for 1 h.

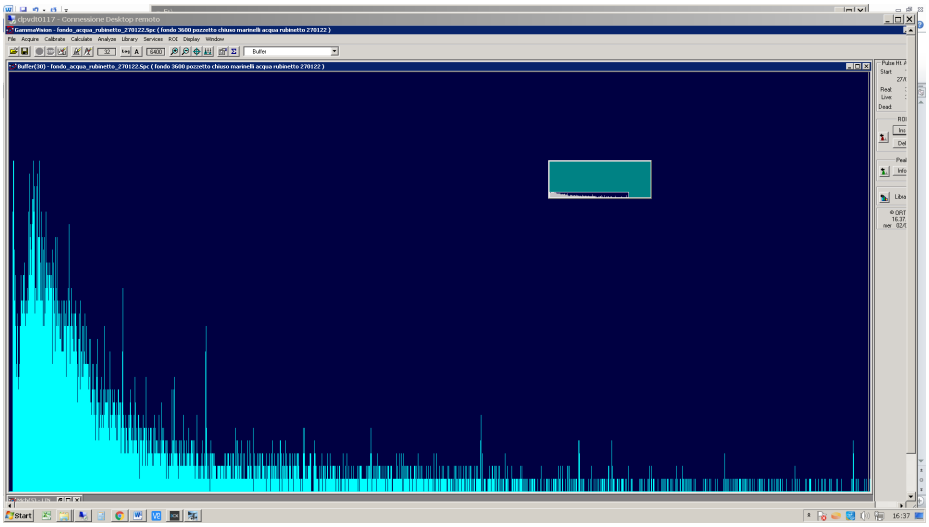

Figure 9.2: Background water spectroscopy

The softened and demineralized water are spilled directly from the two circuit in the synchrotron room during the maintenance day. The collected sample is placed in a *marinelli* measured for 1 h. Thanks to the user-interface Gamma Vision, it is possible to obtain the spectrum and the countrate through the integral of the selected area.

It follows the spectra of the softened water measurement 9.3 and the subtraction of the softened water spectrum from background 9.4.

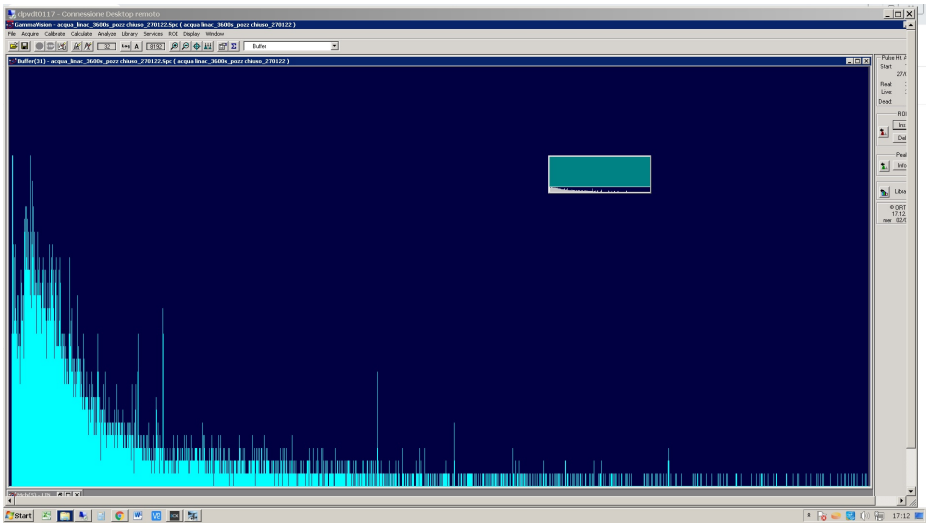

Figure 9.3: Softened water spectrum

As it appears in the figure 9.4, the resulting sample is clean from any kind of radionuclides, because no relevant peak are recognised from a continuum of background noise. Hence, no peak area and countrate are calculated.

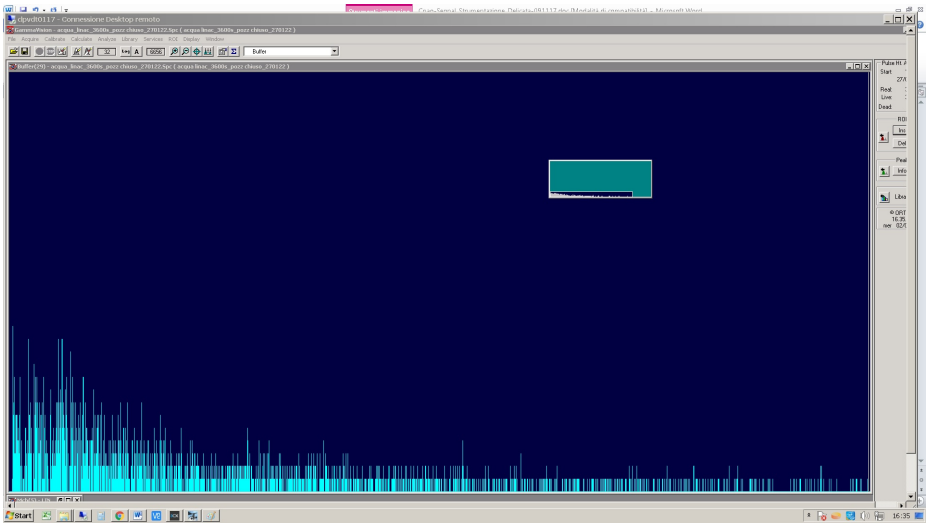

Figure 9.4: Resulting spectrum from softened water

The same procedure is applied for the demineralized water: the sample is placed in a *marinelli* container and measured for $1\,h$. The spectra of the demineralized water 9.5 and the subtraction from the background 9.6 are listed.

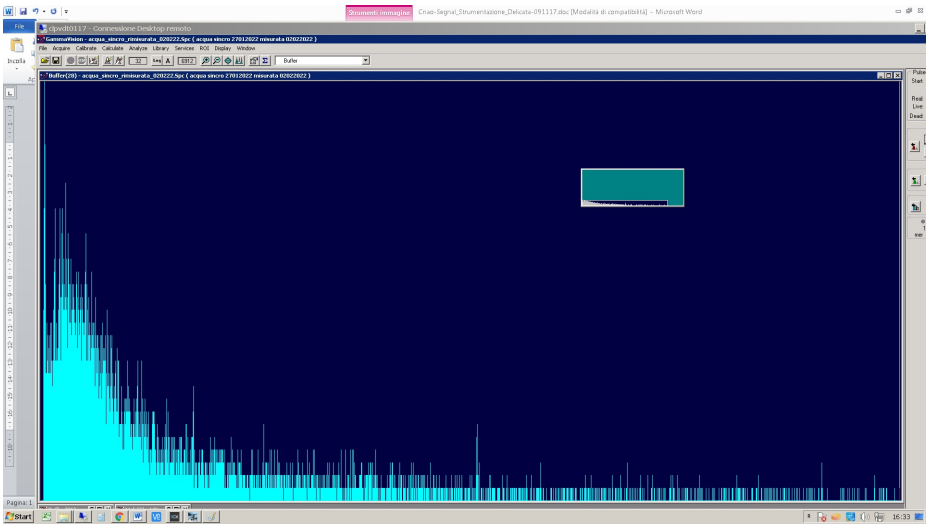

Figure 9.5: Demineralized water spectrum

As a result of the subtraction from the background spectrum, it does not appear any relevant peak and so no radionuclides are detected. The obtained spectrum is similar to the softened water 9.4, where the plot is a continuum produced by noise.

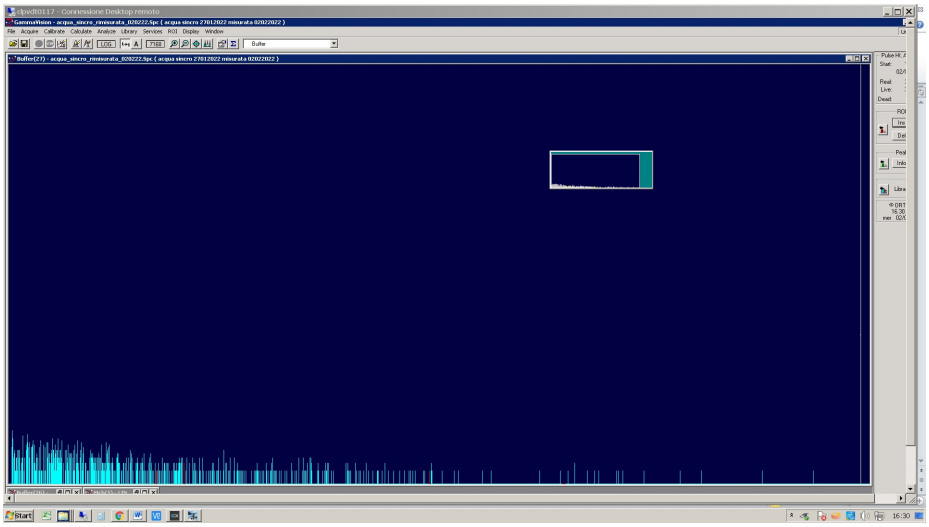

Figure 9.6: Resulting spectrum from demineralized water

9.2. Triathler analysis

Triathler is a liquid scintillator counter, little and portable, that counts one sample at time. It can be optimal to be transported on site and to provide a measurement on spot.

Figure 9.7: Triathler [16]

As regards the technical features, it has one photomultiplier tube and no cooling system. It is set with different protocols that are designed to optimize the counting window for each radionuclide placed on the keyboard. In fact, it has 16 tactile keys, 6 of them to configure the machine to the measurement and the rest to set the radionuclide protocol such as ^{3}H, ^{14}C, ^{32}P. The detectable energy range is from $2\,keV$ to $2000\,keV$. Thanks to 3 adapter, different size vials can be employed in the tank: $20\,ml$ LSC vials, test tubes and micro-tubes. It can be connected to a PC or a printer with an RS-232C serial port.

As every liquid scintillation counter, it is affected by the quenching 8.2.1 and here it follows a solution to correct it.

9.2.1. Quench calibration curve

The quench calibration curve is a method to correct the quenching through the plot of the efficiency versus the quench values. The triathler calculates the quenching parameters as the center of gravity of the spectrum.

The experimental procedure is developed using the following materials: some plastic vials of $20\,ml$ of volume; the capsule sources of ^{3}H in solid form; the AquaLight cocktail, provided by Hidex; the nitromethane as a quench agent; a precision balance; the $1\,ml$ and $5\,ml$ syringes; a $5\,ml$ pipette and some beakers.

The first trial consists of the development of a calibration curve with a 8 samples prepared

in the following way:

1. A capsule of ^3H with an activity of $3137\,Bq$ is placed in a vial and dissolved in $19.981\,g$ of distilled water. After having closed the vial, the sample is shaken to increase the contact between water and the dissolution.
2. After a sufficient time to allow the dissolution, $2\,ml$ of the tritium water solution are added with the help of a syringe to all the 8 vials. Each of them has an activity of $314\,Bq$.
3. It follows the making up to volume with $8\,ml$ of distilled water and $10\,ml$ cocktail, according to the guidance of the cocktail. Then, the vial is shaken to have a sample properly mixed and to avoid the separation of phases.

The vial is set, but it is advisable to wait some hours to stabilize the sample and not having bubbles, that can cover some counts. The instrument is configured to print the calibration curve according to the handbook and the measuring time is set from $1\,min$ to $10\,min$, according to the performed trial. Samples were stored in the darkness and they were kept in the tank of the instrument $15\,min$ to discharge the excitation of the photoluminescence. Moreover, the measurements were conducted in the dark. Nevertheless, it was not possible to obtain a curve. It follows an indicative figure of the situation, different attempts were performed with different measurement times and also varying the resting time in the dark tank.

Technology	Liquid Scintillation
Sample Format	Vial (1x1)
Protocol	H-3
Info	DPM standarisation, current DPM:Lin. interpolation of 0 segment(s) !
Info	DPM:Qp range (49.323 .. 49.323)
Info	Calibration type:Internal Std.
Info	Internal Standard Mode!
Info	Summary:
Info	*** DPM standards ***
Info	Std DPM: 18800
Info	Bad QP value (sd.2) 55.2157
Info	Bad segment(s), used 0 segment(s)
Info	eff qp eff err%
Info	0.02173 55.07 0.00000 -100.00%
Info	0.01905 55.22 0.81340 4168.78%
Info	0.01605 52.25 0.00000 -100.00%
Info	0.01257 64.28 0.96255 7555.10%
Info	0.00980 70.70 1.00000 10103.84%
Info	0.01193 72.92 1.00000 8280.08%
Info	0.00852 83.04 1.00000 11637.85%
Info	0.00884 72.72 1.00000 11210.04%
Info	Values saved

Figure 9.8: Quench curve obtained with 8 vials of composition 10 ml+10ml

The reported high errors are due to the fact that the ^3H spectrum is at low energies as the photo-luminescence peak. So, increasing the quenching level, the spectrum is overlapped to the photoluminescence peak.

As comparison, the photoluminescence peak obtained by a 20 ml cocktail is reported. Even though the sample was stored in a dark place, it was waited for 30 min in the triathler tank before starting the measure to avoid any light excitation. The first spectrum derives from the first vial of the quench curve, that means the one with no quench agent added. It is visible how the two spectra can almost overlap and the ^3H spectrum is barely shaped at a right side of the plot.

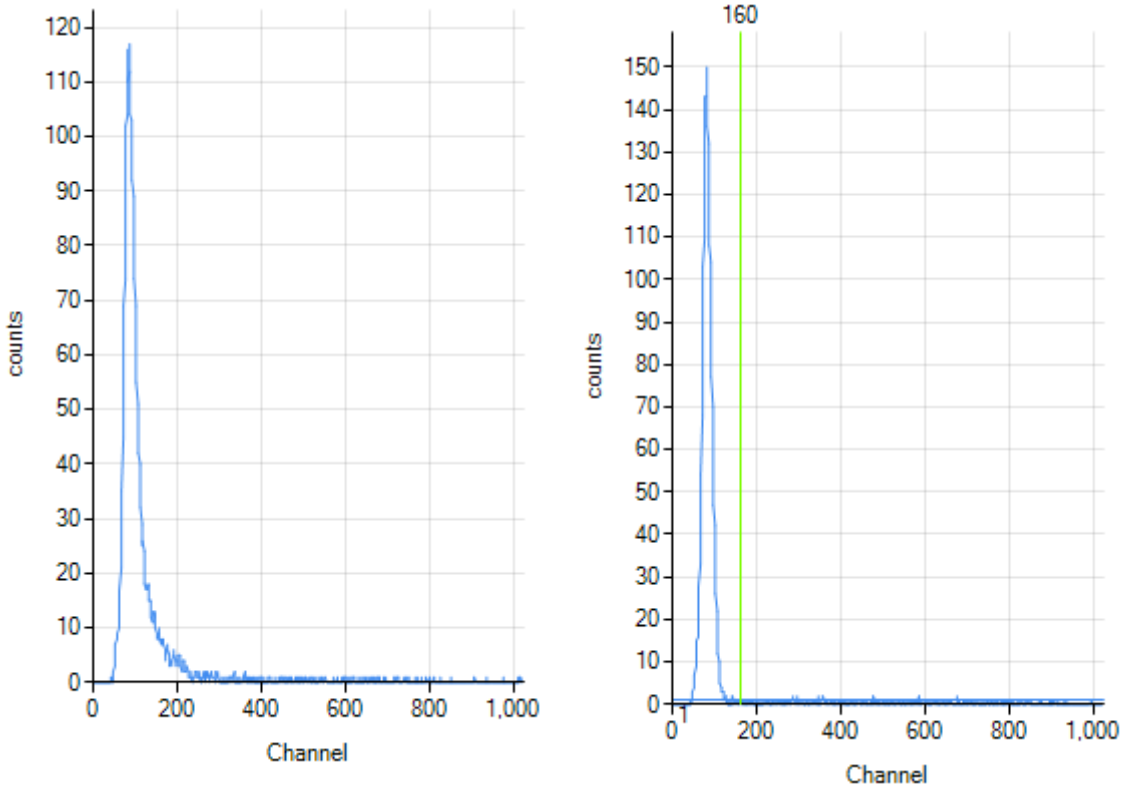

Figure 9.9: 10 ml distilled water+10 ml cocktail+314 Bq ^3H spectrum vs 20 ml cocktail spectrum

Therefore, the first solution is an increasing of activity as the optimal solution to avoid the overlapped spectrum.

The second trial employs a capsule source for each vial, corresponding to an activity of 3135 Bq and 313.5 $\frac{Bq}{g}$. The procedure is the following:

1. in 4 vials a source is placed and dissolved in 10 ml of distilled water.
2. after a proper time to allow the dissolution, 10 ml the of AquaLight cocktail was added. Then, the sample is shaken to ensure the properly mixture and not the separation of the two liquids.

As said for the first trial, a proper time has to pass to allow the stabilization of the sample. The placed figure is just a sample result of all the trials that were performed varying the measurement time and the time of keeping the vials in the dark tank.

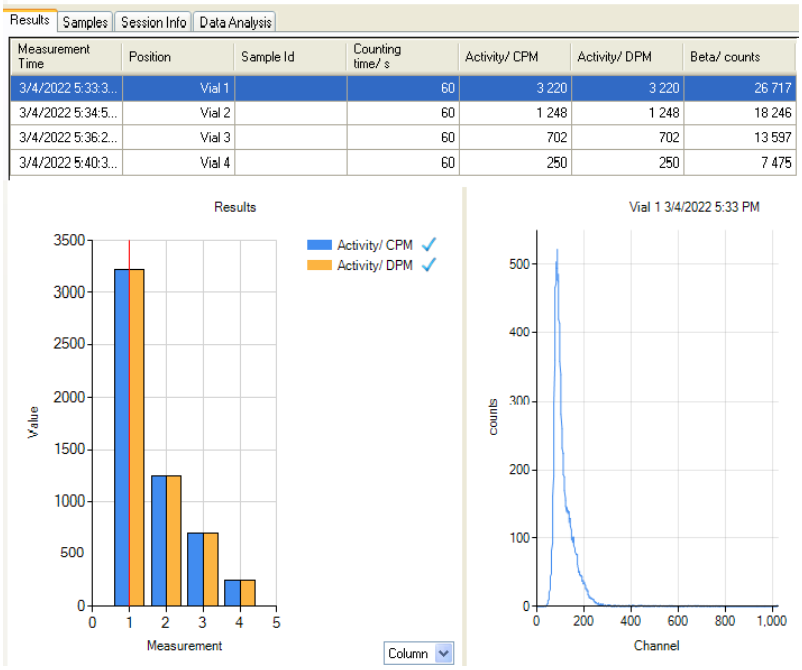

Figure 9.10: Quench calibration curve :10 ml distilled water + 10 ml cocktail + 3135 Bq ^3H

Technology	Liquid Scintillation
Sample Format	Vial (1x1)
Protocol	H-3
Info	DPM standarisation, current DPM:Lin. interpolation of 0 segment(s) !
Info	DPM:Qp range (50.611 .. 50.611)
Info	Calibration type:Internal Std.
Info	Internal Standard Mode!
Info	Summary:
Info	*** DPM standards ***
Info	Std DPM: 185800
Info	Bad QP value (sd.3) 37.4150
Info	Bad segment(s), used 1 segment(s)
Info	eff qp eff err%
Info	0.01733 33.05 0.01733 -0.00%
Info	0.00672 33.02 0.00672 -0.00%
Info	0.00378 37.41 1.00000 26364.22%
Info	0.00135 53.88 1.00000 74104.80%

Figure 9.11: Quench calibration curve error: 10 ml distilled water+ 10 ml cocktail+ 3135 Bq ^3H

Unfortunately, this trial failed. At this point of the experimental procedures, the producers of the instrument were contacted. They suggested to use $8\,ml$ of water, because the cocktail could have reach the limit of solubility. Therefore, the third trial was to perform

a quench calibration curve employing 8 ml of distilled water and 12 ml of cocktail. The procedure remains the same as the second trial and the activity corrected by the half-life.

Even though the changing of concentration, it was not possible to achieve the result. As said for the previous figures, the following figures are an indication of all the performed tests.

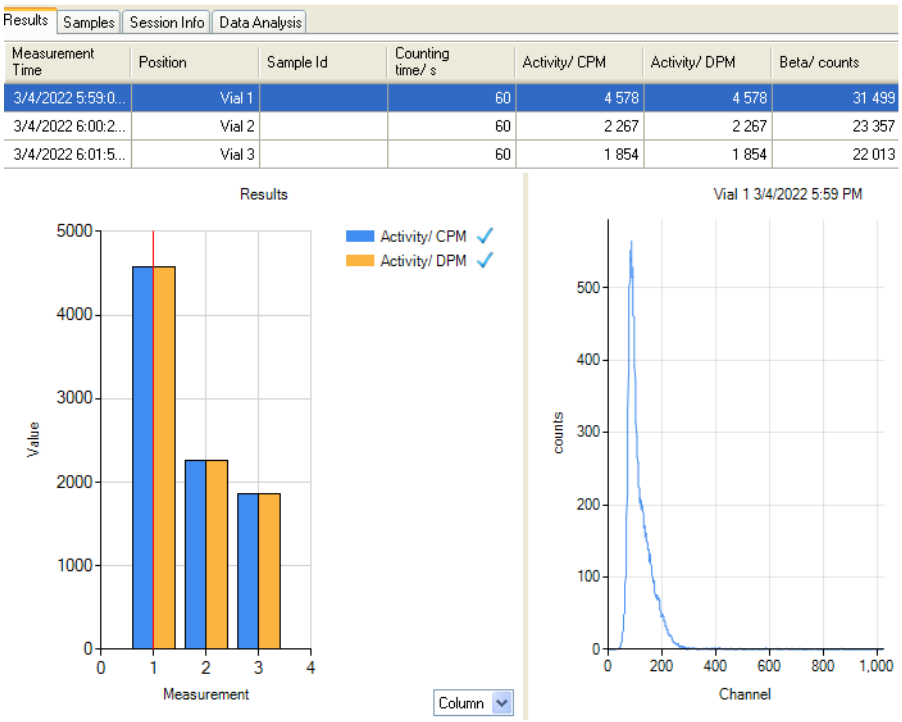

Figure 9.12: Quench calibration curve 8 ml distilled water+ 12 ml cocktail+ 3135 Bq ^3H

Technology	Liquid Scintillation
Sample Format	Vial (1x1)
Protocol	H-3
Info	DPM standarisation, current DPM:Lin. interpolation of 2 segment(s) !
Info	DPM:Qp range (31.125 .. 33.673)
Info	Calibration type:Internal Std.
Info	Internal Standard Mode!
Info	Summary:
Info	*** DPM standards ***
Info	Std DPM: 185800
Info	Bad QP value (sd.3) 32.6157
Info	Bad segment(s), used 1 segment(s)
Info	eff qp eff err%
Info	0.02464 33.52 0.02464 -0.00%
Info	0.01220 31.81 0.01220 -0.00%
Info	0.00998 32.62 0.01805 80.90%

Figure 9.13: Quench calibration curve error: 8 ml distilled water+ 12 ml cocktail+ 3135 Bq ^3H

After this result, the company communicate that the quenching calibration curves were not obtainable in a solution with water, because it is already a quench agent. Moreover, the optimal solution is to have printed different quenching levels with counts higher than $1000\,CPM$ and an efficiency higher than 1%. Therefore, they propose to performed a calibration curve with a quench set industrially prepared and to perform all the measures with vials composed of $15\,ml$ of cocktail and $5\,ml$ or less of distilled water. The quench set solution do not appear as the optimal for this project, because big differences were present between the quench set and the experimental setup:

- the vials are composed of transparent glass, while the experimental one are opaque and in plastic. So, they are not describing the reality and not considering the possibility to have the color quench;
- the cocktail is toluene and is transparent, instead the Aqualight is composed of a mix of aromatic component and appears milky. Again it is not considering the color quench.

Therefore, it was better to perform an internal standard calibration as a measure of an efficiency.

All of these trials failed because the instrument has a photomultiplier tube and it is not able to clean the plot from the photoluminiscence peak. The quench parameter is the spectrum centre of gravity and was falling in the photoluminescence peak, because, increasing the quenching, the spectrum is shifted toward the left of the plot 8.6. For this reason, the instrument was not able to discriminate among different level of quenching and the photoluminescence peak.

9.2.2. Internal standard method

The internal standard method allows a quench correction thanks to an estimation of the efficiency. As explained in the 8.2.1 paragraph, the efficiency of the vial is evaluated performing two measurements: one with an addition of a known activity $DPM_{standard}$ of the studied radionuclide CPM_{x+std} and the other one without CPM_x.

$$efficiency = \frac{CPM_{x+std} - CPM_x}{DPM_{standard}} \tag{9.1}$$

The unknown vial is prepared using the AquaLight cocktail, provided by Hidex, and the demineralized water spilled directly from the pipeline before entering the synchrotron. It is important to shake the vial for some minutes to have a mixture of the two liquids

and not two separated phases. Then, the samples need a couples of hours to stabilize, for not letting the bubbles affecting the measurement. This procedure is chosen to keep in consideration of the exact composition of the water. A demineralized water analysis, conducted in May 2021 by Società Acqua Lodigiana, shows:

Parameter	result	unit of measurement
colony count at 36 °C	<1	UFC/ml
colony count at 22 °C	<1	UFC/ml
coliform bacteria at 37 °C	0	UFC/100ml
escherichia coli	0	UFC/100ml
enterocci	0	UFC/100ml

Table 9.1: Demineralized water analysis

As regards the vial with the addiction of a known activity, a capsule source of ^3H is employed for each vial with an activity equals to 3101 Bq. It is in solid form and is linked to an organic compound, so it is dissolved directly in the cocktail. The vial is shaken to facilitate the dissolution and after a proper time, the distilled water is added. Then, the vial is shaken again to have a proper mixture and not a separation of phases. To avoid to lose counts, the samples need to stabilize for a couple of hours. After the preparation, all the vials are stored in the dark.

Starting from the fact that the company affirmed that the best concentration of water in a 20 ml vial is 5 ml or less, three trials are performed with the following composition:

- 19 ml of cocktail with 1 ml of demineralized water;
- 18 ml of cocktail with 2 ml of demineralized water;
- 15 ml of cocktail with 5 ml of demineralized water.

To reduce as much as possible the photoluminescence, the six samples are stored in a dark place and before the measurement, they are kept 30 min in the dark tank of the triathler. The counting time is equal to a pair of hours, repeated different times. Here, the results are listed, followed by their corresponding spectra:

vial	CPM_x	CPM_{x+std}	efficiency
$19\,ml$+$1\,ml$	120	19100	10.2 %
$18\,ml$+$2\,ml$	124	15580	8.3 %
$15\,ml$+$5\,ml$	133	10564	5.6 %

Table 9.2: Internal standard method result

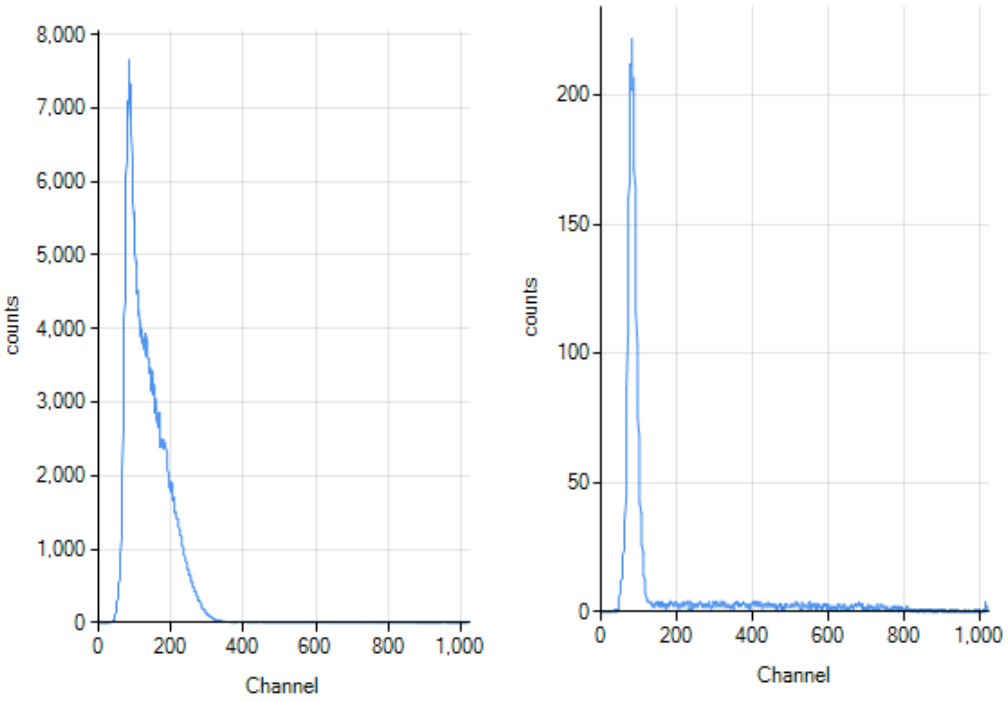

Figure 9.14: $1\,ml$+$19\,ml$+^3H spectrum vs $1\,ml$+$19\,ml$ spectrum

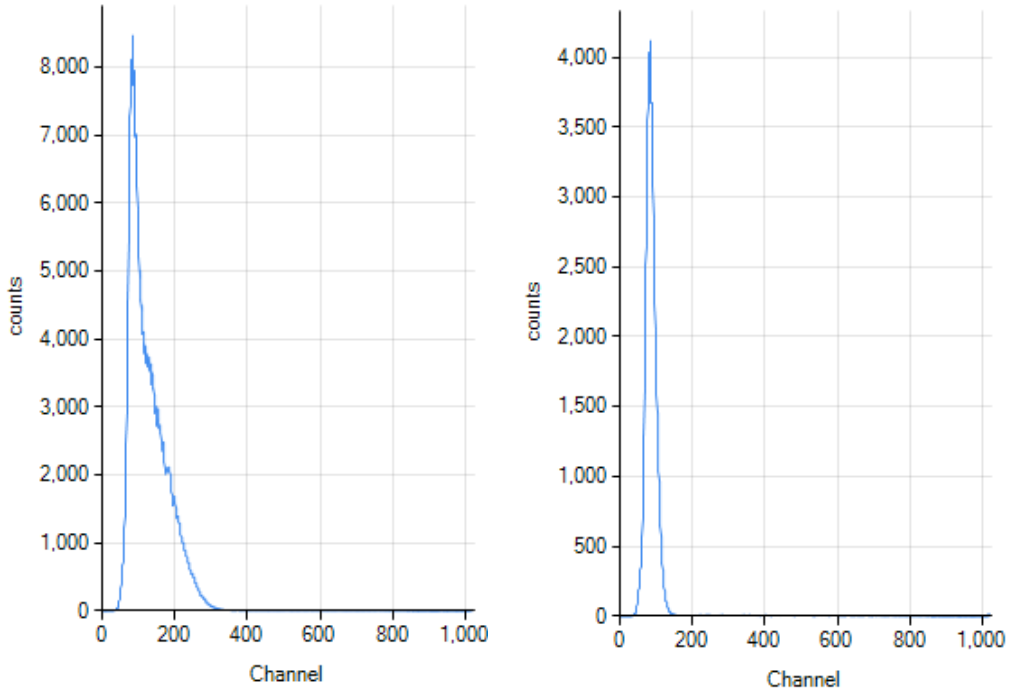

Figure 9.15: $2\,ml{+}18\,ml{+}^{3}H$ spectrum vs $2\,ml{+}18\,ml$ spectrum

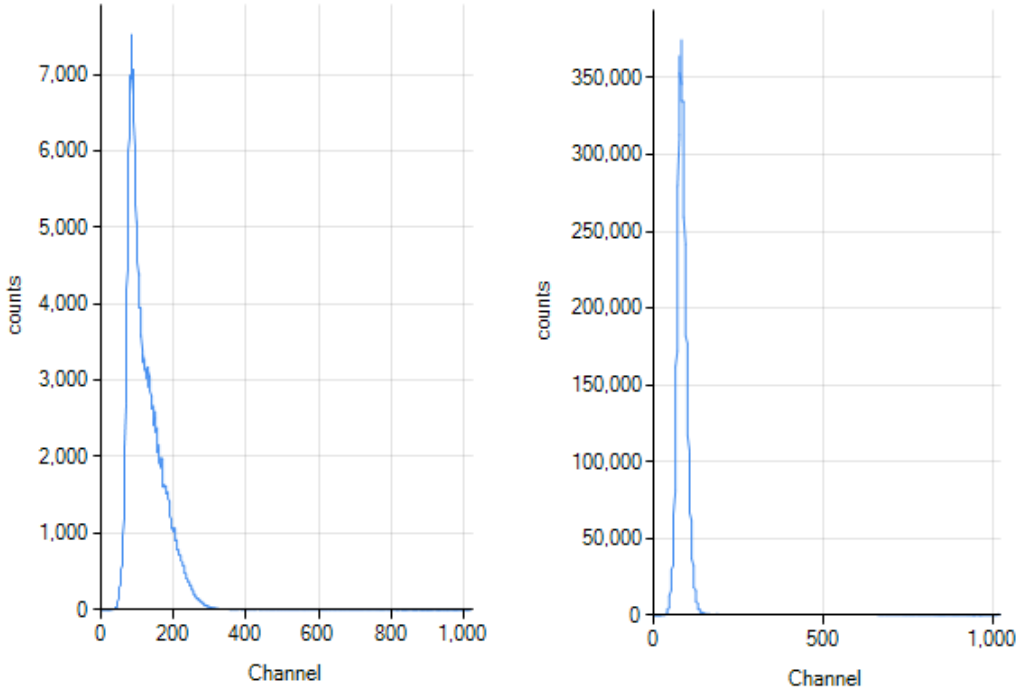

Figure 9.16: $5\,ml{+}15\,ml{+}^{3}H$ spectrum vs $5\,ml{+}15\,ml$ spectrum

The low limits of the detection are calculated with the Currie equation [21], for not having

a false count larger than the 5%:

$$LLD = 4.65\sqrt{N_B} + 2.71 \tag{9.2}$$

where the N_B is the background count-rate. Therefore, the minimum detectable activity in Bq/g is equal to:

$$MDA = \frac{LLD}{\epsilon\, V\, T}\ [Bq/g] \tag{9.3}$$

with V the volume sample, T the measurement time and ϵ the efficiency.

vial	efficiency	MDA for $2h$ as counting time	MDA for $9h$ as counting time
$19\,ml$+$1\,ml$	10.2 %	1.45	0.68
$18\,ml$+$2\,ml$	8.3 %	0.72	0.34
$15\,ml$+$5\,ml$	5.6 %	0.29	0.14

Table 9.3: MDA results varying the concentration

Due to the results obtained, $15\,ml$+$5\,ml$ is chosen as the optimal solution, because it allows to analyze more volume of water and is a good compromise between efficiency and MDA. In fact, considering the vial with $5\,ml$ of water, it is possible to reach optimal values such as $0.29\,Bq/g$ in $2\,h$ [tab:9.3].

Therefore, it follows an evaluation of consistency and reproducibility of the sample to validate the value of efficiency not as a rare event, but as a solid one. Other three samples are prepared with the following composition: $15\,ml$ cocktail with $5\,ml$ demineralized water from CNAO. After an enough time to stabilize the samples, they are measured different times for $2\,h$, before being stored in the dark and having waited for $30\,min$ in the dark tank to reduce the luminescence. The counts are equal to $127\,CPM$, $146\,CPM$, $131\,CPM$ and $136\,CPM$ for an average equal to $135\,CPM$. Moreover, two of the four samples are measured for $15\,h$ for a countrate equals to $131\,CPM$ and $127\,CPM$. According to Poisson distribution, the deviation standard on the total countrate is proving that all the values are included in the distribution.

Furthermore, other three samples are prepared with the addition of the capsule source of ^3H. After the dissolution of the source in $15\,ml$ of AquaLight cocktail, $5\,ml$ of demineralized water from CNAO are added. The measured counts are equal to $10626\,CPM$, $10664\,CPM$, $10721\,CPM$ and $10791\,CPM$. The statistic of these set proves an average equals to $10701\,CPM$. Moreover, the obtained results follow the Poisson distribution.

The evaluation shows a reproducibility in the samples with an efficiency equal to 5.7%.

This value should be checked periodically, for example every year or in correspondence with important movements of the machine to validate the stability and functionality.

10 | Conclusions and future developments

In this work, a method to study the water activation in an hadrontherapy facility is studied with particular observations in the water composition and in the field that generates the activation. Conservative hypotheses are assumed to simulate the worst scenario for a radioprotection purpose. The dissertation is developed with the radioprotection office at CNAO, where an important expansion is programmed with the Hitachi protontherapy and BNCT. For this reason, the investigation deals with their structure and characteristics.

The conducted water activation is realized with *a priori* studio for the expected particles according to the employed water analyses, because the utilities are characterized by softened water, while the accelerator cooling system is composed of demineralized water. Hence, the common radionuclides produced by both water compositions are ^{3}H with traces of ^{10}Be and ^{14}C as regards the long lived particles and for the short lived particles ^{13}N, ^{11}C and ^{15}O. On the other hand, the presence of some milligrams of impurities of the softened water, such as sodium, calcium and chlorides, conducts to the production of important long lived particles as ^{36}Cl and ^{41}Ca and short one as ^{24}Na.

In the actual synchrotron, FLUKA simulations leads to similar results among the different accelerated particles: the activated radionuclides are mainly the listed before, but in different quantities. The main production is due to the acceleration to carbon ions for a year: almost $6\,kBq$ of ^{3}H, $8\,kBq$ of ^{7}Be, some traces of ^{10}Be and ^{14}C and some kBq of ^{11}C and ^{13}N. The activation level is decreasing if accelerating the oxygen, iron, lithium and helium ions and it is minimum for protons.

As regards the Hitachi protontherapy, the water activation of the utilities shows the same produced radionuclides as for the acceleration of protons in the actual synchrotron, but in more quantities. This effect is due to the gantry with its 360° degrees rotation added to the synchrotron and its losses.

In the BNCT facility, the FLUKA codes show just the formation of ^{14}C in the target and of ^{36}Cl and ^{14}C in the HEBL room. Hence, to validate the obtained results, offline

calculus are developed: the HEBL room shows no relevant production of radionuclides, but an increase of activity for ^{3}H and ^{24}Na, while in the target region is highlighted the low activities of ^{14}C and ^{3}H and so the fact that FLUKA could not detect the tritium.

To conclude the cooling water path, the accidental scenario in which the emergency pool failed is studied. The contained radionuclides are ending in the Pavia drainage system where the dose to the workers are evaluated. The dose estimations to the workers during the corrivation, from the depuration tank and the sludge line are under the limit dose to the population of $1\,mSv$ per year.

Thanks to the fact that this work was developed on site, an evaluation of the actual cooling system was possible. This measurement is articulated in two steps: at first, the HPGe allows to exclude the presence of others radionuclides and the second step is a LSC measurement. The HPGe confirms the absence of some emitters that could interfere with the LSC. The second part is developed with the triathler. Its calibration was necessary to avoid the quench effect. The first trial was to perform the quench curve with the addition of a known quantity, but they were not possible to print due to the machine characteristics (1 PMT). Hence, the photoluminiscence peak is overlapped to the ^{3}H spectrum, particularly increasing the quenching level, the plot is shifted and reduced towards left so the centre of gravity was in the photoluminescence peak. At this point, the instrument was not able to differentiate the increasing level of quenching. Therefore, the optimal solution was the internal standard method. Different trials were performed to assure the best concentration of water respect to the scintillation cocktail, as a balance among the efficiency, the analyzed volume and the MDA. Hence, evaluation of reproducibility of the optimal sample validates the consistency of the measurement.

Bibliography

[1] Japanese society of neutron capture therapy (jsnct). what is bnct? URL `http://www.jsnct.jp/e/index.html`.

[2] Fluka. URL `http://www.fluka.org/fluka.php`.

[3] S. Agosteo. *Lecture notes in medical applications of radiation fields*. December 2019.

[4] S. Agosteo, A. Mereghetti, E. Sagia, and M. Silari. Shielding data for hadron-therapy ion accelerators: Attenuation of secondary radiation in concrete. *Nuclear Instruments and Methods in Physics Research Section B: Beam Interactions with Materials and Atoms*, 319:154–167, 2014.

[5] G. Bazzano, A. Ampollini, E. Cisbani, C. De Angelis, S. Della Monaca, P. Nenzi, E. Nichelatti, G. Palmerini, L. Picardi, M. Piccinini, et al. Beam characterization methods at the top-implart proton linear accelerator: an application to space components qualification. In *2021 IEEE 8th International Workshop on Metrology for AeroSpace (MetroAeroSpace)*, pages 37–41. IEEE, 2021.

[6] J. Birks and F. Firk. The theory and practice of scintillation counting. *Physics Today*, 18(8):60, 1965.

[7] F. Campi. *Lecture notes in radioprotection.*

[8] F. CNAO. Fondazione cnao's insitutional website. URL `https://fondazionecnao.it/en`.

[9] R. Craun and D. Smith. Analysis of response data for several organic scintillators. *Nuclear Instruments and Methods*, 80(2):239–244, 1970.

[10] L. Decree. July 2020 no. 101 implementing directive 2013/59/euratom–"attuazione della direttiva 2013/59/euratom, che stabilisce norme fondamentali di sicurezza relative alla protezione contro i pericoli derivanti dall–esposizione alle radiazioni ionizzanti, e che abroga le direttive 89/618/euratom, 90/641/euratom, 96/29/euratom, 97/43/euratom e 2003/122/euratom e riordino della normativa di settore in at-

tuazione dell–articolo 20, comma 1, lettera a), della legge 4 ottobre 2019, n. 117–, 31.

[11] A. Ferrari, P. R. Sala, A. Fasso, and J. Ranft. Fluka. *CERN-library in: http://fluka. web. cern. ch/fluka*, 55(99):100, 2005.

[12] M. Ferrarini. *Caratterizzazione di un rem counter e di un sistema di sfere di Bonner a sensibilità estesa basato sull'utilizzo di rilevatori di CR39 per il monitoraggio ambientale di acceleratori per uso medicale: dottorato in scienza e tecnologia delle radiazioni, 19. ciclo: tesi di dottorato*. 2007.

[13] E. Fokas, G. Kraft, H. An, and R. Engenhart-Cabillic. Ion beam radiobiology and cancer: time to update ourselves. *Biochimica et Biophysica Acta (BBA)-Reviews on Cancer*, 1796(2):216–229, 2009.

[14] I. Governement. Decreto legislativo n. 101 del 31 luglio 2020. attuazione della direttiva 2013/59/euratom, che stabilisce norme fondamentali di sicurezza relative alla protezione contro i pericoli derivanti dall'esposizione alle radiazioni ionizzanti, e che abroga le direttive 89/618/euratom, 90/641/euratom, 96/29/euratom, 97/43/euratom e 2003/122/euratom e riordino della normativa di settore in attuazione dell'articolo 20, comma 1, lettera a), della legge 4 ottobre 2019, n. 117. gu serie generale n. 201 del 12-08-2020—suppl. ordinario n. 29. 2020.

[15] J. Hansman. Why does the neutron elastic scattering cross section increase with decreased energy?, 08 2016.

[16] Hidex. Liquid scintillation measuring procedures, . URL `https://hidex.com/ebooks/liquid-scintillation-measuring-procedures/introduction/quenching//`.

[17] Hidex. Application for radiometric measurements, quench, . URL `https://www.perkinelmer.com/it/lab-products-and-services/application-support-knowledgebase/radiometric/quench.html`.

[18] IAEA. Practical applications of short-lived radioisotopes. .

[19] S. IAEA. Safety reports series no. 19. .

[20] M. J. Kessler. *Liquid Scintillation Analysis: science and technology*. Packard Instrument, 1989.

[21] G. F. Knoll. *Radiation detection and measurement*. John Wiley & Sons, 2010.

[22] C. W. Lee, Y.-O. Lee, Y.-S. Cho, and S. Ahn. Analysis of the neutron thermalization

in an accelerator room. *Journal of Nuclear Science and Technology*, 45(sup5):39–41, 2008.

[23] NEA. Janis web. URL `https://www.oecd-nea.org/janisweb/`.

[24] A. Noujaim, C. Ediss, and L. Weibe. *Liquid scintillation: science and technology*. Academic Press, 2013.

[25] N. C. on Radiation Protection and Measurements. *NCRP Report No. 144. Radiation protection for Particle Accelerator Facilities*. 2003.

[26] C. Peng. Quenching correction in liquid scintillation counting. *Advances in tracer methodology*, pages 81–94, 1966.

[27] R. Protection. Icrp publication 103. *Ann ICRP*, 37(2.4):2, 2007.

[28] M. Pullia. Status report on the centro nazionale di adroterapia oncologica (cnao). *IEEE transactions on applied superconductivity*, 16(2):1708–1711, 2006.

[29] S. Rossi. The national centre for oncological hadrontherapy (cnao): status and perspectives. *Physica Medica*, 31(4):333–351, 2015.

[30] TAE. Tae web. URL `https://taelifesciences.com/alphabeam-neutron-system/`.

[31] I. TECDOC et al. Current status of neutron capture therapy. *TECDOC-1223*, 2001.

[32] M. Umezawa, F. Ebina, Y. Fujii, K. Matsuda, K. Hiramoto, K. Umegaki, and H. Shirato. Development of compact proton beam therapy system for moving organs. *Hitachi Rev*, 64506:13, 2015.

[33] J. Varmuza, K. Katovsky, O. Šťastný, and M. Zeman. The spectrum of neutrons and its importance for nuclear power engineering. pages 1–5, 05 2017. doi: 10.1109/EPE.2017.7967301.

[34] H. Vega C, E. Manzanares A, V. Hernandez D, G. Mercado, M. Iniguez, and A. Martin M. Thermalization of monoenergetic neutrons in a concrete room. 2006.

[35] H. R. Vega-Carrillo, E. Gallego, E. Manzanares-Acuña, A. Lorente, R. Barquero, A. Martin-Martin, and J. Gutierrez-Villanueva. Neutron room return effect. *Revista mexicana de física*, 54:63–66, 2008.

List of Figures

List of Tables

List of Symbols

Variable	Description
ab-BNCT	accelerator-based Boron Neutron Capture Therapy
BNCT	Boron Neutron Capture Therapy
CNAO	Centro Nazionale di Adroterapia Oncologica
CPM	Counts Per Minute
CPS	Counts Per Second
D.Lgs.	Decreto Legislativo
ESD	Eletrostatic Deflector
FLUKA	FLUktuierende KAskade
FORTRAN	FORmula TRANslator
HEBL	High Energy Beam Line
HEBT	High Energy Beam Transfer Line
HPGe	Hiperpure Germanium
IAEA	International Atomic Energy Agency
IC	Isocenter
ICRP	International Commission on Radiological Protection
ICRU	International Commission on Radiological Units and Measurements
IMPT	Intensity Modulated Proton Therapy
INFN	Istituto Nazionale di Fisica Nucleare
LEBT	Low Energy Beam Transfer Line
LET	Linear Energy Transfer
LINAC	Linear Accelerator
LSC	Liquid Scintillation Counting
MDA	Minimum Detectable Activity
MEBT	Medium Energy Beam Transfer Line
OER	Oxygen Enhancement Ratio
PMT	Photo Multiplier Tube
RFQ	Radio Frequency Quadrupole
SOBP	Spread Out Bragg Peak